Study of the Optical Properties of Solids by using Full Potential Linear Augmented Plane Wave (FP-LAPW) method

Dissertation Submitted in Fulfillment of the

Requirements for the Degree of

Doctor of Philosophy

in Physics

By

Lalmuanpuia

To

Department of Physics

Mizoram University, Aizawl

Mizoram, India

May 2011

Study of the Optical Properties of Solids by using Full Potential Linear Augmented Plane Wave (FP-LAPW) method

Dissertation Submitted in Fulfillment of the

Requirements for the Degree of

Doctor of Philosophy

in Physics

By

Lalmuanpuia

Registration No. Ph. D/ 163/ 17. 12. 2007

To

Department of Physics

Mizoram University, Aizawl

Mizoram, India

May 2011

Ê¨ÉWÉÉä®ú¨É

Ê´É·ÉÊ´ÉtÉ±É¤É

¦ÉÉèÊiÉEò Ê´ÉYÉÉxÉ

Ê´É¦ÉÉMÉ

MIZORAM UNIVERSITY
DEPARTMENT OF PHYSICS
AIZAWL 796 009 MIZORAM
Phones : 0389 - 2330435, - 2330522
FAX : 0389 - 2330522
E-mails : hod_phymzu@rediffmail.com
rktt@sancharnet.in

Dr. R. K. Thapa

MZU-1/P-14/03/PHY/Ph.D./ Dated: 6th May, 2011

Certificate

This is to certify that the thesis entitled '*Study of the optical properties of solids by using full potential linear augmented plane wave (FP-LAPW) method'* submitted by Shri Lalmuanpuia, for the degree of Doctor of Philosophy of the Mizoram University, Aizawl, embodies the record of original investigations carried out by him under my supervision. He has been duly registered and the thesis presented is worthy of being considered for the award of the Ph. D. degree. This work has not been submitted for any degree of any other university.

(R.K.Thapa)

Supervisor

Declaration of the Candidate

Mizoram University

Aizawl: Mizoram

Department of Physics

I declare that I wrote this work myself and carried out the computational study described in it, without using any other sources and aids than those that are stated under the supervision of Dr. R. K. Thapa, Reader in Physics, Mizoram University, Tanhril, Aizawl and that I have not submitted this work to any other University or Institute for any other degree.

I also declare that the present investigation relates to bonafide research and the title of the thesis is '**STUDY OF THE OPTICAL PROPERTIES OF SOLIDS BY USING FULL POTENTIAL LINEAR AUGMENTED PLANE WAVE (FP-LAPW) METHOD'.**

(Dr. R. K. THAPA) **(LALMUANPUIA)**

Supervisor **Candidate**

Department of Physics,
Mizoram University, **Dated: 4th May, 2011**

Aizawl, Mizoram.

Acknowledgement

First of all, I am most grateful to my supervisor Dr. R.K. Thapa who has encouraged my studies in many different ways during the past years. Not only did he support me in scientific issues, but also managed to create this warm and relaxed atmosphere which turned working in his group into an enjoyable experience.

I also would like to thank all the other group members M.P. Ghimire, Sandeep, Dibya and Rosangliana since they are responsible for the nice atmosphere and for the encouraging discussions in our group.

I would also like to express my sincere gratitude to Mrs. Kamala Thapa for her generosity and warm welcome extended towards us.

And last, but not least, I would like to say thanks to my father Mr. Hrangthanpuia and my mother Mrs. Thangzawni for their steady support during all the years of my studies.

Dated: 9th. May 2011

Mizoram University

Aizawl, Mizoram. (LALMUANPUIA)

CONTENTS

List of Figures

LIST OF TABLES

A synopsis for the Ph. D. Programme
Of
Physics Department, Mizoram University

'Study of the Optical Properties of Solids by using Full Potential Linear Augmented Plane Wave (FP-LAPW) method'

Submitted by

Lalmuanpuia

Date of Admission : 17th August 2007
Date of approval by BPGS: 30th October 2007

Supervisor

Dr.R.K.Thapa
Department of Physics
Mizoram University
Tanhril : Mizoram

October 2007

Study of the Optical Properties of Solids by using Full Potential Linear Augmented Plane Wave (FP-LAPW) method

INTRODUCTION

One of the most powerful tools for studying the properties of solids is the measurement and the analysis of their optical properties. In this work some of the results required for such an analysis is presented. It is now almost twenty-five years since doped poly-acetylene has been shown to reach electrical conductivities comparable to conventional metals (Chiang *et al*.1977). These findings marked the birth of a whole new field of research focusing on the electronic and optical properties of conjugated polymers. These novel materials combine the mechanical flexibility, the low molecular weight, and the low cost processibility which is typical for 'plastic' materials with the electro-optical properties known from inorganic semiconductors and metals. Moreover they are low dimensional systems, which opens new possibilities for applications, and which is also interesting from a purely scientific point of view. Optical properties of solids are a major topic, both, in basic research as well as for industrial applications. While for the former origin and nature of different excitation processes is of fundamental interest, the latter can make use of them in many opto-electronic devices .These wide interests require experiment and theory to go hand in hand, and thus asks for reliable theoretical concepts.

SURVEY OF LITERATURE

Applied scientific research depends on the existence of accurate theoretical models. In particular, highly reliable ab-initio methods are indispensable for designing novel materials as well as for a detailed understanding of their properties. The development of such theories describing the electronic structure of atoms, molecules, and solids has been one of the success stories of physics in the 20^{th} century. Among these, density functional theory (DFT) (Hohenberg 1964, Kohn 1964, Sham 1966, Jones 1989, Gunnarsson 1989) has proven to yield ground state properties for a vast

number of systems in a very precise manner. Indeed, DFT forms the basis of all electronic ground state calculations carried out in the present work.

Excited states, on the other hand, are not contained within the framework of DFT, and are –generally speaking –much more demanding. However, it is these properties that are probed in spectroscopic methods, and that are utilized for technological applications. Therefore, it is necessary to develop and test ab-initio techniques that are capable of predicting excited state quantities equally reliable as, for instance, DFT does for the ground state properties. In this work, we are mainly interested in optical properties, thus we are concerned with the interaction of external electro-magnetic with electron-hole excitations in the system. This can be treated rigorously within many-body perturbation theory, express in terms of the equation of motion for the electron-hole two – particle Green's function, the so called Bethe-Salpeter equation (BSE) (Sham 1966, Hanke 1975, Strinati 1982). The interaction between the electron and the hole is characterized by an effective interaction kernel, which has to be approximated in an appropriate manner. To zeroth order, the electron and the hole can be treated as independent particles, which results in the random phase approximation (RPA) for the optical properties. However, solutions of the BSE in an ab-initio framework, appearing in the literature in the past few years, have shown that electron-hole interactions are indeed important in order to correctly describe quantitative (oscillator strengths) as well as qualitative (bound excitons) features of optical spectra of semi-conductors and insulators (Albrecht 1997, Benedict 1998, Rohlfing 1998, Van der Horst 1999, Arnaud 2001).

SCOPE OF STUDY

The development of new materials and the understanding of their physical properties is at the heart of technological as well as scientific progress. Optical properties of solids are a major topic, both, in basic research as well as for industrial applications. Optical properties of solids are a major topic, both, in basic research as well as for industrial applications. . To date, the range of applications covers light emitting diodes [Tang (1987), Burroughes (1990), Braun (1991), Grem (1992), Friend (1999)] photo diodes and photovoltaic cells (Sariciftci 1992, Halls 1995) and also fully organic transistors (Garnier 1990, Srivastava 1994, Dodalpur 1995). Recently, outstanding electronic and optical properties have been studied in molecular crystals

consisting of conjugated molecules. Devices based on polyacene single crystals are efficient photovoltaic cells (Schon, 2000), ambipolar field effect transistors (Berg et *al.* 2000), show electrically driven laser emission (Schon *et al.* 2000), and exhibit the integral as well as the fractional Quantum Hall effect (Schon *et al.* 2000).Lead salts had been widely used as optical detectors, and hence these semiconductors have technological importance. We intend to study the optical properties of these systems by using the latest method called FP-LAPW. Optical properties like variation of ε_1, ε_2, absorption coefficients, refractive indices etc. against photon energies, will be calculated with the help of standard computer code named as WIEN2K. The primary scope of our study will be hence to update the existing data on optical and band structure properties.The reason being that we will be using the DFT approach as proposed by Hohenberg and Kohn (1964).

OBJECTIVE

The purpose of this work is therefore (i) to develop the necessary tools in order to solve the BSE for crystalline systems, and (ii) to apply these techniques to semiconductor systems like PbS, PbTe, and PbSe. The first point again consists of two steps:

All wave functions entering the calculations are commonly expressed in terms of given basis functions. In the present work, we choose linearized augmented plane waves (LAPW). They form the basis of the full- potential LAPW method (Andersen 1975), which is one of the most accurate and successful band structure methods available. The BSE is adopted for this basis set by deriving the appropriate formulae, and a computer program is implemented which is performing the required computational steps. We have chosen the full potential linearized augmented plane wave (FP-LAPW) method where no shape approximation for potential is made. We have developed the formalism of treating optical properties within the random phase approximation (RPA) taking into account interband as well as intraband contributions. In terms of applications we focus on metallic cases for the following reasons. (1) Metals don't suffer from the band gap problem; (2) metals are quite well described by the LDA, and (3) the RPA is justified due to the effective screening.

THEORY

(A) **Optical response**:

The optical properties of solids are given by the response of the electron system to a time - dependent electromagnetic perturbation caused by the incoming light. As such, the calculation of these properties is reduced to the calculation of a response function that is the complex dielectric tensor or equivalently the polarizability. An exact expression for it is of course not known and we have to resort to the usual technique of many- body perturbation theory to derive the approximations. The first of these is the RPA.

A particular case of the general expression for the dielectric function in the RPA is the well known Lindhard formula (Ashcroft and Mermin 1976),

$$\varepsilon(q,\omega) = 1 + \frac{2V(q)}{\Omega_c} \sum_k \frac{f_0(\varepsilon_{k+q}) - f_0(\varepsilon_k)}{\varepsilon_{k+q} - \varepsilon_k - \omega} \Omega_c$$

where $V(q)=\frac{4\pi e^2}{[q]^2}$ is the Coulomb interaction, Ω_c the unit cell volume, f_0 the Fermi distribution function, and ε_k the single particle energy. The factor 2 comes from the summation over the spin.

(B) **Symmetry**:

The dielectric tensor is symmetric with up to six independent components according to the symmetry of the crystal. Therefore the general expression for the imaginary part of ε is:

$$\begin{pmatrix} Im\varepsilon_{xx} & Im\varepsilon_{xy} & Im\varepsilon_{xz} \\ Im\varepsilon_{xy} & Im\varepsilon_{yy} & Im\varepsilon_{yz} \\ Im\varepsilon_{xz} & Im\varepsilon_{yz} & Im\varepsilon_{zz} \end{pmatrix}$$

(C) **Kramers- Kronig relations and optical constants**:

From the imaginary part of the dielectric tensor component $\mathrm{Im}\,\varepsilon_{ij}$ the corresponding real part is obtained by

$$\mathrm{Re}\,\varepsilon_{ij} = \delta_{ij} + \frac{2}{\pi}\wp\int_0^\infty \frac{\omega' \,\mathrm{Im}\,\varepsilon_{ij}(\omega')}{\omega'^2 - \omega^2} d\omega'$$

Given the real part, the inverse transformation has to be used.

With the knowledge of the complex dielectric tensor components all other frequency – dependent optical constants can be obtained.

(D) **Sumrules**:

There are three sumrules which obtain information about the absorption process:

$$\int_0^{\omega'} \sigma(\omega)\omega d\omega = N_{eff}(\omega')$$

$$\int_0^{\omega'} \mathrm{Im}\left(\frac{-1}{\varepsilon(\omega)}\right)\omega d\omega = N_{eff}(\omega')$$

$$\int_0^{\infty} \mathrm{Im}\left(\frac{-1}{\varepsilon(\omega)}\right)\frac{1}{\omega} d\omega = \frac{\pi}{2}$$

The first two give an effective number of electrons contributing to the absorption process as a function of energy. Typically, in the low energy region the contribution to the intraband spectrum should sum up to the number of the outermost valence electrons.

The LAPW basis set:

In band structure calculations based on density-functional theory (Hohenberg and Kohn 1964) the single particle electronic states $\{\Psi_{nk}(r)\}$ and energies $\{\varepsilon_{nk}\}$ are desribed by the solutions of the Kohn-Sham (KS) equation [Kohn, Sham 1965]

$$\left[-\frac{\hbar^2}{2m}\nabla^2 + V_{eff}(r)\right]\Psi_{nk}(r) = \varepsilon_{nk}\,\Psi_{nk}(r) \ldots\ldots\ldots\ldots\ldots (1)$$

With the effective potential $\{V_{eff}(r)\}$ being the sum of the bare Coulomb potential of the atomic nuclei $\{V_{latt}(r)\}$, The Hatree potential $\{V_H(r)\}$ and the exchange correlation potential $\{V_{xc}(r)\}$. In practical calculations, equation (1) is solved via the Rayleigh-Ritz variational principle.

METHODOLOGY

We will give a short account of the full potential LAPW method and discuss the implementation of the solution to the BSE in terms of the LAPW method. The actual formulae required for the coding are derived and numerical test are presented. For this purpose, we intend to use the computer programme called WIEN2K code developed by Peter *et al*. Full fledged standard code called WIEN2K code for the calculations of optical properties systems under studies. The code consists of several FORTRAN programmes for doing calculations of density of states (DOS), band structure and optical properties etc. This code runs on LINUX operating system and is compatible with the Lahey Fujitsu FORTRAN 95 compiler.

The code had been used by several authors successfully. For example, Daoudi *et al* (2007) had used it for the calculation of ground state properties of nitride compounds. Optical properties of rare earth compounds like hexaborides (sing *et al.* 2007), zinc choleozenides (Reshak *et al.* 2007), sesquioxides (Singh *et al.* 2006), etc. had been also studied successfully by using this particular.

ORGANISATION

Tentative arrangement of the thesis in the form of chapters will be as follows:

Chapter 1: Introduction.

Chapter 2: Theoretical background of Random Phase Approximation and Linear Augmented Plane Wave method.

Chapter 3: Study of Optical response within the LAPW method and Band structure calculations.

Chapter 4: Conclusions followed by references.

REFERENCES

[1] Ali Hussain Reshak and Sushil Auluck, Physica B 388, issues 1-2, 34-42 (2007)

[2] A. Dodabalapur, L. Torsi, H.E. Katz, Science **268,** 270 (1995)
B Daoudi, M Sehil, A. Boukraa, H Abid, Int. J. Mater. Sci. Simu., 1, 91- 106, (2007)

[3] B. Arnaud, M. Alouani, Phys .Rev. B **63**, 085208 (2001)

[4] Braun, A.J. Heeger, Appl. Phys. Lett**.58,** 1982 (1991)

[5] C.K. Chiang, C.R. Fincher, Y.W. Park, A.J. Heeger, H. Shirakawa, E.J. Louis, S.C. Gau, A.G. Mac Diarmid, Phys. Rev Lett. **39**, 1098 (1977)

[6] C.W. Tang, S.A. Van Slyke, Appl. Phys. Lett.**51**, 913 (1987).

[7] F. Garnier, G. Horowitz, X.Peng, D.Fichou, Adv. Mat. **2**, 592 (1990)

[8] F. Garnier, R.Hajlaoui, A. Yasser, P.Srivastava, Science **26**, 1684 (1994)

[9] G.Grem, G. Leditzky, B. Ullrich, G. Leising, Adv. Mat **4**, 36 (1992)

[10] G. Strinati, Phys Rev Lett. **49**, 1519 (1982)

[11] G. Strinati, Phys Rev Lett. B **29**, 5718 (1984)

[12] J.H. Burroughes, D.D.C. Bradley, A.R. Brown, R.N. Marks, K.Mackay, R.H.Friend, P.L. Burn, A. Kraft, A.B. Holmes, Nature **347**, 539 (1990)

[13] J.H. Schon, S. Berg, C. Kloc, B. Batlogg, Science **287**, 1022 (2000)

[14] J.H. Schon, C. Kloc, R.C. Haddon, B. Batlogg, Science **288**, 656 (2000)

[15] J.H. Schon, C. Kloc, B. Batlogg, Science **406**, 702 (2000)

[16] J.H. Schon, C. Kloc, A. Dodabalapur, B. Batlogg, Science **289**, 599 (2000)

[17] J.H. Schon, C. Kloc, B. Batlogg, Science **288**, 2338 (2000)

[18] J.W. van der Horst, P.A. Bobbert, M.A.J Michels, G. Brocks, P.J. Kelly, Phys. Rev. Lett. **83**, 4413. (1999)

[19] J.J.M. Halls, C.A. Walsh, N.C Greenham, E.A. Marseglia, R.H.Friend, S.C. Moratti, A.B. Holmes, Nature **376**, 498 (1995)

[20] L.J. Sham, T.M. Rice, Phys. Rev. **144**, 708 (1966)

[21] LX. Benedict, E.L. Shirley, R.B Bohn, Phys. Rev. Lett. **80**, 4514 (1998)

[22] M. Rohlfing, S.G. Louie, Phys. Rev. Lett.**81**, 2312 (1998)

[23] M. Rohlfing, S.G. Louie, Phys. Rev. Lett.**82**, 1959 (1999)

[24] Nirpendra Singh, Sapan Mohan Saini, T. Nautiyal, and Sushil Auluck, Journal of Physics: Condensed Matter. 19 346226 (2007)

[25] Nirpendra Singh, Sapan Mohan Saini, T. Nautiyal, and Sushil Auluck, Journal of Applied Physics 100, 083525 (2006)

[26] N.S. Sariciftci, L Smilowitz, A.J. Heeger, F. Wudl, Science **258**, 1474 (1992).

[27] Neil W. Ashcroft and N. David Mermin, Solid State Physics, (Saunders College Publishing, Fort Worth, TX, U.S.A., 1976) p-344

[28] O.K. Andersen, Phys. Rev B **12**, 3060 (1975)

[29] P. Hohenberg, W. Kohn, Phys. Rev. **136**, B 864 (1964)

[30] R.H. Friend, R.W. Gymer, A.B. Holmes, J.H. Burroughes,R.N. Marks, C. Taliani, D.D.C. Bradley, D.AD. Santos, J.L. Bredas, M. Logdlund, W.R. Salaneck, Nature **397**, 121 (1999)

[31] R.O. Jones, O. Gunnarsson, Rev. Mod. Phys **61**, 689 (1989)

[32] S. Albrecht, G.Onida, L.Reining, Phys.Rev. B **55**, 10278 (1997)

[33] S. Albrecht, L.Reining, R. Del Sole, G.Onida, Phys.Rev. Lett.**80**, 4510 (1998)

[34] W. Hanke, L.J. Sham, Phys. Rev. B **12**, 4501 (1975)

[35] W. Hanke, Adv. Phys. **27**, 287 (1978)

[36] W. Hanke, L.J. Sham, Phys. Rev. Lett.**43**, 387 (1979)

[37] W. Hanke, L.J. Sham, Phys. Rev. Lett.B **21**, 4656 (1980)

[38] W. Kohn, L.J. Sham, Phys.Rev. **140**, A1133 (1965)

[39] W. Kohn, Rev. Mod. Phys. **71**, 1253 (1999)

Chapter 1

Introduction

The development of new materials and the understanding of their physical properties is at the heart of technological as well as scientific progress. The study of semiconductors opens new possibilities for applications which make it interesting from a purely scientific point of view. The range of applications covers infrared detectors, in light emitting devices, as infrared lasers in fibre optics (Agarwal *et al.,*1993), as thermoelectric materials, in solar energy panels, and in window coatings and in quantum dots as monolayer (Justo *et al.,*2010; Hicks *et al.,* 1996; Chatterjee *et al*.,1993; Nair *et al*., 1990; Bozin *et al.,*2010). Ferroelectric substance has wide applications in non-linear optics, ceramics, micro wave and sensor industries (Tagantsev *et al*.,2003; Kell,1963) as well as in microelectronics.

Applied scientific research depends on the existence of accurate theoretical models. In particular, highly reliable *ab-initio* methods are in-dispensable for designing novel materials as well as for a detailed understanding of their properties. The development of such theories describing the electronic structure of atoms, molecules, and solids has been one of the success stories of physics in the 20^{th} century. Among these, density functional theory (DFT) of Hohenberg and Kohn (1964), Kohn *et al.,* (1965) and others (Jones *et al.,* 1989; Kohn, 1999) have proven to yield ground state properties for a vast number of systems in a very precise manner. DFT forms the basis of all electronic ground state calculations carried out in the present work.

In this work, we are mainly interested in optical properties, thus we are concerned with the interaction of external electro-magnetic waves with electron-hole excitations in

the system. We will limit our calculations to weak external perturbations which can be treated within the linear response regime. This can be treated rigorously within many-body perturbation theory, expressed in terms of the equation of motion for the electron-hole two-particle Green's function, the so-called Bethe-Salpeter equation (BSE) (Sham *et al.,* (1966); Hanke *et al.,* (1975), (1979), (1980); Hanke, (1975); Strinati, 1982,1984). To zeroth order, the electron and the hole can be treated as independent particles, which results in the random phase approximation (RPA) for the optical properties. However, solutions of the BSE in an *ab-initio* framework, appearing in the literature in the past few years, have shown that electron-hole interactions are indeed important in order to correctly describe quantitative (oscillator strengths) as well as qualitative (bound excitons) features of optical spectra of semi-conductors and insulators (Albrecht *et al*.,1997,1998 ; Benedict *et al*.,(1998), Rohlfing *et al.,*1998 ,1999; Van der Horst *et al.*,1999; Arnaud *et al.,* 2001).

In the present work, we choose full potential linearized augmented plane waves (FP-LAPW) method (Hashemifar *et al.,* 2005; Hedin *et al.,* 1971), which is one of the most accurate and successful band structure methods available. We will apply this method to semiconductors and ferroelectric materials. All wave-functions entering the calculations are commonly expressed in terms of given basis functions. We have used a computer program WIEN2k code of Blaha *et al.,* (2008) which is an implementation of the full-potential LAPW method, for all computations presented in this thesis. The calculations focus mainly on the influence of inter-molecular interactions on the electronic and optical properties of semiconductors.

This work is organized as follows. In Chapter 2 we give a short description of density functional theory (DFT) which provides the framework for treating ground state

properties of systems of interacting electrons. We will discuss the basic theorems and equations that form the foundations of DFT (Hohenberg *et al.*, 1964; Kohn *et al.,* 1965), and the relevant approximations entering the theory. In chapter 3 we will give a detailed method for the full potential linearized augmented plane waves (FP-LAPW) method. In chapter 4, we will discuss a methodology for optical study starting from Maxwell's equations in the presence of matter and we will derive the macroscopic dielectric function (DF) in the random phase approximation by using the self-consistent field method following the presentation of Adler (1962) and Wiser (1963). Chapter 4 contains the main outcome of the theoretical developments attained within this work.

In Chapter 5, the density of states, electronic band structures and optical properties for systems like BeX, PbX, ZnX, (where X= S, Se, Te) and ferroelectric material $SbTaO_4$ will be presented. In chapter 6, we will present the conclusion of the thesis, which will be followed by references and appendices.

Chapter 2

Density Functional Theory

Since its introduction in the 1960s (Hohenberg *et al*.,1964; Kohn *et al*.,1965) density functional theory (DFT) has evolved into a powerful tool that is widely used in condensed matter theory and computational materials science for the calculation of electronic, magnetic and structural properties of solids. The method has been remarkably successful in predicting, reproducing and explaining a wide variety of materials phenomena such as predictions of magnetic, electronic properties and understanding various physical properties of the systems. Thomas and Fermi proposed a scheme based on the density of electrons to discuss the properties of a system of interacting electrons, such as a molecule or a solid. They assumed that the motions of the electrons are un-correlated, and the kinetic energy can be described by a local approximation based on the free electron result. Although the Thomas-Fermi approximation has only limited success in treating real materials, it is the basis of the density functional formalism. The promising aspect of using the electron density instead of the many-particle wave function as basic variable is of course, that it is much easier to obtain than the precise details of the wave function ψ, and also the scaling with system size is much better for methods based on the density of the system. The equations that govern interactions between the electrons and nuclei of solids have been well known for decades, but finding their exact solution for a complex solid is beyond the limits of current computing power. However, using a series of approximations, the electronic structure and the total energy of most materials can be calculated quite accurately. A wide variety of first-principles methods are used to determine the behavior of materials. Materials have different types of

bonding interactions and therefore some approximations are better suited than others for a particular system of interest.

Density functional theory (DFT) enables the description of the ground state properties of a real system in terms of its ground state electronic charge density $n(r)$, a parameter simply depending on a single spatial coordinate r, instead of the wave functions which depend on all the electronic coordinates r_i. In this formalism, all the physical quantities related to the ground state, are expressed as functional of the charge density, $F[n(r)]$. As was shown by Hohenberg and Kohn (1964), all ground state properties of a crystal are uniquely determined by the electron charge density.

2.1 The Hohenberg-Kohn Theorem

The DFT is based on two theorems.

Theorem 1. For a given external potential v, the total energy of a system is a unique functional of the ground state electron density.

To prove this we consider a Hamiltonian, H=T+V+W, where T represents the kinetic energy of the system, V the interaction of the electrons with an external potential (including the potential coming from the atomic nuclei in the solid) and W the electron-electron interaction. For N electrons the solution to this Hamiltonian results in a ground state many body wave function $\psi(r_i, r_2, ...r_N)$ and we have

$$H\,\psi = E_o\,\psi. \tag{2.1}$$

The electron density can be calculated from

$$n(r) = \langle \psi \left| \sum_{i=1}^{N} \delta(r - r_i) \right| \psi \rangle \tag{2.2}$$

and the interaction V is written as $V = \int n(r)v(r)d^3r$, where $v(r)$ is the external potential. Now, to proof that two different external potentials $v(r)$ and $v'(r)$ must give rise to different ground state electron densities for a system with potential $v'(r)$ we have

$$H'\psi' = E'_0\psi' \tag{2.3}$$

Let $n(r)$ be the non-degenerate ground-state density of N electrons in the external potential $v(r)$, corresponding to the ground state characterized by the many-electron wave function ψ and its total energy E_o. Then, we can write

$$E_0 = \langle\psi|H|\psi\rangle \tag{2.4}$$

$$= \int n(r)v(r)d^3r + \langle\psi \mid T+V \mid \psi\rangle \tag{2.5}$$

$$E_0 = \int n(r)v(r)d^3r + F[n(r)] \tag{2.6}$$

$$F[n(r)] = \langle\psi \mid T+V \mid \psi\rangle \tag{2.7}$$

Now suppose that there exists a second external potential $v'(r)$, which differs from $v(r)$ not just by a constant, leading to the same density $n(r)$. If we denote its ground state wave function and energy with ψ' and E'_0 respectively, we obtain

$$E'_0 = \langle\psi'|H|\psi'\rangle \tag{2.8}$$

$$= \int n(r)v'(r)d^3r + \langle\psi' \mid T+V \mid \psi'\rangle \tag{2.9}$$

The Rayleigh-Ritz minimal principle for ψ gives the following inequality

$$
\begin{aligned}
E_0 &< \langle \psi' | H | \psi' \rangle \\
&= \int n(r) v'(r) d^3 r + \langle \psi' | T + V | \psi' \rangle \\
&= E_0' + \int [v(r) - v'(r)] n(r) d^3 r
\end{aligned}
\tag{2.10}
$$

A similar argument for the ground state of ψ′ leads to the expression

$$
\begin{aligned}
E_0' &< \langle \psi | H' | \psi \rangle \\
&= E_0 + \int [v'(r) - v(r)] n(r) d^3 r
\end{aligned}
\tag{2.11}
$$

Adding Eqs. (2.3) and (2.4) leads to the contradiction

$$E_0 + E'_0 < E_0 + E_0' \tag{2.12}$$

which is clearly wrong. Hence $n'(r) \neq n(r)$ and we conclude that two different potentials, $v(r)$ and $v'(r)$ give rise to different densities $n(r)$ and $n'(r)$. Therefore, knowledge of the electron density $n(r)$, implies that it was calculated from a Hamiltonian with a specified external potential $v(r)$. As the kinetic energy T, and electron-electron interactions W, are known and specified one concludes that knowledge of the ground state electron density determines the entire Hamiltonian and hence the ground state energy, which proves Theorem 1. We can thus express a functional relationship between the ground state energy and the corresponding electron density as

$$E[n(r)] = \mathrm{T}[n(\mathrm{r})] + V[n(r)] + W[n(r)]. \tag{2.13}$$

The second important theorem of DFT is

Theorem 2. The exact ground state density minimizes the energy functional $E[n(r)]$. To prove Theorem 2 one starts from Theorem 1 and for a given external potential $v_0(r)$ writes

$$E_{v_0}[n(r)] = \langle \psi[n(r)] | T + W + V_0 | \psi[n(r)] \rangle \tag{2.14}$$

where the subscript v_0 indicates that this is the energy functional for a system with external potential $v_0(r)$. Since the ground state density specifies the Hamiltonian, it also specifies the wave function (of the ground state and of excited states) and hence the notation ψ [$n(r)$]. If the ground state electron density is denoted by $n_0(r)$, the ground state can be expressed as ψ [$n_0(r)$]. From the variational principle one again obtains

$$\langle \psi[n_0(r)] | T + W + V_0 | \psi[n_0(r)] \rangle < \langle \psi[n(r)] | T + W + V_0 | \psi[n(r)] \rangle \tag{2.15}$$

which can also be expressed as

$$E_{v_0}[n_0(r)] < E_{v_0}[n(r)] \tag{2.16}$$

i.e., the ground state density minimizes the energy functional $E[n(r)]$. This is the Hohenberg-Kohn minimum principle (Hohenberg *et al.*,1964) stating that the total energy is a functional of the density, and that the ground state density $n(r)$ minimizes this functional resulting in the ground state energy $E = E[n(r)]$. If we have an explicit form for $E[n(r)]$ we could minimize it with respect to the electron density and in this way calculate the ground state energy. But, due to the complexity provided by the electron-electron interactions, approximations are necessary to obtain an explicit expression for $E[n(r)]$.

2.2 The Kohn-Sham equation

The equation of Kohn and Sham are a practical procedure to obtain the ground state density and turn density functional theory into a method of finding energy bands.

$$F[n(r)] = \langle \psi | T + V | \psi \rangle \tag{2.17}$$

Hohenberg and Kohn demonstrated that there exists a unique universal functional $E[n(r)]$of the ground state electron density, which satisfies the variational principle with respect to the electron density:

$$E_0 = \int n(r)v(r)d^3r + \langle \psi \mid T + V \mid \psi \rangle \tag{2.18}$$

$$= \int n(r)v(r)d^3r + F[n(r)] \tag{2.19}$$

$$F[n(r)] = \langle \psi \mid T + V \mid \psi \rangle \tag{2.20}$$

where $F[n(r)]$ contains the electronic kinetic energy (T) and the electronic Coulomb interaction (V) and $v(r)$ represents the Coulomb potential due to the nuclei of the solid. The fundamental Hohenberg-Kohn theorem of the density functional theory states that the ground state energy can be obtained by minimization of the functional (2.19), constrained with the conservation of the total charge.

Unfortunately, the universal functional $F[n(r)]$ is not known. To solve this problem, Kohn and Sham (1965) introduced an additional development by mapping the original interacting problem into an effective and non-interacting problem with a slightly different potential $V_{KS,}$ called the effective Kohn-Sham potential. The density functional F[n(r)] for the interacting system is given by the sum of the kinetic energies of a non-interacting electron gas with the same density $n(r)$ as the original one, and additional terms that describe the inter-particle interactions

$$F[n] = T_s[n] + J[n] + E_{xc}[n] \tag{2.21}$$

where $T_s[n]$ is the kinetic energy of a non-interacting electron gas, $J[n]$ is the classical Coulomb energy (often referred as Hartree term)

$$J[n]=\frac{e^2}{2}\iint\frac{n(r')}{|r-r'|}d^3r' \tag{2.22}$$

and $E_{xc}[n]$ is called exchange-correlation energy and contains all many-body effects not described by the other terms. In other words, $E_{xc}[n]$ describes the difference between the real system and the effective non-interacting system (including the correction for the kinetic energy and the Coulomb interactions):

$$E_{xc}[n]=\{T(n)+V(n)\}-\{T(n)+J(n)\} \tag{2.23}$$

The difference is usually expected to be small, and $E_{xc}[n]$ principally contains the correction of $J(n)$ arising from the correlations between electrons.

From equation 2.21 it is possible to extract the effective Kohn-Sham potential V_{KS}, by imposing that the energy functional $E[n(r)]$ for the interacting problem must be minimized by the same electron density $n(r)$ that minimizes the energy $E_s[n(r)]$ of the non-interacting electron gas.

$$\left[-\frac{\hbar^2}{2m_e}\vec{\nabla}_i^2+V_{KS}\right]\phi_i(\vec{r})=\varepsilon_i\phi_i(\vec{r}) \tag{2.24}$$

where

$$V_{KS}=v_r+e^2\int\frac{n(\vec{r}')}{|\vec{r}-\vec{r}'|}d\vec{r}'+\frac{\delta E_{xc}[n(r)]}{\delta n(r)} \tag{2.25}$$

With the Kohn-Sham potential V_{KS}, the effective Hamiltonian describes a non-interacting system, since all interactions have been included in V_{KS}. In addition, the electronic problem can now be tackled using a one-particle system, and the charge density becomes:

$$n(\vec{r}) = \sum_{i=1}^{N} \left[\phi_i(\vec{r}) \right]^2 \tag{2.26}$$

The exchange-correlation potential is the variational derivative of the exchange correlation energy functional:

$$V_{xc}(r) = \frac{\delta E_{xc}[n(r)]}{\delta n(r)} \tag{2.27}$$

The wave function $\phi_i(\mathrm{r})$ appearing in the Kohn-Sham equations describe electronic orbitals for the auxiliary non-interacting gas; they are the eigenstates of the effective single electron non-interacting problem and should not be considered as wave functions for the electrons of the real system. It is only the total energy and the electronic density $n(r)$ that have a physical meaning. However, usually the Kohn-Sham energy levels give good description of band structure of the real crystalline solids.

2.3 Local density approximation

Although the exchange correlation energy, $E_{xc}[n(r)]$ is well defined as a concept, its expression is not known precisely, and therefore an approximate expression is necessary to obtain the ground state energy $E[n(r)]$. The local density approximation (LDA) is a simple expression for $E_{xc}[n(r)]$ and it is based on the assumption that the real $E_{xc}[n(r)]$ is equal to the exchange correlation energy per electron of a homogeneous electron gas of the same density $n(r)$:

$$E_{xc}[n] = \int n(r)\varepsilon_{xc}n(r)d^3r \tag{2.28}$$

where ε_{xc} is the exchange-correlation energy per electron of a uniformly interacting electron gas of the same density n (Kohn *et al*.,1965). The correlation part was first calculated by Ceperly and Alder using Quantum Monte Carlo method. The LDA is

strictly valid only if $n(r)$ is varying slowly, and many extensions exist which give improved accuracy for systems with localized electrons.

2.4 Generalized gradient approximation

To extend the density approximation to systems with more significant non-homogeneous densities, several techniques have been proposed. The most successful one is the generalized gradient approximation (GGA), where the real $E_{xc}[n(r)]$ is expressed as a functional of the density $n(r)$ and its gradient $\nabla n(r)$:

$$E_{xc}[n] = \int n(r)\varepsilon_{xc}n(r)d^3r + \int F_{xc}[n(r)|\nabla n|]d^3r \tag{2.29}$$

where F_{xc} is a correction. In principle this method should be called as LDA+GGA, but for short one uses only the term GGA. The GGA formalism gives a better description of inhomogeneous systems, like transition metals, and it significantly improves the binding energy, predicting good results also in the cases where LDA fails. GGA accounts specifically for density gradients that are neglected in pure LDA. For the GGA calculations performed in this work, the Perdew-Burke-Ernzerhof (PBE96) (1996) parameterization for the exchange-correlation functional was used.

Chapter 3

Full-Potential Linearized Augmented Plane Wave Method (FP-LAPW)

In order to solve the Kohn-Sham equations for periodic crystals systems plane waves $e^{i[(k+K)]r}$ would be a natural choice of basis functions compatible with the periodic boundary conditions. Here, *k* denotes a vector from the first Brillouin zone, and *K* is a reciprocal lattice vector. However, an unrealistically large number of plane waves would be necessary to achieve an appropriate description of the wave functions near the atomic nuclei. It was the idea of Slater (1937) to augment the plane waves by atomic-like functions in the vicinity of the atomic nuclei. Since Slater first proposed the method in 1937, the augmented plane wave (APW) method and its descendents has been among the most popular schemes for solving the electronic structure using density-functional theory. The APW method in its modern general potential and linearized forms combines a conceptual simplicity with high accuracy for a general system. During the years, there have been important developments of the original APW method, for instance the full-potential implementation and of course the linearization of the secular problem as proposed by Andersen (1975).

While the LAPW method yields accurate results for close-packed metal systems the restrictions to the potential (shape-approximations) become difficult to justify for crystals with open structures such as silizides, perovskides, surfaces or clusters. In LAPW method, a basis set is introduced which is especially adapted to the problem. This adaptation is achieved by dividing the unit cell into two regions, namely (i) non-overlapping atomic spheres (centered at the atomic sites) and (ii) an interstitial region

(region II) as shown in Fig. 3.1. For the construction of basis functions, the muffin tin approximation (MTA) is used according to which the potential is assumed to be spherically symmetric within the atomic spheres in which an atomic-like function is used and constant outside in which plane waves are used.

The basis functions for the two regions are:

(1) Inside atomic sphere I, of radius R_i, a linear combination of radial functions times spherical harmonics $Y_{lm}(r)$ is used

$$\phi_{kn} = \sum \left[A_{lm,k_n} u_l(\vec{r}, E_l) + B_{lm,k_n} \dot{u}_l(\vec{r}, E_l) \right] Y_{lm}(\hat{r}) \qquad (3.1)$$

where $u_l(\vec{r}, E_l)$ is the regular solution of the radial Schroedinger equation for energy E_l and the spherical part of the potential inside sphere I; $\dot{u}_l(\vec{r}, E_l)$ is the energy derivative of u_l evaluated at the same energy E_l. A linear combination of these two functions constitutes the linearization of the radial function. The coefficients A_{lm} and B_{lm} are functions of k_n determined by requiring that this basis function matches each plane wave (PW) the corresponding basis function of the interstitial region. u_l and $\dot{u}_l$ are obtained by numerical integration of the radial Schrödinger equation on a radial mesh inside the sphere.

(2) In the interstitial region a plane wave expansion is used

$$\phi_{k_n} = \frac{1}{\sqrt{\omega}} e^{i\vec{k}_n \cdot \vec{r}} \qquad (3.2)$$

where $\vec{k}_n = \vec{k} + \vec{K}_n$; $\vec{K}_n$ are the reciprocal lattice vectors and $\vec{k}$ is the wave vector inside the first Brillouin zone. Each plane wave is augmented by an atomic-like function in

every atomic sphere. The solutions to the Kohn-Sham equations are expanded in this combined basis set of LAPW's according to the linear variation method

$$\psi_k = \sum_n c_n \phi_{k_n} \tag{3.3}$$

and the coefficients c_n are determined by the Rayleigh-Ritz variational principle.

In order to improve upon the flexibility of the basis set and to make possible a consistent treatment of semicore and valence states in one energy window, adding additional basis functions to the usual LAPW basis set called 'local orbitals (LO)' was suggested by Singh (1994). They are local in the sense that they are completely confined within the muffin tin spheres. Local orbitals consists of a linear combination of two radial functions at two different energies and one energy derivative and is given as

$$\phi_{lm}^{LO} = \sum \left[A_{lm} u_l(\vec{r}, E_{1,l}) + B_{lm} \dot{u}_l(\vec{r}, E_{1,l}) + C_{lm} u_l(\vec{r}, E_{1,l}) \right] Y_{lm}(\hat{r}) \tag{3.4}$$

In the applications of APW and LAPW methods, the potential in the unit cell $V(r)$ was typically approximated by

$$V(r) = \begin{cases} V_I^0 = const & outside\, sphere \\ V_{MT}^0(r) & inside\, sphere \end{cases} \tag{3.5}$$

using a constant potential in the interstitial region and a spherically symmetric potential inside each sphere.

The full-potential Linearized Augmented Plane Wave (FP-LAPW) method is one of the most accurate methods used for the solution of the Kohn-Sham equations for semiconducting systems. The code that has been used for all calculations in this work (WIEN2k) is a full-potential LAPW code developed by Blaha and co-workers (2008). The idea of the FP- LAPW method is to divide the unit cell into two different regions: non-overlapping spheres around the positions of the nuclei, and the remaining interstitial region, schematically depicted in Fig. 3.1.

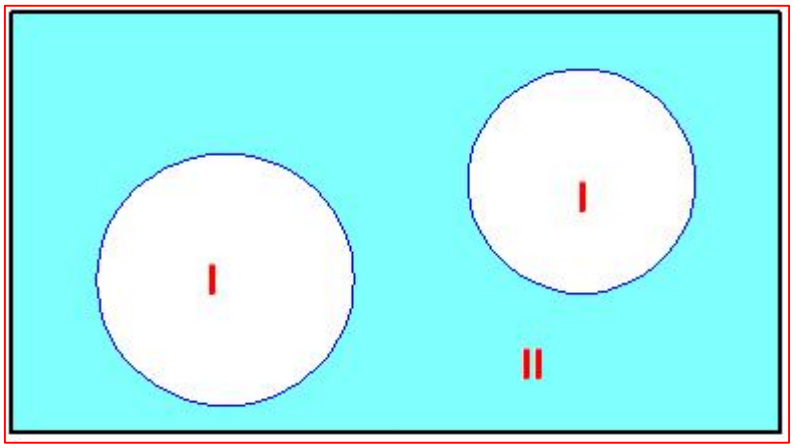

Figure 3.1: Partitioning of the unit cell into atomic spheres (I) and an interstitial region (II).

In the two regions, different sets of basis functions are used for the wave functions as well as for the electron density and the crystal potential. The choice of these basis functions is guided by the observation that near the nuclei the wave functions remain atomic-like even in a crystalline environment, whereas they are more plane-wave like between the atoms. The same argument also applies for the density as well as for the potential.

In the full-potential LAPW method (Hashemifar *et al*., 2005; Hedin *et al*., 1971) there are no shape-approximations in the interstitial region and inside the muffin-tin spheres. The constant interstitial potential V_I^0 is replaced by the warped potential $\sum_K V_K e^{i\vec{K}\cdot\vec{r}}$ and to the spherical muffin-tin potential the non-spherical term is added.

$$V(r)=\begin{cases}\sum\limits_{LM} V_{LM}(\vec{r})Y_{LM}(\hat{r}) & \textit{inside sphere}\\ \sum\limits_{K} V_K e^{i\vec{K}\cdot\vec{r}} & \textit{outside sphere}\end{cases} \qquad (3.6)$$

The charge density *n*(r) is represented in the same way as the potential:

$$n(r)=\begin{cases}\sum\limits_{LM} n_{LM}(\vec{r})Y_{LM}(\hat{r}) & \textit{inside sphere}\\ \sum\limits_{K} n_K e^{i\vec{K}\cdot\vec{r}} & \textit{outside sphere}\end{cases} \qquad (3.7)$$

3.1 The Muffin-Tin A- and B-Coefficients

Within FPLAPW the electron wavefunctions are expanded differently in the interstitial region and the muffin-tins. Each basis function consists of a planewave in the interstitial, which is matched to the radial functions and spherical harmonics in the muffin-tins. The coefficients of the function inside the spheres are determined from the requirement, that the basis functions and their derivatives are continuous at the sphere

boundaries. These coefficients play an important role, therefore we will discuss how the matching conditions can be solved and what properties they induce.

In many systems where the FP-LAPW method can be applied, some atoms are symmetry equivalent, i.e. these atoms can be mapped onto each other by a space group operation $\{R|\tau\}$ Such a group of atoms is called an atom type, represented by one of the atoms. Let $\{R^{\mu}|\tau^{\mu}\}$ be the operation that maps the atom μ onto its representative. This atom can now be assigned a local coordinate frame S^{μ} where the origin of S^{μ} is at the atoms position p^{μ} .The local frame is chosen such that the unit vectors of the local frame S^{μ} are mapped onto those of the global frame by $R^{g}\left(R^{\mu}S^{\mu}=S^{g}\right)$. The local frame of the representative atom S^{α} is only translated with respect to the global frame, i.e. the same rotation R^{μ} maps S^{μ} onto S^{α}. The potential (and other quantities) inside the muffin-tins can now be written in terms of the local coordinate system. Due to the symmetry we find $V_{MT^{\alpha}}(r^{\alpha})=V_{MT^{\mu}}(r^{\mu})$ where (r^{α}) and (r^{μ}) are expanded in terms of the local frames S^{α} and S^{μ} respectively. As a consequence the radial functions $u_l(r)$ and the Hamiltonian matrices are the same for all atoms of the same type. This way symmetry is exploited to save memory and computing time (during the calculation of the t-matrices) and (r^{μ}) are expanded in terms of the local frames S^{α} and S^{μ} respectively. As a consequence, the radial functions $u_l(r)$ and the Hamiltonian matrices are the same for all atoms of the same type. This way symmetry is exploited to save memory and computing time (during the calculation of the t-matrices).

Any plane wave can be expanded into spherical harmonics via the Rayleigh expansion,

$$e^{iKr}=4\pi\sum_{L}i^{l}\,j_l(rK)\,Y_L^{*}(\hat{K})\,Y_L(\hat{r}) \tag{3.8}$$

where r = |r|, K = |K| and K abbreviates (G + k). Looked at from the local frame K and p^{μ} appear rotated, besides the origin of the local frame is shifted. Therefore, the planewave has the following form in the local frame:

$$e^{i(R^{\mu}K)(r+R^{\mu}p^{\mu})} \tag{3.9}$$

Thus, the Rayleigh expansion of the planewave in the local frame is given by:

$$e^{iKp^{\mu}} 4\pi \sum_{L} i^{l}\, j_{l}(rK)\, Y_{L}^{*}(R^{\mu}\hat{K}) Y_{L}(\hat{r}) \tag{3.10}$$

The requirement of continuity of the wavefunctions at the sphere boundary leads to the equation

$$\sum_{L} \left[A_{lm}^{\mu G}(k_n) u_l(\vec{r}, E_l) + B_{lm}^{\mu G}(k_n) \dot{u}_l(\vec{r}, E_l) \right] Y_{lm}(\hat{r})$$

$$= e^{iKp^{\mu}} 4\pi \sum_{L} i^{l}\, j_{l}(rK)\, Y_{L}^{*}(R^{\mu}\hat{K}) Y_{L}(\hat{r}) \qquad (3.11)$$

where $A_{lm}^{\mu G}$ and $B_{lm}^{\mu G}$ are matching co- efficient which are functions of k_n determined by requiring that this basis function matches each plane wave (PW) the corresponding basis function of the interstitial region. The second requirement is, that the derivative with respect to r, denoted by *d/dr* = ', is also continuous

$$\sum_{L} \left[A_{lm}^{\mu G}(k_n) u_l'(\vec{r}, E_l) + B_{lm}^{\mu G}(k_n) \dot{u}_l'(\vec{r}, E_l) \right] Y_{lm}(\hat{r})$$

$$= e^{iKp^{\mu}} 4\pi \sum_{L} i^{l}\, j_{l}'(rK)\, Y_{L}^{*}(R^{\mu}\hat{K}) Y_{L}(\hat{r}) \qquad (3.12)$$

These conditions can only be satisfied, if the coefficients of each spherical harmonic $Y_L(\hat{r})$ are equal. Solving the resulting equations for $A_{lm}^{\mu G}(k_n)$ and $B_{lm}^{\mu G}(k_n)$ yields:

$$A_{lm}^{\mu G}(k_n) = e^{iKp^{\mu}} 4\pi \frac{1}{W} i^{l} Y_{L}^{*}(R^{\mu}\hat{K}) [u_l(\vec{r}, E_l) k j_l'(\vec{r}, k) - \dot{u}_l'(\vec{r}, E_l) j_l(\vec{r}, k)] \tag{3.13}$$

$$B_{lm}^{\mu G}(k_n) = e^{iKp^{\mu}} 4\pi \frac{1}{W} i^{l} Y_{L}^{*}(R^{\mu}\hat{K}) [u_l'(\vec{r}, E_l) j_l(\vec{r}, k) - u_l(\vec{r}, E_l) k j_l'(\vec{r}, k)] \tag{3.14}$$

The Wronskian W is given by:

$$W = [\dot{u}_l(\vec{r})u'_l(\vec{r}) - u_l(\vec{r})\dot{u}'_l(\vec{r})] \tag{3.15}$$

Thus their form is completely general so that such a scheme is termed full-potential calculation. In order to have a small number of LM values in the lattice harmonics expansion a local coordinate system for each atomic sphere is defined according to the point group symmetry of the corresponding atom. This specifies a rotation matrix that relates the local to the global coordinate system of the unit cell.

Chapter 4

Methodology for optical study

4.1 Linear Optical Response

In this chapter we will set up methods that will enable us to calculate the linear optical response of periodic solids from first principles. The microscopic Maxwell equations will be discussed as a prerequisite that will enable us to calculate the linear optical response of periodic solids from first principles. The concept of the dielectric matrix and some of its general properties are also discussed. Following the work of Ehrenreich et al., (1959), Adler (1962) and Wiser (1963), we then describe the linear optical properties of solids in terms of the self-consistent field method. Ehrenreich and Cohen (1959) derived an expression for the dielectric function of solids by assuming that electrons and holes move independently of each other in a self-consistent potential arising from the externally applied electric field plus a screening field. This is the widely-used random phase approximation (RPA) or equivalently the time-dependent Hartree-approximation. Adler (1962) and Wiser (1963) generalized the RPA description by allowing the screening field to vary on an atomic scale, giving rise to the so-called local field corrections. A presentation of the optical properties of solids on the RPA level can be found in a book by Wooten (1972). In the last section, we go beyond the RPA by including excitonic effects. These electron-hole interactions have important consequences in the description of the optical properties of semiconductors.

4.2 Microscopic Maxwell Equations

The Maxwell equations of electrodynamics in the presence of matter and on a microscopic (atomic) scale can be written in the form

$$\nabla \llcorner D = 4\pi\rho_{ext} \tag{4.1}$$

$$\nabla \times E = -\frac{1}{c}\frac{\partial B}{\partial t} \tag{4.2}$$

$$\nabla \llcorner B = 0 \tag{4.3}$$

$$c^2 \nabla \times B = 4\pi j_{ex} + \frac{\partial D}{\partial t} \tag{4.4}$$

where the electric displacement D is connected to the electric field E via the polarization P, as $D = E + P$. The Maxwell equations in the form (4.1-4.4) correspond to systems which are described by the external charge density ρ_{ex} with the current density j_{ex}. Thus, the fields entering the Maxwell equations are difference fields between the perturbed and the unperturbed system. The most general form of the dielectric tensor ε is defined by linearly relating the electric displacement D to the electric field E

$$D_i(r,t) = \int d^3r' dt' \varepsilon_{ij}(r,r';t-t')E_j(r',t') \tag{4.5}$$

where ε_{ij} is a tensor of second rank for crystals other than cubic symmetry, and we have used the summation convention for double appearing indices j in the above equation. In a perfect crystal, we have translational symmetry, and the dielectric tensor remains unchanged when both coordinates r and r' are shifted by a lattice vector R. Hence,

$$\varepsilon_{ij}(r+R,r'+R;t-t') = \varepsilon_{ij}(r,r';t-t') \tag{4.6}$$

and the dielectric tensor can be Fourier analyzed with the following convention to be used for all lattice-periodic two-point functions in this thesis (Appendix A. I)

$$\varepsilon_{ij}(r,r';t-t') = \frac{1}{\Omega}\sum_{q}\sum_{GG'} e^{-i[(q+G)r-\omega t]}\varepsilon_{ij}(q+G,q+G';\omega)e^{i[(q+G')r'-\omega t]} \tag{4.7}$$

Here, q is a vector within the first Brillouin zone, G and G' are reciprocal lattice vectors, and Ω denotes the crystal volume. By transforming D and E to reciprocal space and to

the frequency domain, and using the Fourier expansion for ε, expression (4.5) can be written as

$$D_i(q+G;\omega) = \sum_{G'} \varepsilon_{ij}(q+G, q+G';\omega) E_j(q+G';\omega) \tag{4.8}$$

Eq. (4.8) can be interpreted in the following way: The (q, ω) Fourier component of the dielectric displacement D is a vector in the reciprocal lattice vectors G, and the same is true for the electric field. Then, the (q, ω) component of the dielectric displacement D is related to the (q, ω) component of the electric field via a matrix multiplication with the dielectric matrix corresponding to (q, ω), and having the matrix indices GG'.

4.3 Longitudinal and the transverse dielectric tensor

In this section, we follow a practice introduced by Lindhard (1954) and describe the dielectric response in terms of the longitudinal and the transverse dielectric tensor describing the response to a longitudinal and transverse electric field, respectively. In the case of a homogeneous system, for instance the free-electron gas, a longitudinal (transverse) current cannot be induced by a transverse (longitudinal) electric field. Consequently, the longitudinal and transverse dielectric tensors give a complete description of the linear dielectric properties of the homogeneous electron gas. In inhomogeneous systems, such as periodic solids, however, a purely transverse or purely longitudinal electric field induces both transverse and longitudinal currents. We are interested in the response to an optical perturbation, which is a transverse electro-magnetic field. Therefore, the optical properties have to be calculated using the transverse-response formalism, with a term A • p as perturbation. Here, A denotes the vector potential, and p is the momentum operator. In the limit of vanishing q vectors, however, it can be shown that a longitudinal perturbation described by a scalar potential leads to the same result. This property is referred to as the gauge invariance of optical properties and was shown by Ambegaokar *et al*. (1960) for cubic crystals, and by Del

Sole *et al*., (1984) for systems with lower than cubic symmetry. For this reason, it is sufficient to consider the longitudinal dielectric tensor, if one is interested only in the limit $q \rightarrow 0$. Therefore, we will restrict the discussion in the following sections to the description of the longitudinal dielectric function only.

4.4 Macroscopic Quantities

When we are interested in the response to an optical perturbation, we are interested in the average response of the system due to the large wave length of light in the visible region as compared to an atomic scale. We define the macroscopic quantity f_M corresponding to its microscopic counterpart f by averaging the microscopic quantity over one unit cell. We can express f in terms of the Fourier representation such that

$$f(r) = \frac{1}{\Omega} \sum_{qG} f_G(q) e^{-i(q+G)r} \tag{4.9}$$

The average over one unit cell with volume Ω_0 at the position R defines the macroscopic quantity in the following way

$$f_M(R) = \frac{1}{\Omega_0} \int_{\Omega_0} d^3 r f(r+R) \tag{4.10}$$

Taking into account the definition (4.9) and using the fact that |q| is assumed to be much smaller than |G|, the term e^{-iqr} is approximately 1, which leads to the result

$$f_M(R) = \sum_q f_0(q) e^{-iqR} \tag{4.11}$$

The above relation simply says that the q Fourier component of any macroscopic quantity is just the $\{q, G = 0\}$ component of the corresponding microscopic quantity. We will make use of this result in the next sections, when we derive an expression for the macroscopic dielectric function.

4.5 The Self-Consistent Field Method

In this section, we want to describe the longitudinal dielectric response of solids by following the derivation of the longitudinal dielectric matrix for periodic crystals in the random phase approximation as given by Adler (1962) and Wiser (1963). An alternative description using field theoretical techniques is due to Nozieres and Pines (1958a, 1958b, 1958c). The starting point for the discussion is the single particle Liouville-von-Neumann equation

$$i\frac{\partial \hat{n}}{\partial t} = \left[H, \hat{n}\right] \tag{4.12}$$

Here, $\hat{n}$ denotes the density operator of the system and the Hamiltonian $\hat{H}$ consists of a time-independent part $\hat{H}_0$ describing the unperturbed system plus the self-consistent potential *V(r,t)*

$$\hat{H} = \hat{H}_0 + V(r,t) \tag{4.13}$$

The self-consistent potential *V(r,t)* is the sum of the externally applied potential V_{ext} and the screening potential V_s due to the rearrangement of the electrons in response to the external perturbation

$$V(r,t) = V_{ext}(r,t) + V_s(r,t) \tag{4.14}$$

We have assumed the response V_s to be a classical electro-static screening potential, and we did not allow for exchange and correlation effects here. This approximation accounts for the fact that we treat electrons and holes as independent particles. It is assumed that the motion of the electrons in the unperturbed case can be described by an effective single-particle potential such as the Kohn-Sham potential of density functional theory, which we write in the form

$$\hat{H}_0 \left| mk \right\rangle = \varepsilon_{mk} \left| mk \right\rangle \tag{4.15}$$

Here, $|mk\rangle$ denotes the Bloch state of band number *m* and wave vector *k* with the single-particle energy ε_{mk}. The action of the density operator of the unperturbed system $\hat{n}_0$ on the eigenstates $|mk\rangle$ is given by

$$\hat{n}_0|mk\rangle = f_0(\varepsilon_{mk})|mk\rangle \tag{4.16}$$

where f_0 is the Fermi-Dirac distribution function. We now assume that the density operator of the perturbed system can be written as

$$n = \hat{n}_0 + \hat{n}_1 \tag{4.17}$$

where $\hat{n}_1$ denotes the density change due the perturbation. By neglecting a term $(V, \hat{n}_1)$, containing products of the density change and the self-consistent perturbing potential, we obtain the linear response regime, and arrive at the linearized form of the Liouville equation for the density change $\hat{n}_1$,

$$i\frac{\partial \hat{n}_1}{\partial t} = [H_0, \hat{n}_1] + [V, \hat{n}_0] \tag{4.18}$$

Moreover, we assume that the time dependence of the external potential V_{ext} is given by

$$V_{ext} \sim e^{-i\omega' t}e^{\delta t} = e^{-i\omega t} \tag{4.19}$$

where δ is an infinitesimal positive number producing an adiabatic switching on of the perturbation. In the following it is understood that ω contains the appropriate infinitesimal δ. In the linear response regime all quantities exhibit the same time dependence as the external perturbation. Taking the matrix elements of Eq. (4.18) between the states $\langle lk|$ and $|mk+q\rangle$, using the relations (4.15) and (4.16), and taking into account the $e^{-i\omega t}$ time dependence leads to

$$\langle lk|\hat{\rho}_1|mk+q\rangle = \frac{f_0(\varepsilon_{mk+q}) - f_0(\varepsilon_{lk})}{\varepsilon_{mk+q} - \varepsilon_{lk} - \omega}\langle lk|V|mk+q\rangle \tag{4.20}$$

Hence, we have found a relation between the induced density and the self-consistent potential from which we will get the polarizability of the system.

4.6 Neglecting Local Fields

In this section we will discuss an approximation which greatly simplifies the computation of the macroscopic dielectric function. The macroscopic external perturbation which is described by the scalar potential V_{ext} only produces a screening potential V_s on a macroscopic scale. Therefore, both V_{ext} and V_s as well as the total perturbing potential V can be expressed in a Fourier series

$$V(r,t) = \sum_q V(q,t) e^{-iqr} \tag{4.21}$$

We can derive an expression for the polarization $\hat{P}^0$ that is relating the change in the density n to the total potential V.

$$n(q,\omega) = \hat{P}^0(q,\omega) V(q,\omega) \tag{4.22}$$

$$\hat{P}^0(q,\omega) = \frac{1}{\Omega} \sum_{lmk} \frac{f_0(\varepsilon_{mk+q}) - f_0(\varepsilon_{lk})}{\varepsilon_{mk+q} - \varepsilon_{lk} - \omega} [M^0_{lm}(k,q)]^* M^0_{lm}(k,q) \tag{4.23}$$

The matrix elements involved in the equation (4.23) can be evaluated for small q by perturbation theory [Appendix II]. Application of Poisson's equation and using the relation $V_{ext} = \varepsilon V$ directly leads to the macroscopic dielectric function in the RPA which is a well known Lindhard formula (Ashcroft and Mermin 1976),

$$\varepsilon_M(q,\omega) = 1 + V(q) \hat{P}^0(q,\omega) \tag{4.24}$$

The above expression is easy to evaluate, because only the G = G' = 0 component of the irreducible polarization $\hat{P}^0$ has to be computed, and moreover no matrix inversion is involved.

4.7 The Long Wavelength Limit

Our main interest in this chapter is to describe the linear response of solids to optical perturbations. Since the wave length of electro-magnetic waves at optical frequencies is much larger than the characteristic momenta in solids, optical perturbations can be described by taking the limit of vanishing q vectors. On account of the Coulomb potential appearing for instance in Eq. (4.24) this limit has to be taken analytically, because simply setting $q = 0$ would result in an indeterminate expression for the dielectric function. This follows from the fact that the matrix elements $M^0_{lm}(k,q)$ entering Eq. (4.23) are given by Kronecker deltas, when q is identically 0

$$M^0_{lm}(k,q=0) = \delta_{lm} \tag{4.25}$$

The reason is of course the fact that the normalized Bloch states belonging to different bands are orthogonal to each other. We can, however, derive an expression for the matrix elements $M^0_{lm}(k,q)$ in the limit of vanishing wave vector q by using $k \bullet p$ perturbation theory (Appendix II). One obtains

$$M^0_{lm}(k,q\to 0) \quad = \quad \delta_{lm} \quad + \quad \frac{\langle lk \mid qp \mid mk\rangle}{\varepsilon_{mk} - \varepsilon_{lk}}(1-\delta_{lm}) \tag{4.26}$$

where p denotes the momentum operator. Thus, making use of the relation (4.26) we get an expression for the polarization in the limit of small q

$$\hat{P}^0(q\to 0,\omega) \quad = \quad 4q^2 \sum_{vck} \frac{\langle vk \mid p_i \mid ck\rangle\langle ck \mid p_j \mid vk\rangle}{(\varepsilon_{ck} - \varepsilon_{vk} - \omega)(\varepsilon_{ck} - \varepsilon_{vk})^2} \tag{4.27}$$

Remembering that the frequency ω contains the infinitesimal imaginary number $i\delta$, we can use the identity

$$\mathrm{Im}\frac{1}{\varepsilon_{ck} - \varepsilon_{vk} - \omega + i\delta} \quad = \quad -\pi\delta(\varepsilon_{ck} - \varepsilon_{vk} - \omega) \tag{4.28}$$

We finally arrive at an expression for the imaginary part of the macroscopic dielectric function in the independent particle approximation where local field effects are neglected

$$\mathrm{Im}\,\varepsilon_M(q\to 0,\omega) \;=\; \frac{16\pi^2}{\Omega\omega^2}\sum_{lmk}\langle vk\,|\,p_i\,|\,ck\rangle\langle ck\,|\,p_j\,|\,vk\rangle\delta(\varepsilon_{ck}-\varepsilon_{vk}-\omega) \tag{4.29}$$

Note that the prefactor $1/\omega^2$ is a consequence of the square of the energy difference in the denominator of Eq. (4.27) and the delta function due to the replacement by equation (4.28). It has been shown that in the limit of vanishing *q*, the response to a transverse perturbation is equivalent to that of a longitudinal perturbation, as has already been discussed in Sec. 4.3. This is not only true for cubic systems (Ambegaokar *et al*., 1960) but also for crystals with lower symmetry (Del Sole *et al*., 1984). For that reason, Eq. (4.29) describes the response to an optical perturbation, where the tensor character of $\mathrm{Im}\,\varepsilon_M(q\to 0,\omega)$ takes into account the anisotropy of crystals with symmetries lower than cubic. We note that the real part of ε_M can be obtained by using the well-known Kramers-Kronig relations.

4.8 Kramers- Kronig relations

From the imaginary part of the dielectric tensor component $\mathrm{Im}\,\varepsilon_{ij}$ the corresponding real part is obtained by

$$\mathrm{Re}\,\varepsilon_{ij}=\delta_{ij}+\frac{2}{\pi}\wp\int_0^\infty\frac{\omega'\,\mathrm{Im}\,\varepsilon_{ij}(\omega')}{\omega'^2-\omega^2}d\omega' \tag{4.30}$$

Given the real part, the inverse transformation has to be used. With the knowledge of the complex dielectric tensor components all other frequency – dependent optical constants can be obtained.

4.9 Dielectric Response within DFT

In this section, we want to consider exchange-correlation (XC) effects in the response function resulting from the XC energy appearing in density functional theory. We have to add to the classical, electro-static screening potential V_s a term V_{xc} stemming from the change in the exchange-correlation potential (2.27) due to the external perturbation given by the scalar potential V_{ext}. Thus, we can write for the self-consistent potential V

$$V_H = V_{ext} + V_s + V_{xc} \tag{4.31}$$

where V_s is just the Hartree potential due to the density change n, which is given by

$$V_s(r) = \int d^3r' \frac{n(r')}{|r-r'|} \tag{4.32}$$

The variation of the XC potential with the density, V_{xc}, is obtained from

$$V_{xc} = \int d^3r' K_{xc}(r,r') n(r') \tag{4.33}$$

where the exchange-correlation kernel K_{xc} is defined as the functional derivative of the XC potential with respect to the density, or equivalently, as second functional derivative of the exchange-correlation energy,

$$K_{xc} = \frac{\delta^2 E_{xc}}{\delta n(r) \delta n(r')} \tag{4.34}$$

Taking into account the definition of the independent particle polarizability $\hat{P}_0$ as the response to the total change in the effective potential, and the full polarizability P as the response to the external potential, we obtain in matrix notation (Levine et al., 1989, 1991; Hybertson et al., 1987).

$$P = (1 - v\hat{P}^0 - K_{xc}\hat{P}^0)^{-1}\hat{P}^0 \tag{4.35}$$

This expression differs from the corresponding RPA expression used in the previous section, by the additional term $K_{XC}\hat{P}_0$ involving the exchange-correlation kernel. If the exchange-correlation energy E_{xc} is a local function, as is the case in the framework of density functional theory, then also the kernel K_{xc} is a local function and given by

$$K_{xc}(r,r') = \frac{dV_{xc}}{dn}\Big|_{n(r)}\delta(r-r') \tag{4.36}$$

As a consequence of the delta function in the above equation, the reciprocal-space expression of K_{xc} is independent of q,

$$K^{xc}_{GG'} = K^{xc}(G-G') \tag{4.37}$$

It is in the limit $q\rightarrow 0$, which is relevant for the description of optical properties. Therefore, we neglect the exchange-correlation term appearing in the polarization function in Eq. (4.35) and work with the RPA expressions when calculating the dielectric function in the framework of density functional theory. In the remaining part of the chapter, however, we develop a method to go beyond the RPA which allows us to incorporate electron-hole interactions into the description of the optical response of semiconductors.

4.10 Inclusion of Excitonic Effects

The connection of the irreducible polarization $\hat{P}$ and complete polarization P to the dielectric matrix ε is given by the following relation

$$\varepsilon = (1-v\hat{P}) \tag{4.38}$$

$$\varepsilon = (1-v\hat{P}) \tag{4.39}$$

Again, v denotes the Coulomb potential as usual and ε^{-1} is the inverse of the dielectric matrix. Equations (4.38) and (4.39) can be combined to yield a generalized Dyson's equation for the complete polarization

$$P = \hat{P} + \hat{P}vP \tag{4.40}$$

From that expression we see that the polarization P is the sum of two contributions termed proper and improper polarization parts, respectively. The proper polarization part, which is equal to the irreducible polarization $\hat{P}$, describes just the electron-hole polarizations which are due directly to the excitations by the external applied field. The improper part, $\hat{P}vP$, contains the polarization part due to the induced field coming from the polarization of all other electron-hole pairs.

4.11 The Long-Range Part of the Coulomb Potential

For the calculation of the optical response we are interested in the long wave-length limit, thus $|q| \to 0$. In this case, the term $\hat{P}vP$ in Eq. (4.40) contains divergent Coulomb factors. These divergent factors can, however, be isolated following a procedure due to Ambegaokar and Kohn (1960). We define the new polarization function $\bar{P}$ as the sum of all polarization processes not involving the long-range part of the Coulomb interaction. In analogy to (4.40) we obtain a generalized Dyson equation for $\bar{P}$

$$\bar{P} = \hat{P} + \hat{P}\bar{v}\bar{P} \tag{4.41}$$

where v denotes a modified Coulomb potential defined in the way

$$\bar{v}(q+G) = \begin{cases} 0 & for \quad G = 0 \\ v(q+G) & for \quad G \neq 0 \end{cases} \tag{4.42}$$

It has been shown by Kohn that, for insulating crystals, the irreducible polarization $\hat{P}$ is proportional to q^2 for small q vectors. Moreover, due to the cut off Coulomb potential v the polarization function $\bar{P}$ defined above shows the same behavior as $\hat{P}$ for small q.

Thus, we can combine Eqs. (4.40) and (4.41) in order to derive the following relation between the G = G' = 0 components of P and $\bar{P}$ in the limit of vanishing q

$$P_{00}(q,\omega) = \frac{\bar{P}_{00}(q,\omega)}{1-v(q)\bar{P}_{00}(q,\omega)} \tag{4.43}$$

By using the above expression we can now rewrite Eq. (4.43) in the form

$$\begin{aligned} \varepsilon_{00}^{-1}(q,\omega) &= 1+v(q)P_{00}(q,\omega) \\ &= \frac{1}{1-v(q)\bar{P}_{00}(q,\omega)} \end{aligned} \tag{4.44}$$

By the definition of the macroscopic dielectric function via the G = G' = 0 element of the inverse of the dielectric matrix, we finally obtain

$$\varepsilon_M(q,\omega) = 1-v(q)\bar{P}_{00}(q,\omega) \tag{4.45}$$

Chapter 5

Study of the Optical Properties of Solids by using Full Potential Linear Augmented Plane Wave (FP-LAPW) method.

We have used the FP-LAPW method within the framework of density functional theory (DFT) (Hohenberg *et al*.,1964) as implemented in the WIEN2k code (Blaha *et al*., 2008) for relativistic computation of electronic structure, the density of state (DOS) and optical properties for berrylium chalcogenides (BeS, BeSe and BeTe), lead chalcogenides (PbS, PbSe, and PbTe), zinc chalcogenides (ZnS,ZnSe,and ZnTe) and stibiotantalite. We will be using Eqn. (4.29) of chapter 4 to find the imaginary part of the dielectric function ε_2 for all three types of chalcogenides and ferroelectric material stibiotantalite. The exchange-correlation potential was calculated with generalized gradient approximation (GGA) based on Perdew *et al.,* (1996). Kohn-Sham wave functions (Kohn *et al*., 1965) were expanded in terms of spherical harmonic functions inside the non-overlapping muffin-tin spheres surrounding the atomic sites and in Fourier series in the interstitial region. We use $R_{MT} \times K_{max} = 7$ to determine the matrix size, where K_{max} is the plane-wave cut off and R_{MT} is the muffin tin sphere radii. In the atomic region, the basis set consists of spherical harmonics with angular quantum number $l = 10$ and a non spherical contribution with $l = 4$. The self-consistent iterations are considered to be converged when the total energy of the system are stable within 10^{-3} mRy.

5.1 Beryllium Chalcogenides:

The beryllium chalcogenides crystallize in the zinc-blende structure at ambient pressure and temperature. Recently, the electronic and physical properties of BeS, BeSe and BeTe compounds have been studied. For example, the lattice parameters of beryllium chalcogenides were initially measured by Zachariasen (1922). Yim *et al*., (1972) have confirmed the crystalline structure to be zinc-blende. Stukel (1970) and Sarkar *et al*., (1977) have studied the energy bands of beryllium chalcogenides using the first principle self-consistent orthogonalized-plane wave (OPW) and the augmented-plane wave (APW) methods. Kalpana *et al*., (1998) have also studied these systems theoretically by using the tight-binding linear muffin-tin orbital method (TB-LMTO). The electronic band structures of Be chalcogenides were also studied by Waag *et al*., (1996) with first principle self consistent orthogonalized-plane wave (OPW) and the augmented–plane wave (APW) methods. Hassan *et al.,* (2006) have performed the theoretical investigation of the ground state properties and the structural phase transition by using the FP-LAPW method within DFT to confirm the indirect band gap occurring between Γ and X for BeS and BeSe. First principle electronic structure calculations were also performed by Heciri *et al*., (2007) using full potential augmented plane wave plus local orbitals (APW+lo) within DFT for BeS, BeSe and BeTe to compare the results obtained from GGA with those from conventional local density approximation (LDA) exchange-correlation energy functional (Perdew *et al.,*1996). High pressure phase transitions in these compounds were also studied by Berghout *et al*., (2006) using FP-LAPW and the plane wave pseudopotential (PPsPW) methods, to show the existence of wide indirect band gaps for these compounds in their band structures and DOS.

5.1.1 Computational methods

The electronic configurations of elements in beryllium chalcogenides are Be : [He] $2s^2$; S : [Ne] $3s^2$ $3p^4$; Se : [Ar] $3d^{10}$ $4s^2$ $4p^4$ and Te : [Kr] $4d^{10}$ $5s^2$ $5p^4$ The *l*-expansion of the wave function were carried out up to l_{max} = 10 inside the muffin-tin spheres of radius R_{MT}. The wave functions in the interstitial region were expanded in the plane waves with a cut-off of $K_{max} = 7/R_{MT}$ in order to achieve energy eigen values convergence. The R_{MT} values used were 1.8 a.u. for Be, while for S, Se and Te 2.0 a.u, 2.2 a.u and 2.4 a.u were used respectively. The berrylium chalcogenides BeS, BeSe and BeTe crystallize in the zinc-blende structure at ambient pressure and temperature with lattice parameter 4.870Å for BeS, 5.137 Å for BeSe and 5.617 Å for BeTe. A mesh point of 5000 k-points were used to obtain 111 special *k*-points in the irreducible wedge of the Brilloiun zone for BeS, BeSe, BeTe. Both the muffin-tin radius and number of *k*-points were varied to ensure total energy convergence.

The components of the imaginary or the absorptive part of the dielectric function, $\varepsilon^{ij}_2(\omega)$ was calculated. The real part $\varepsilon_1(\omega)$ can be obtained from the imaginary part $\varepsilon_2(\omega)$ by using the Kramers-Kronig dispersion relation.

5.1.2 Results and discussions

The total densities of states for all the three compounds are shown in Fig. 5.1a, 5.1b, 5.1c. From the total density of states, we observe energy gap at around 0 eV which is taken as Fermi energy level. The partial densities of states are shown in Fig. 5.2. It is seen that just below the Fermi level, the bands are dominated by chalcogen p states, with some contribution coming from the Be-2s states. In the region above the Fermi level, p states also dominate. From the partial state densities, it is clear that the main bonding mechanism in beryllium chalcogenides is the hybridization between the Be-2s states and

chalcogen p states. The bond is strongly covalent and partially ionic in character, covalent since the Be-2s states and chalcogen p states are strongly hybridized and degenerate over a large part of their extension, and ionic since the relative amount of Be-2s states and chalcogen p states is different above and below Fermi level. Below the Fermi level, the chalcogen p states dominate and above Fermi level, the Be-2s states strongly hybridized with the chalcogen s, p and d states. From simple argumentation using the relative electro-negativity of the chalcogen and beryllium, we expect that BeS should be the most ionic and BeTe the most covalent of the three systems since (according to Pauling) S, Se and Te have electro-negativities 2.5, 2.4, and 2.1 respectively. This conclusion compares well with what we expect from Fig.5.2. The calculated band structures along symmetry lines L, Γ, X, W, are displayed in Fig. 5.3a, 5.3b and 5.3c.

5.1.3 Band structures

In Fig. 5.3a, 5.3b, and 5.3c., we show the plots of energy bands in the case of BeS, BeSe and BeTe. It is seen that BeS, BeSe and BeTe have indirect band gap of 3.1eV, 2.6 eV and 1.9 eV respectively from Γ to X along Δ-direction. The highest valence bands are observed at 0 eV which is taken as Fermi energy level at Γ symmetry point. These bands are due to the p-state electrons of chalcogen atoms as seen from the partial density of states in Fig. 5.2. The lowest conduction bands observed at 3 eV, 2.6 eV, and 2 eV lies at symmetry point X which are due to the contributions from both the beryllium s states and chalcogen s, p and d states. The calculated band-gaps for the compounds under study have been tabulated with the experimental and theoretical results provided by others in table 5.1.

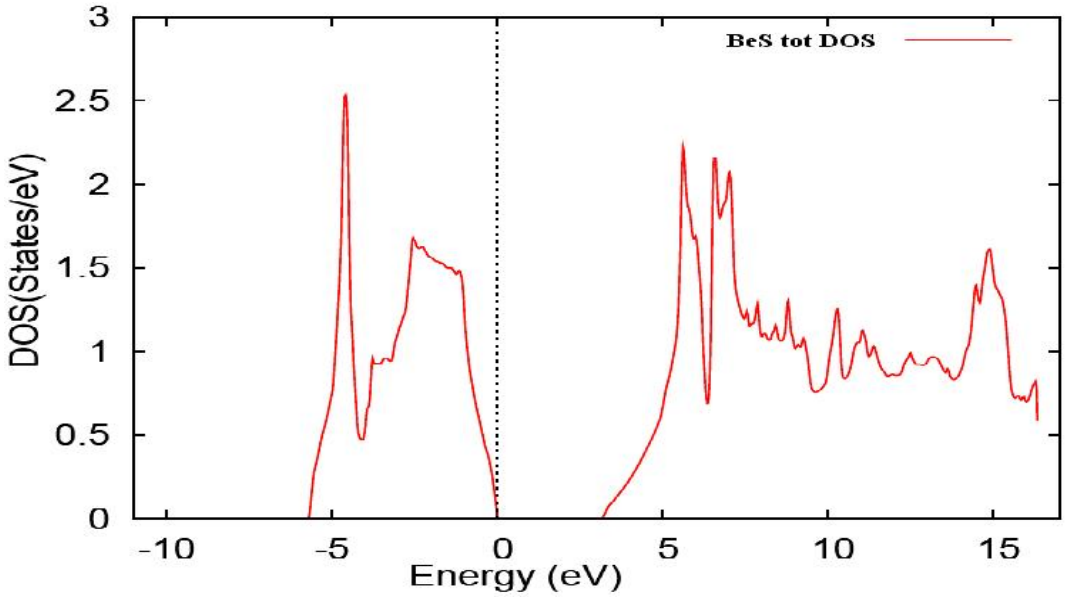

Fig. 5.1a. Total DOS for BeS. The vertical dotted line at E = 0 eV indicates the Fermi energy level.

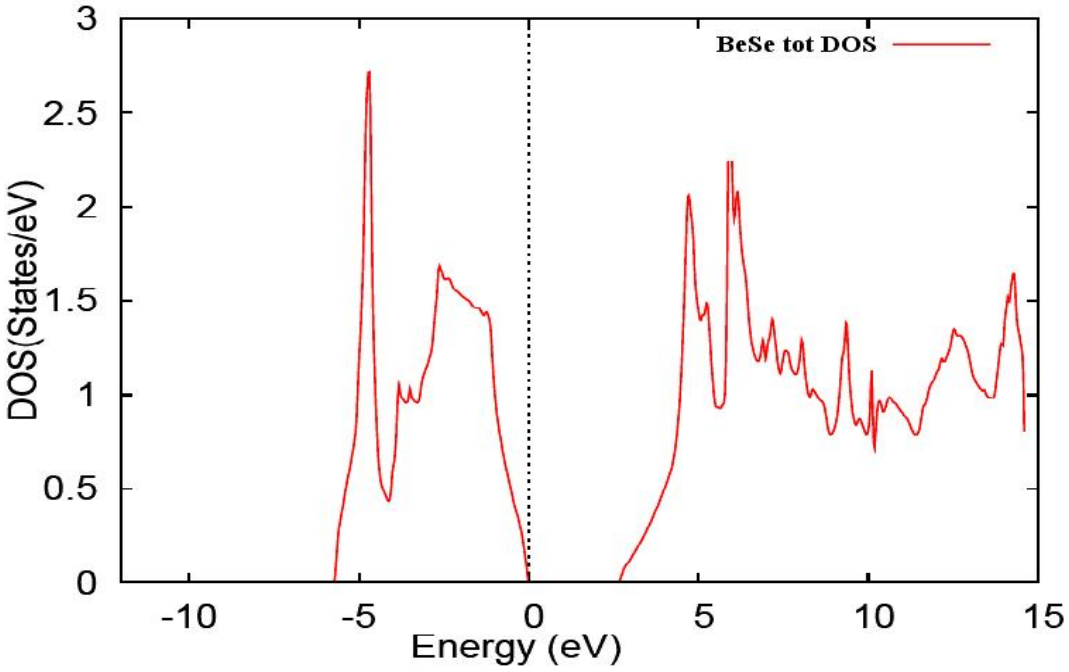

Fig. 5.1b. Total DOS for BeSe. The vertical dotted line at E = 0 eV indicates the Fermi energy level.

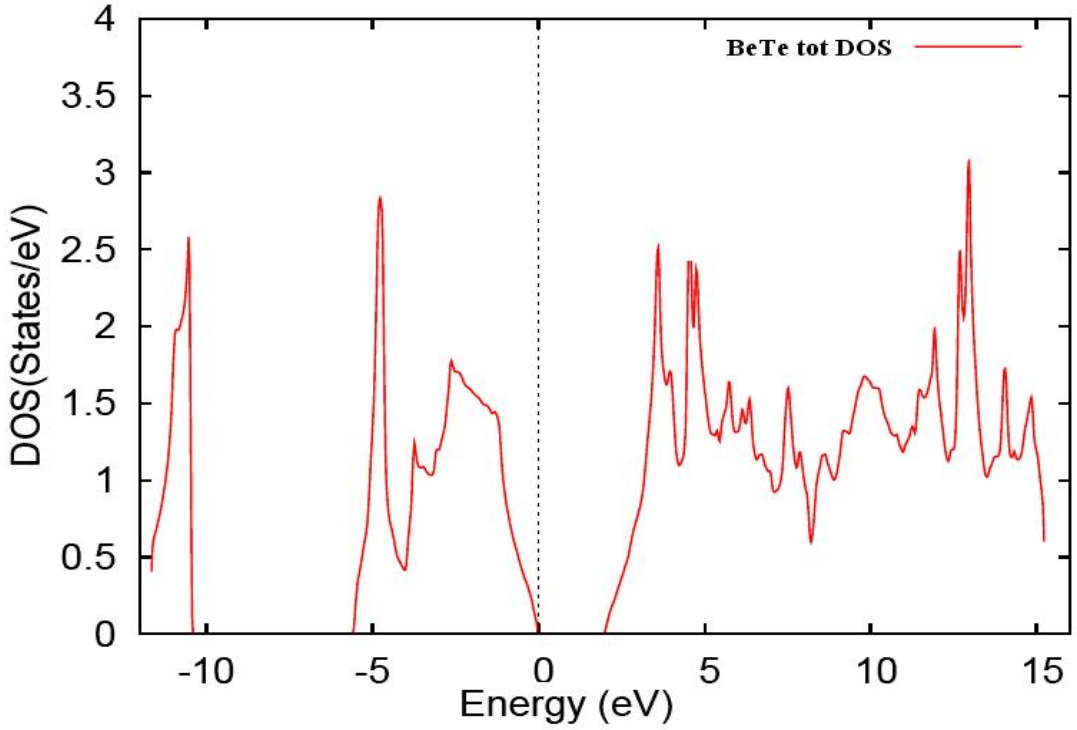

Fig. 5.1c. Total DOS for BeTe. The vertical dotted line at E = 0 eV indicates the Fermi energy level.

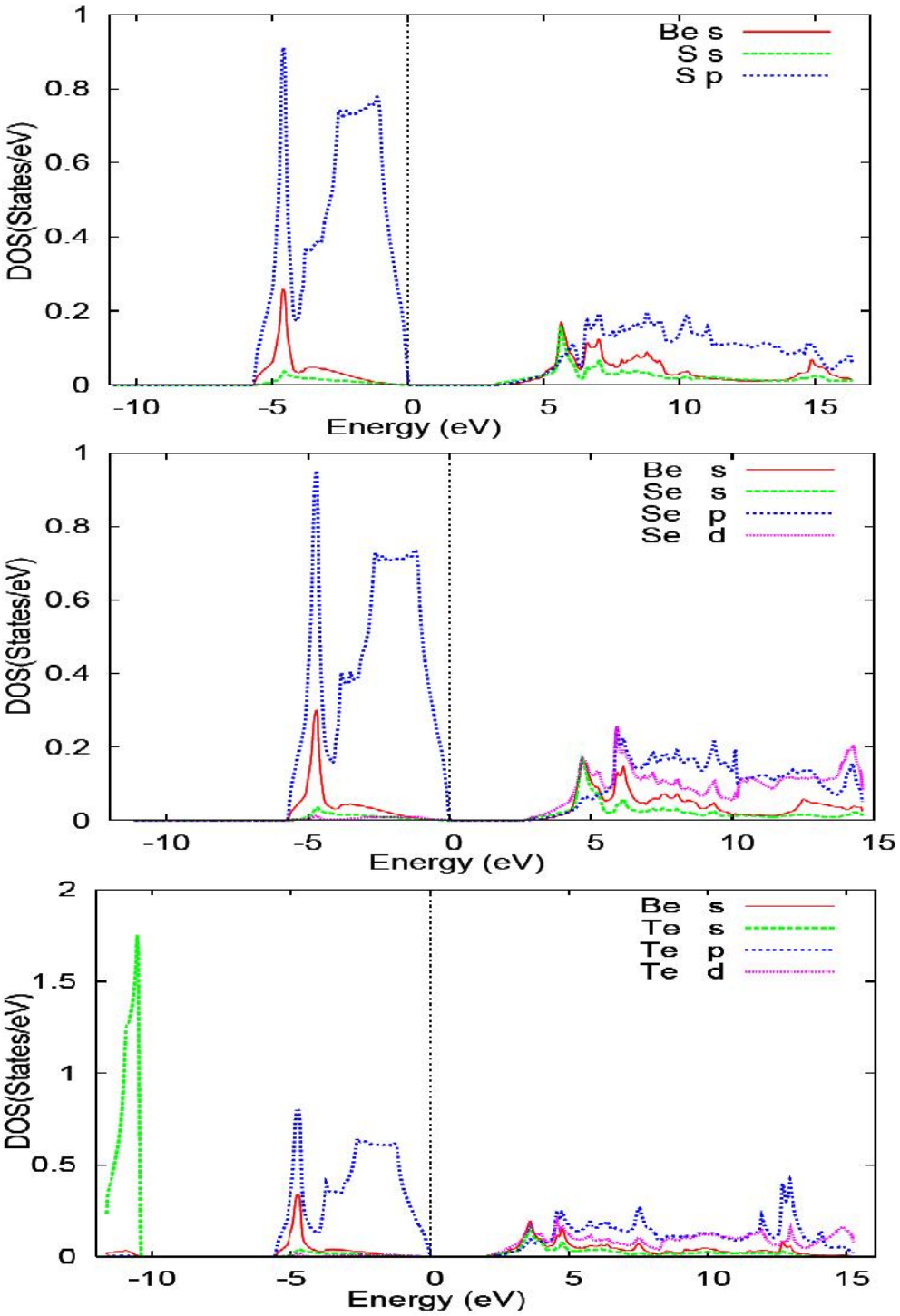

Fig. 5.2. Partial DOS for BeS, BeSe, and BeTe. The vertical dotted line at E = 0 eV indicates the Fermi energy level.

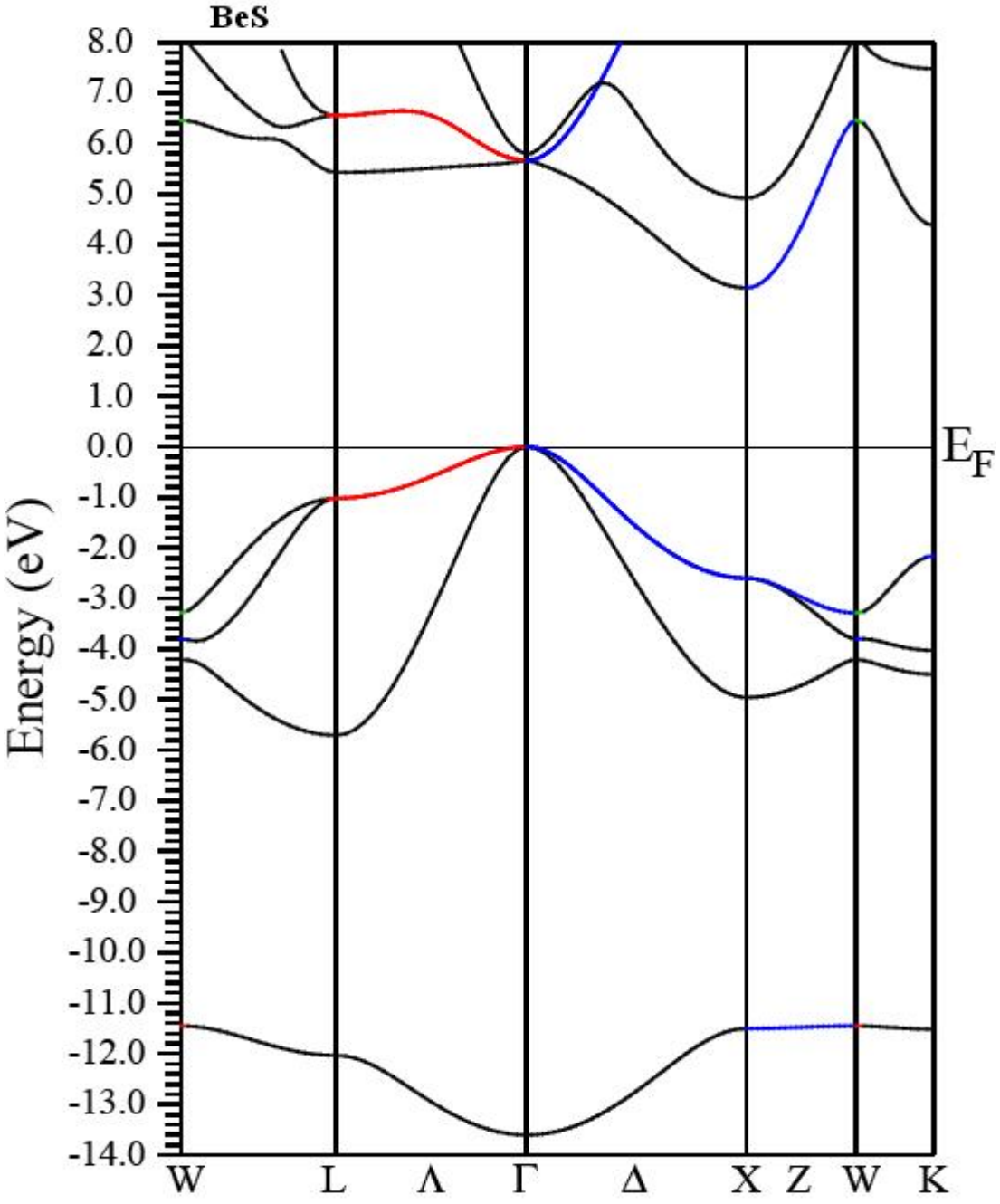

Fig. 5.3a. Energy band structure for BeS along the high symmetry directions.

E_F = 0 eV corresponds to the Fermi level.

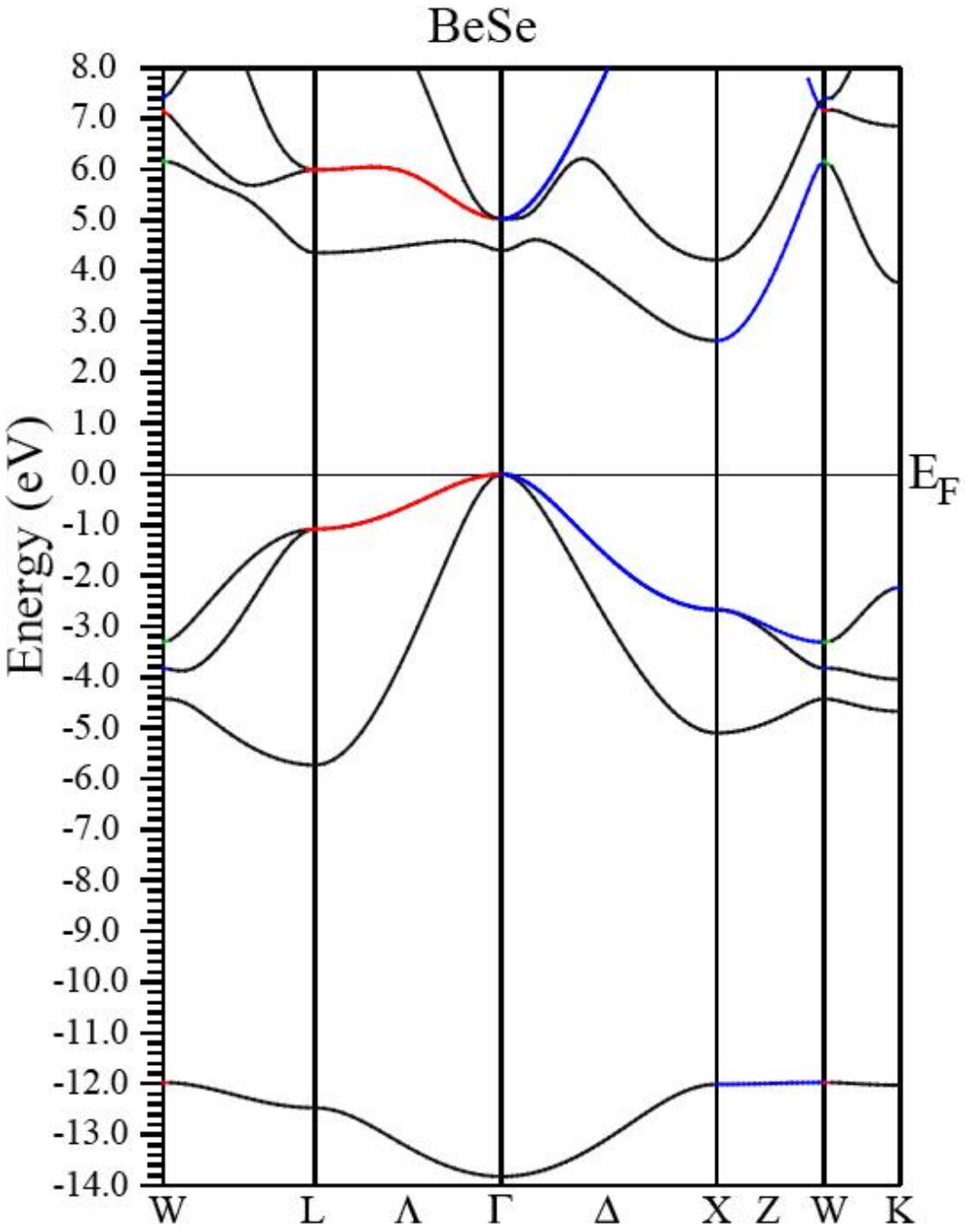

Fig. 5.3b. Energy band structure for BeSe along the high symmetry directions.

E_F = 0 eV corresponds to the Fermi level.

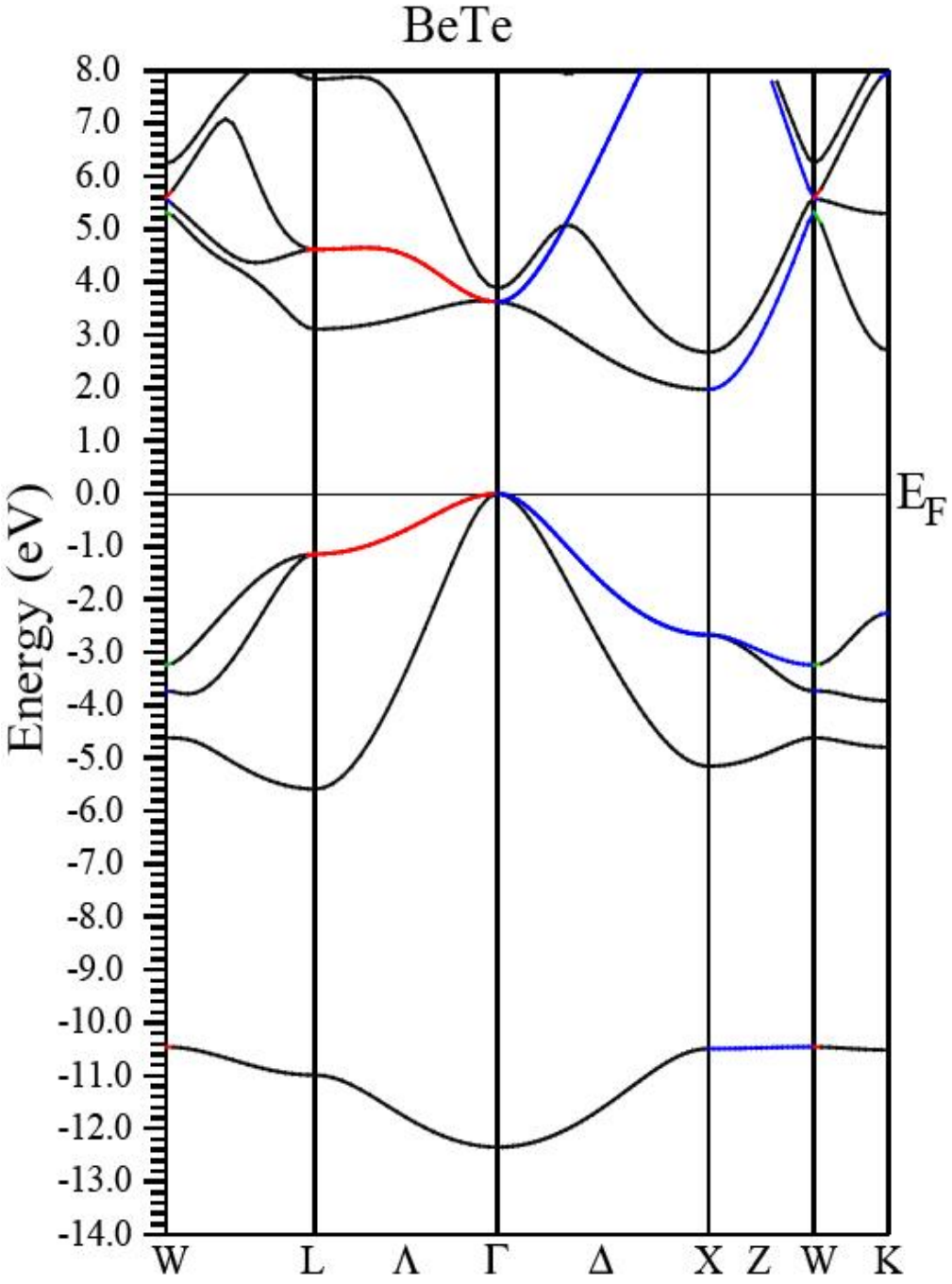

Fig. 5.3c. Energy band structure for BeTe along the high symmetry directions.

E_F = 0 eV corresponds to the Fermi level.

Table 5.1: Calculated indirect (Γ- X) energy band gap values using GGA under FP-LAPW and the results of the experimental and theoretical band gaps using various techniques for BeS, BeSe and BeTe.

Systems study	Expt. Band gaps (Γ-X) (eV)	Theoretical Band gaps (Γ-X) (eV)	Our Calculated Band-gap (Γ- X) (eV)
BeS	>5.5eV	2.75 eV	3.1 eV
BeSe	4-4.5eV	2.31 eV	2.6 eV
BeTe	2.7 eV	1.6 eV	2.6 eV

The experimental band gaps are taken from Zachariasen (1922), the theoretical band gap for BeS is taken from Luo *et al*., (1995); BeSe and BeTe are taken from Fleszar *et al.*, (2000).

5.1.4 Optical properties

The absorptive part of the dielectric function $\varepsilon_2(\omega)$ is shown in Fig.5.4a., 5.4b., 5.4c. The trends in $\varepsilon_2(\omega)$ may be linked to the trends observed in the DOS and band structures From the partial state densities in Fig. 5.2, it is obvious that the p states play a major role in these optical transitions, both as initial and final states. Of the s states, the Be state primarily serves as initial state, whereas the chalcogen states are mostly final state. The beryllium and chalcogen s, p and d states are primarily final states. Optical transitions between bands that are parallel or nearly so in the Brillouin Zone tend to result in peaks in the optical spectrum. Fig. 5.4a, 5.4b, 5.4c displays the imaginary (absorptive) part of the dielectric function $\varepsilon_2(\omega)$ for BeX. Our analysis of the $\varepsilon_2(\omega)$ curves show that the first critical points of the dielectric function occurs at 5.6 eV, 4.5 eV and 3.5 eV. These critical points are followed by the main peaks in the spectra situated at 6.8 eV in BeS, 6.2 eV in BeSe and 5.1 eV in BeTe related to direct transition. These

peaks are primarily due to transition between valence band and conduction band above the Fermi energy along symmetry lines L, Γ, X, W. As there should be one-to-one correspondence between band structure and optical spectrum, we first look at the imaginary part of the dielectric function $\varepsilon_2(\omega)$. For BeS, BeSe and BeTe the energy peak at 6.8 eV, 6.2 eV and 5.1 eV in the $\varepsilon_2(\omega)$ arises from the interband transition between the maximum of valence band at Γ - edge and the bottom most conduction band at *W* - edge. These main peaks are followed by sharp energy peak at 7.5 eV, 7.1 eV, and 5.7eV for BeS, BeSe and BeTe due to the interband transition from the highest valence band -1.0 eV and the second lowest conduction band at L - edge. Our optical calculation shows that transitions between highest lying valence band (HVB) and lowest lying conduction band (LCB) account for almost all structures in optical spectra at energy below 6 eV.

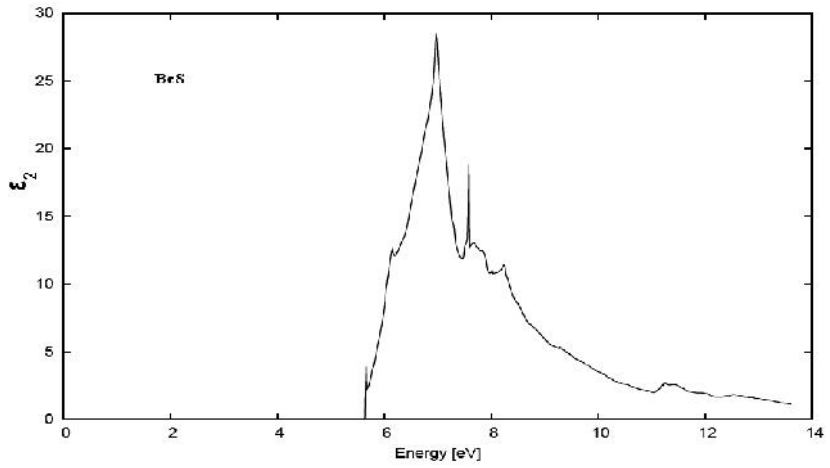

Fig. 5.4a. Imaginary or absorptive part of dielectric function for BeS.

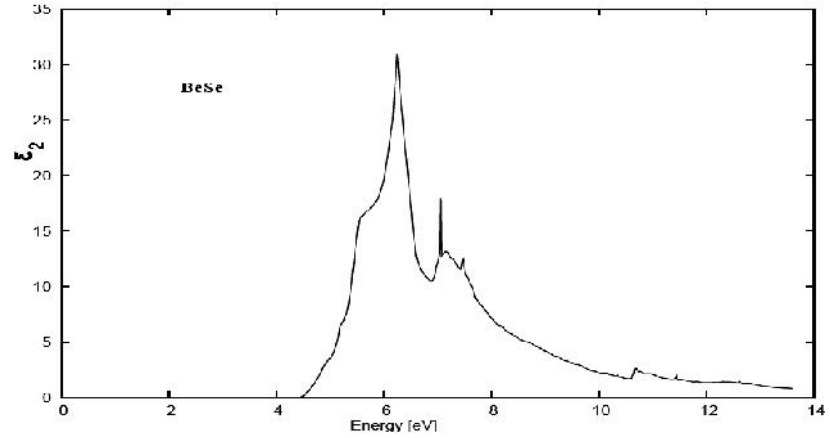

Fig. 5.4b. Imaginary or absorptive part of dielectric function for BeSe.

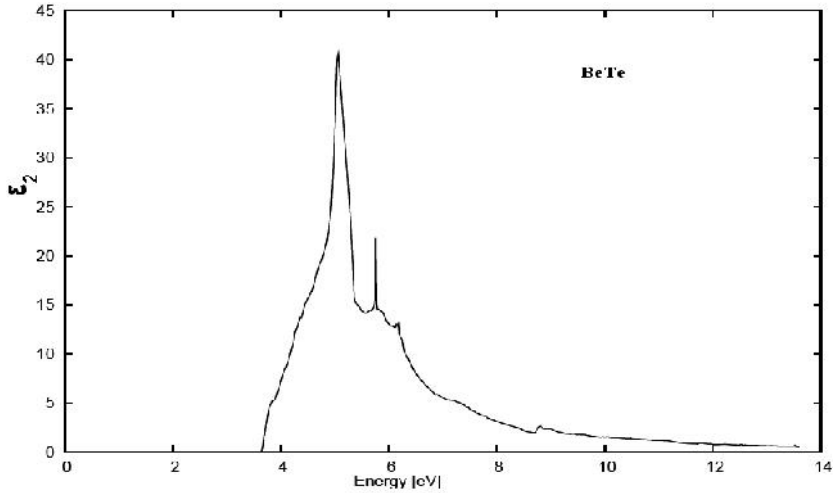

Fig. 5.4c. Imaginary or absorptive part of dielectric function for BeTe.

5.2 Lead chalcogenides:

5.2.1 Calculational method

A lead salt is stable in rock-salt structure and have direct minimum energy band gap at the L symmetry point in the Brillouin Zone (BZ). For our calculation, we used lattice parameters a = 5.54 Å, 6.13 Å, and 6.5Å for PbS, PbSe, and PbTe respectively, which was found out from volume optimization with the optimized wave vector k = 4000 and atomic sphere radii 2.5 Å for Pb, 2.4 Å, 2.4 Å and 2.6 Å respectively for S, Se and Te.

5.2.2 Results and discussions

The total density of states for PbX are shown in Fig.5.5a, 5.5b, 5.5c. From the total density of states, we observe a small energy gap at around 0 eV which is taken as Fermi energy level. The partial densities of states are shown in Fig. 5.6. It is seen that just below the Fermi level, the bands are dominated by chalcogen p states, with some contribution coming from the Pb-6p states. In the region above the Fermi level, p states also dominate. From the partial state densities, it is clear that the main bonding mechanism in PbTe is the hybridization between the Pb-6p states and chalcogen p states. The bond is both ionic and covalent in character, covalent since the Pb-6p states and chalcogen p states are strongly hybridized and degenerate over a large part of their extension, and ionic since the relative amount of Pb-6p states and chalcogen p states is different above and below Fermi level. Below the Fermi level, the chalcogen p states dominate and above Fermi level, the Pb-6p states dominate. The calculated band structures along symmetry lines L, Γ, X, W, are displayed in Fig. 5.7a, 5.7b, 5.7c. Experimentally, it is well known that PbX have a narrow band gap at the L point. We

also find energy gap of 0.40 eV, 0.24 eV, and 0.60 eV for PbS, PbSe, and PbTe respectively at the L point.

Table 5.2: Our calculated direct (L-L) energy band gap values using GGA under FP-LAPW and the results of the experimental and theoretical band gaps for PbS, PbSe and PbTe.

Systems study	Expt. Band gaps (L-L) (eV)	Theoretical Band gaps (L-L) (eV)	Our Calculated Band-gaps (L-L) (eV)
PbS	0.41	0.069	0.40
PbSe	0.27	0.141	0.24
PbTe	0.31	0.032	0.60

Experimental band gaps are taken from Strehlow *et al*., (1973) and theoretical band gaps are taken from Anna Delin *et al.,* (1997).

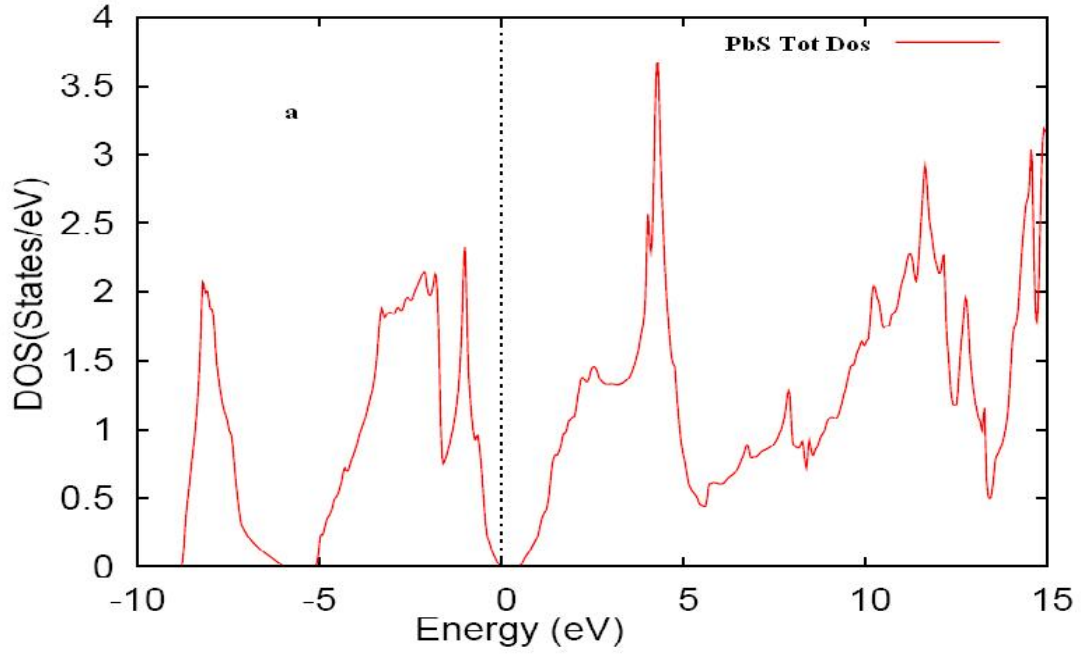

Fig. 5.5a. Total DOS for PbS. The vertical dotted line at E = 0 eV indicates the Fermi energy level.

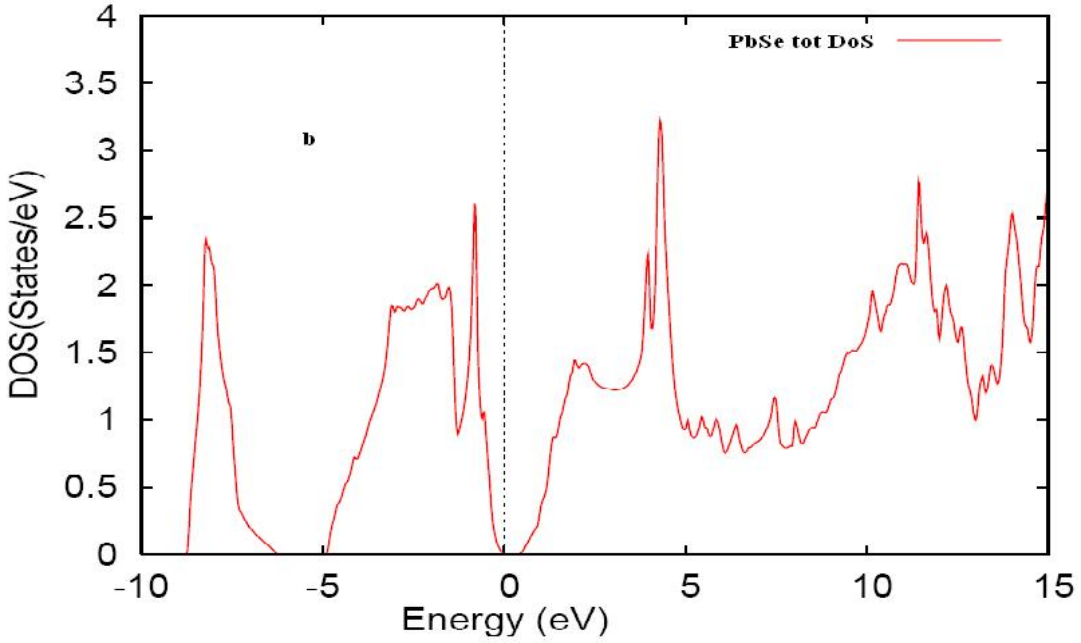

Fig. 5.5b. Total DOS for PbSe. The vertical dotted line at E = 0 eV indicates the Fermi energy level.

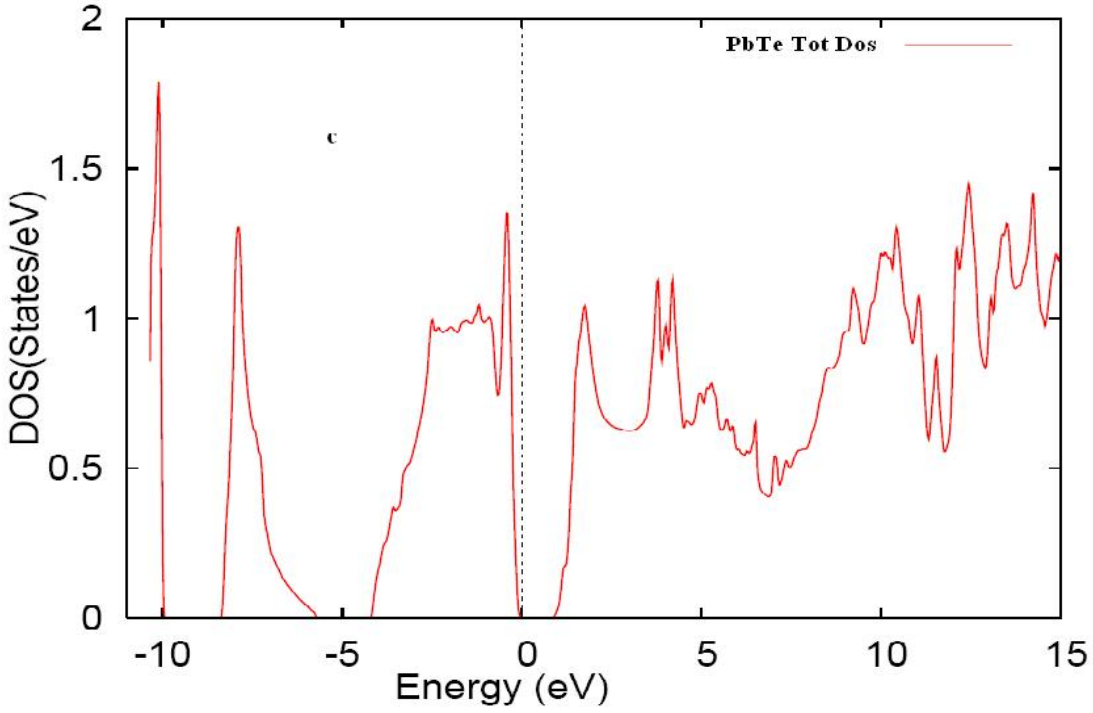

Fig. 5.5c. Total DOS for PbTe. The vertical dotted line at E = 0 eV indicates the Fermi energy level.

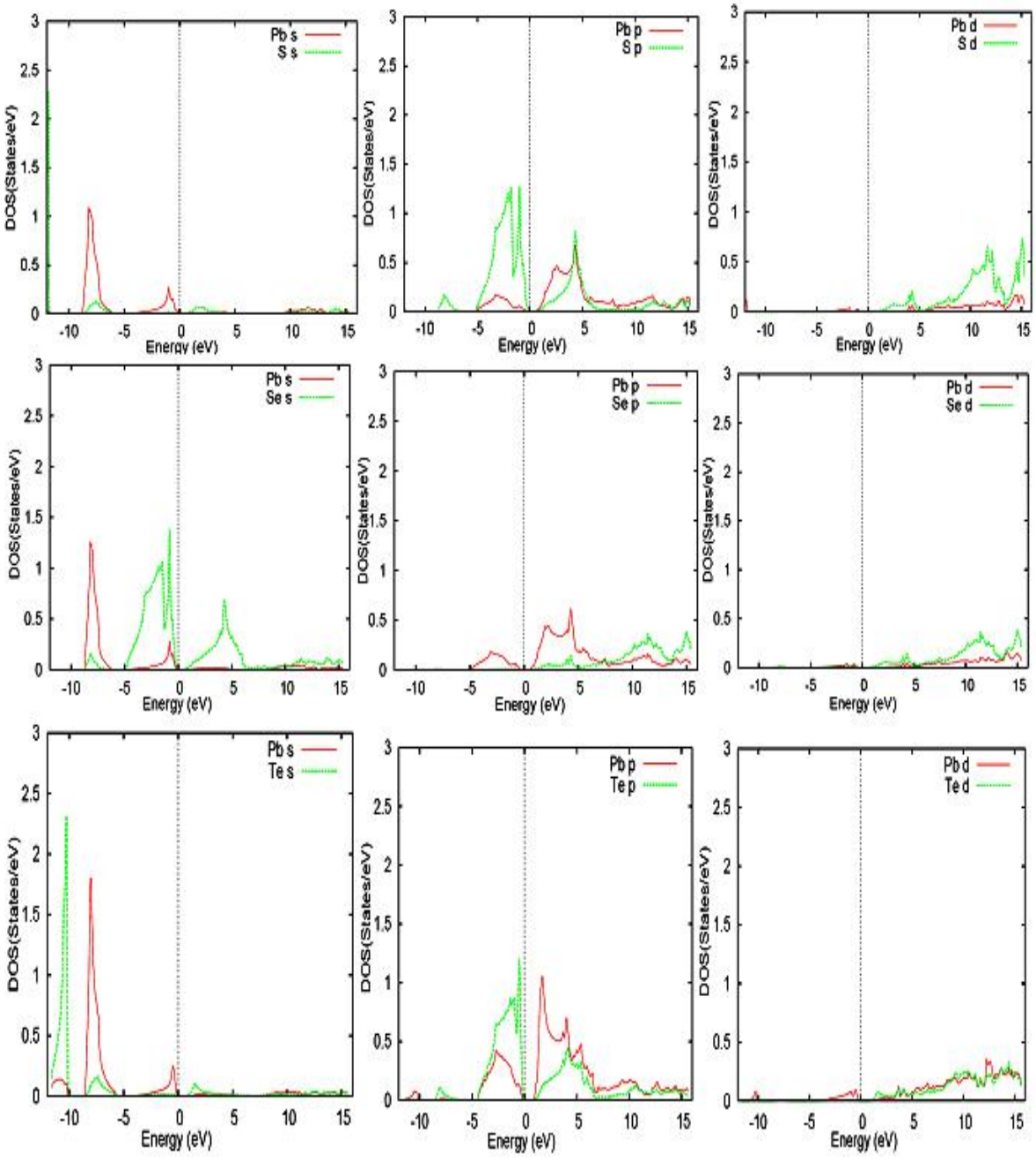

Fig. 5.6. Partial DOS for PbS, PbSe, and PbTe. The vertical dotted line at E = 0 eV indicates the Fermi energy level.

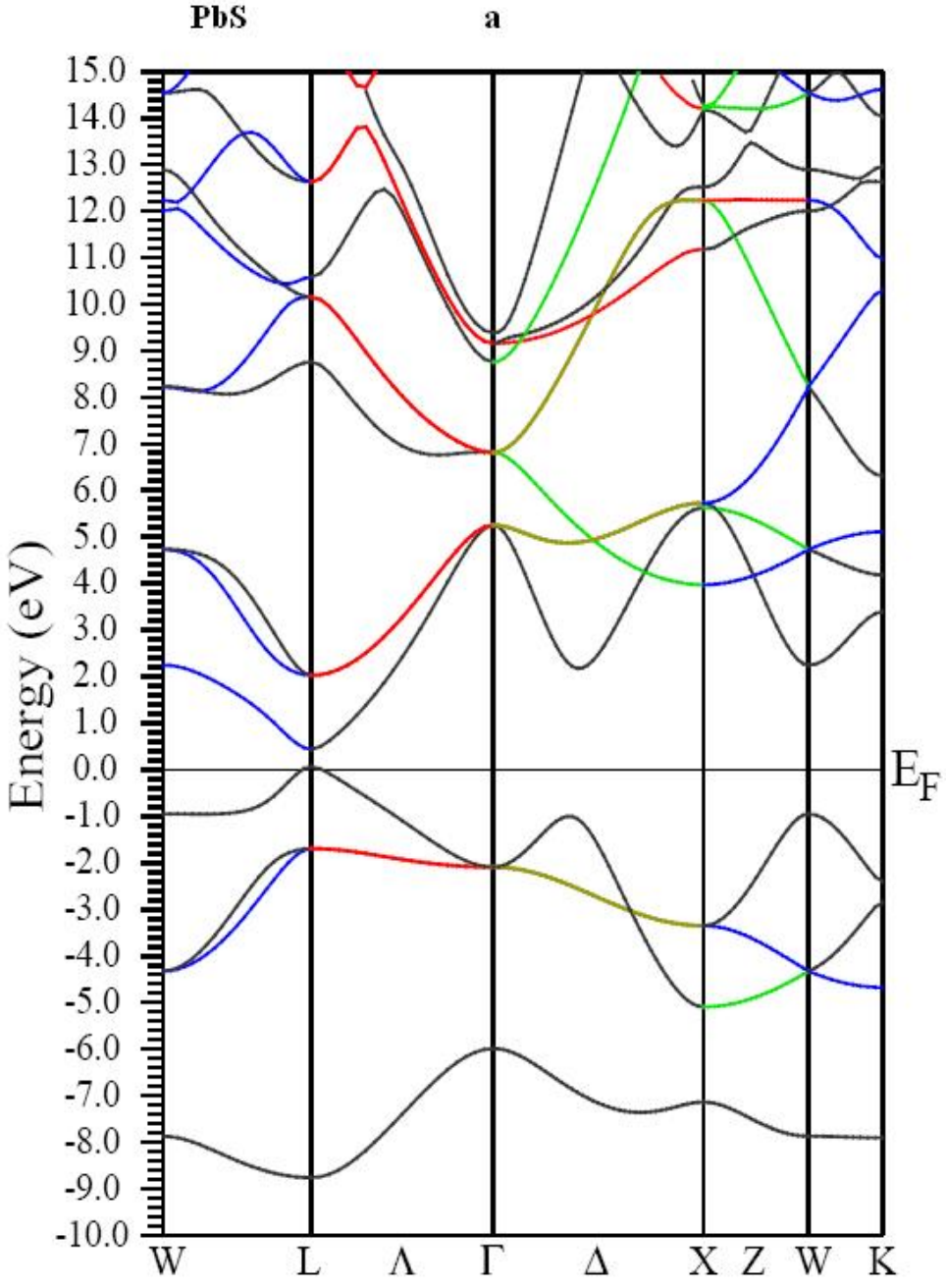

Fig. 5.7a. Energy band structure for PbS along the high symmetry directions. E_F = 0 eV corresponds to the Fermi level.

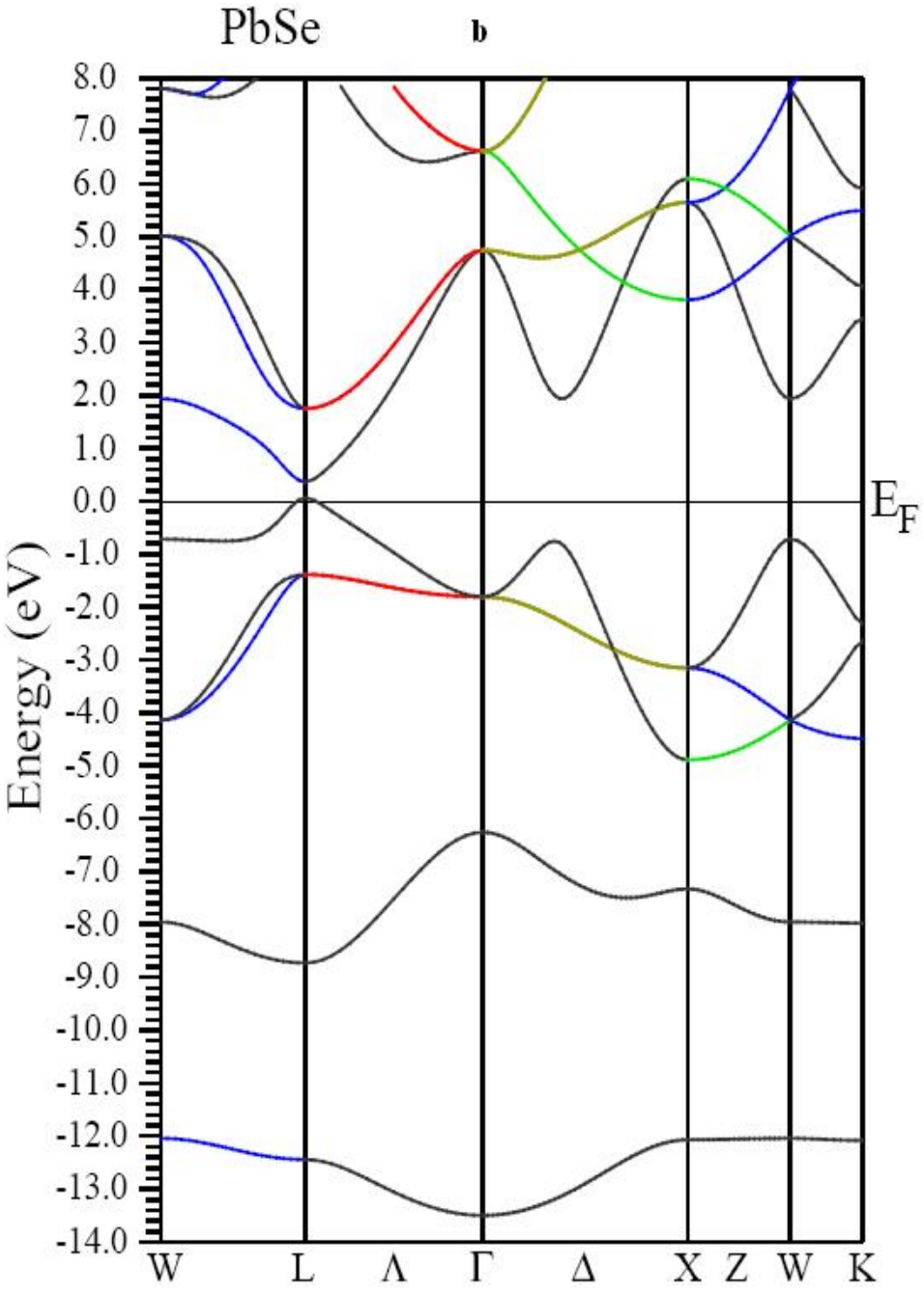

Fig. 5.7b. Energy band structure for PbSe along the high symmetry directions. $E_F = 0$ eV corresponds to the Fermi level.

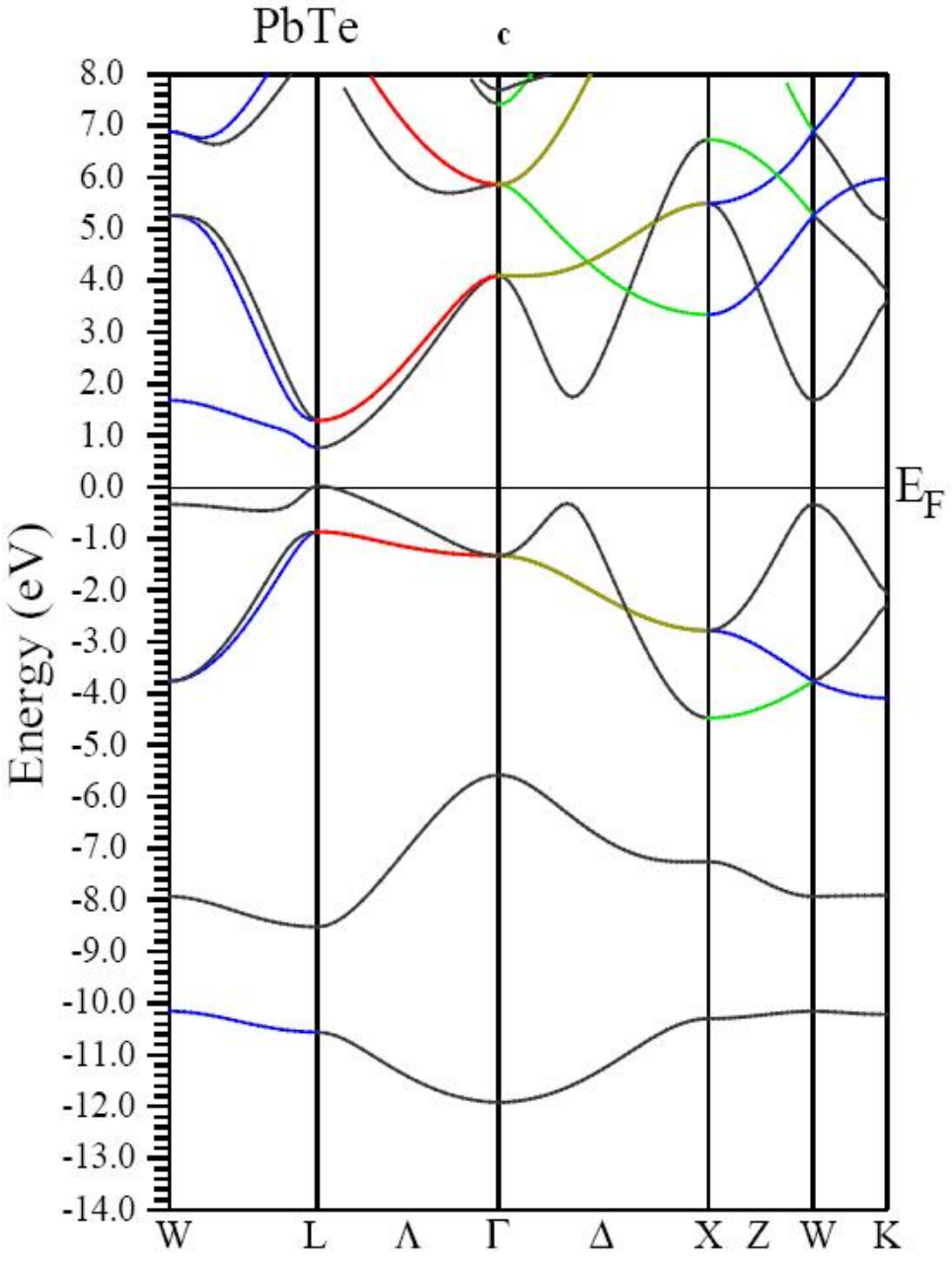

Fig. 5.7c. Energy band structure for PbTe along the high symmetry directions. E_F = 0 eV corresponds to the Fermi level.

5.2.3 Optical properties

The absorptive part of the dielectric function $\varepsilon_2(\omega)$ is shown in Fig. 5.8a, 5.8b and 5.8c. From the partial state densities in Fig. 5.6, it is obvious that the p states play a major role in these optical transitions, both as initial and final states. Of the s states, the Pb state primarily serves as initial state, whereas the chalcogen states are mostly final state. The lead and chalcogen d states are primarily final states. Fig. 5.8, displays the imaginary (absorptive) part of the dielectric function $\varepsilon_2(\omega)$ for PbX. Our analysis of the $\varepsilon_2(\omega)$ curves show that the first critical points of the dielectric function occurs at 0.5 eV, 0.45 eV and 0.8 eV. These critical points are followed by the main peaks in the spectra situated at 3.1 eV in PbS, 2.6 eV in PbSe and 2.2 eV in PbTe related to direct transition. These peaks are primarily due to direct transition between valence band and conduction band above the Fermi energy along symmetry lines L, Γ, X, W. Since the optical spectra are obtained from the interband transitions, the peak structures in Fig. 5.8a, 5.8b and 5.8c can be explained through our band structures Fig.5.7a, 5.7b, 5.7c. For PbS the energy peak at 3.1eV in the $\varepsilon_2(\omega)$ arises from the interband transition between the valence band in -0.9 eV and the bottom most conduction band at W- edge. The sharp energy peak at 2.6 eV for PbSe is due to the interband transition from the highest valence band -0.7 eV to the lowest conduction band at W- edge. The energy peak at 2.2 eV for PbTe is due to the interband transition between the valence band in -0.3 eV and the conduction band in 1.9 eV. The experimental measurement localized the main peaks at 2.5 eV, and 2.0 eV for PbSe and PbTe (Suzuki *et al*., 1994; 1995). In comparison with the experimental data, there is slight energy shift in the main peaks. The dispersive part of the dielectric function $\varepsilon_1(\omega)$ have been obtained by Kramers-Kronig relation. All the features obtained shows satisfactory result with the experimental spectra (Suzuki *et al*., 1995).

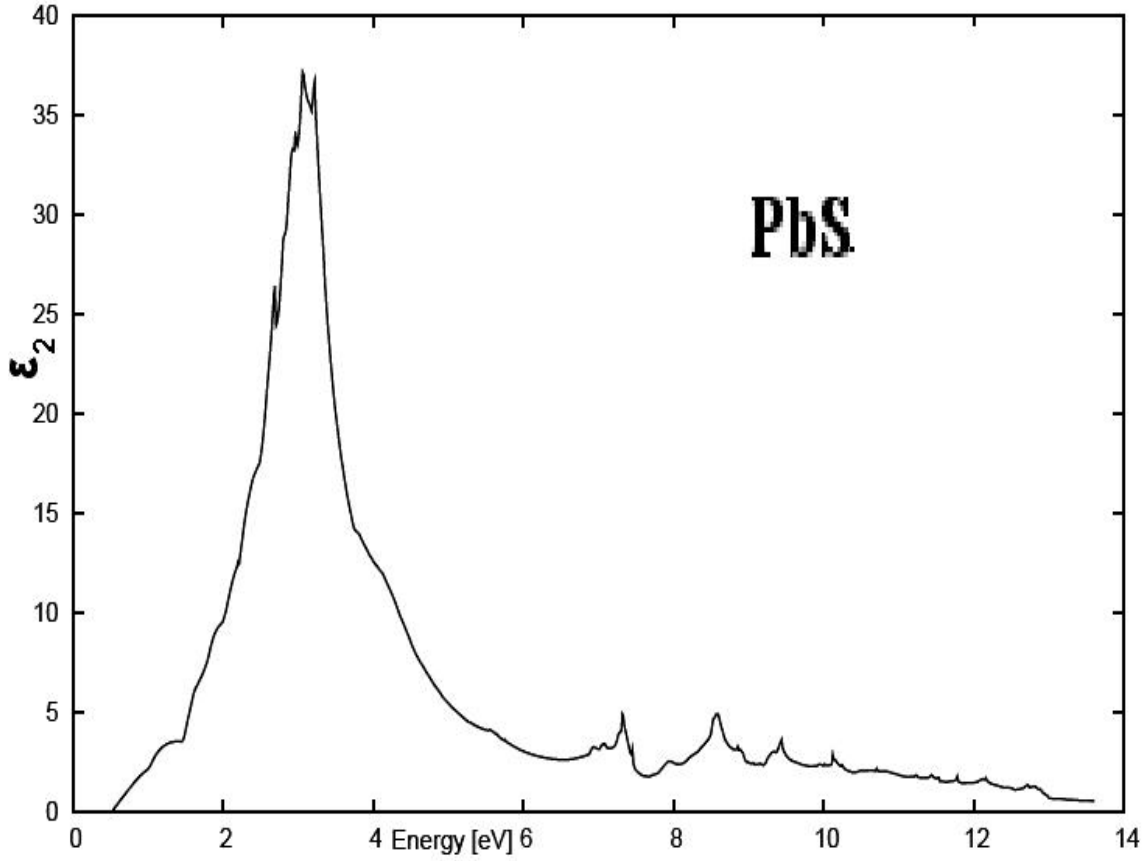

Fig.5.8a. Calculated Imaginary part of dielectric function for PbS.

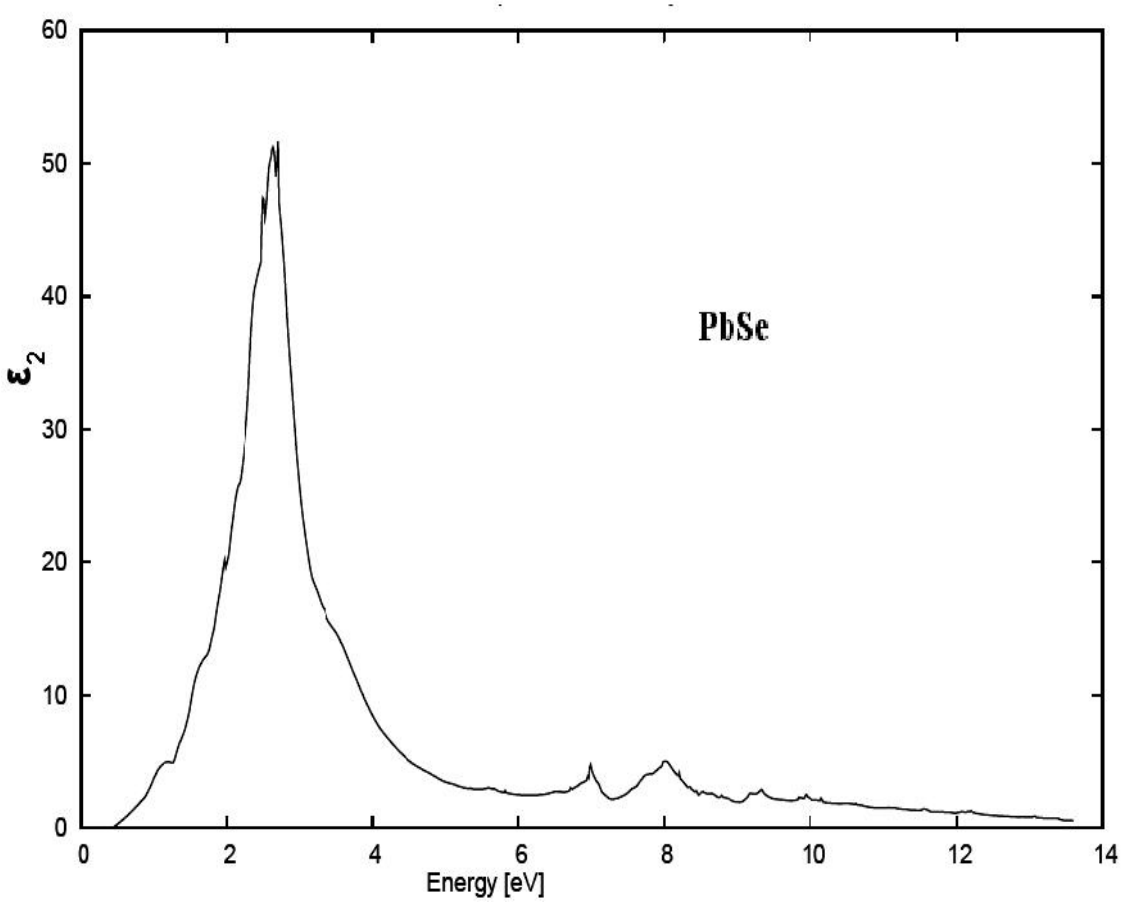

Fig.5.8b. Calculated Imaginary part of dielectric function for PbSe.

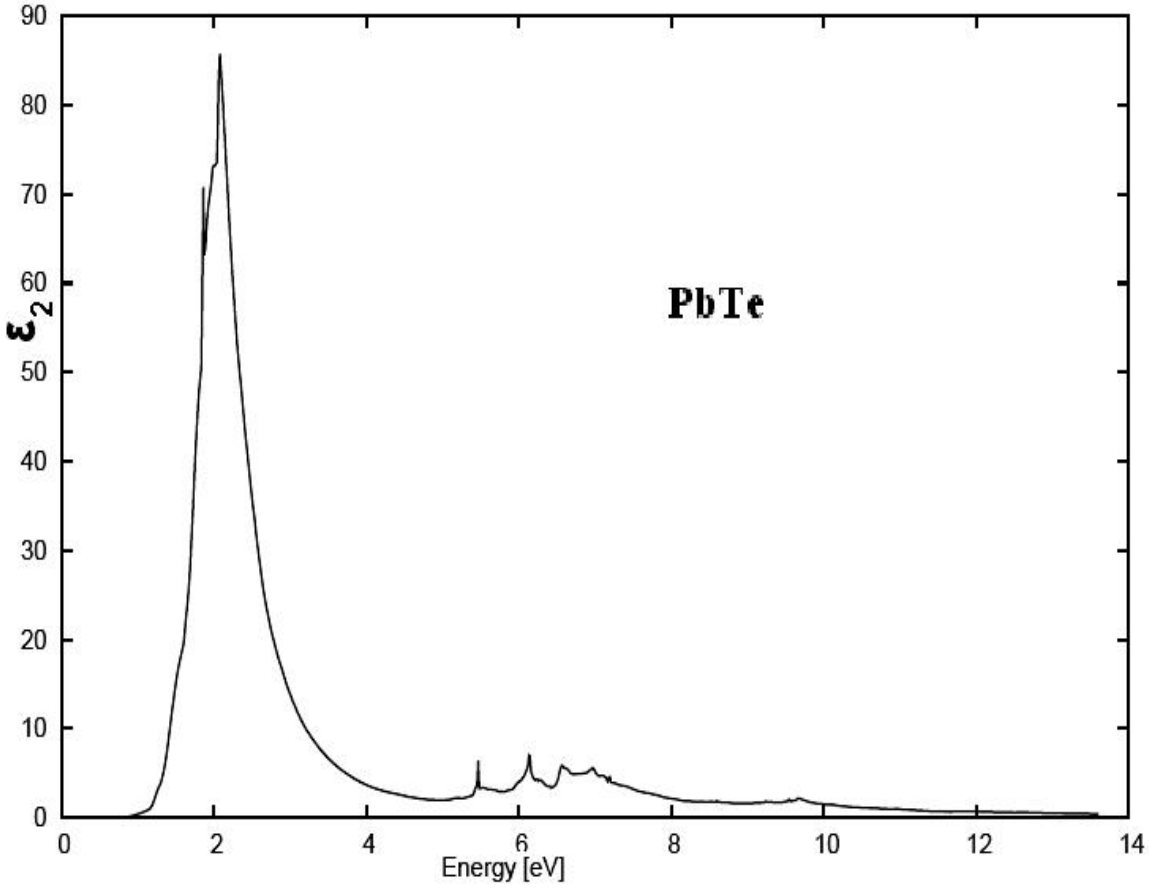

Fig.5.8c. Calculated Imaginary part of dielectric function for PbTe.

5.3 Zinc chalcogenides:

Zinc chalcogenides have been extensively studied experimentally for their intrinsic optical properties (Adachi *et al*., (1991), Kim *et al*., (1993, 1996, 1997), Dahmani *et al*., (1994), Ronnow *et al*., (1999), Samara *et al*., (1983), Walter *et al*., (1970), Ves *et al*., (1990), Wagner *et al.,* (1998), Freeouff (1970)) because of their potential use in device capable for operating at high temperature.

5.3.1. Calculational method:

Zinc chalcogens have direct minimum energy band gap at the Γ symmetry point in the Brillouin Zone (BZ). For our calculation, we used lattice parameters a = 5.13 Å**,** 5.6 Å, and 6.0Å for ZnS, ZnSe, and ZnTe respectively, which was found out from volume optimization with the optimized wave vector k = 5000 and atomic sphere radii 2.20 Å for Zn, 1.8Å, 1.9 Å and 2.2 Å respectively for S, Se and Te. We use $R_{MT} \times K_{max} = 7$ to determine the matrix size, where K_{max} is the plane-wave cut off and R_{MT} is the muffin tin sphere radii. In the atomic region, the basis set consists of spherical harmonics with angular quantum number l = 10 and a non spherical contribution with l = 4. The semiconducting Zinc chalcogenides crystallized in the zinc-blende structure. The space group is F-43 m. The Zn atom is located at the origin and the X atom is located at (1/4, 1/4, 1/4).

5.3.2. Results and discussions

The calculated total density of states, the partial density of states and band structures for zinc chalcogenides are shown in Fig. 5.9a, 5.9b, 5.9c, Fig.5.10a, 5.10b, 5.10c. and Fig.5.11a, 5.11b, 5.12c. The valence band maximum (VBM) and conduction band minimum (CBM) are occurs at the Γ point. Thus the energy gap is direct between

the top of the valence band and the bottom of conduction band at Γ point. It is clearly seen that the band gap are on the whole underestimated in comparison with experiments results. This underestimation of the band gaps is mainly due to the fact that the simple form GGA do not take into account the quasiparticle self energy correctly (Rashkeev *et al*., 2001) which make it not sufficiently flexible to accurately reproduce both exchange correlation energy and its charge derivative.

Table 5.3: Our calculated direct (Γ - Γ) energy band gap values using GGA under FP-LAPW and the results of the experimental and theoretical band gaps for ZnS, ZnSe and ZnTe.

Systems study	Expt. Band gaps (Γ - Γ) (eV)	Theoretical Band gaps (Γ - Γ) (eV)	Our Calculated Band-gaps (Γ - Γ) (eV)
ZnS	3.80	2.4	2.8
ZnSe	2.82	1.6	1.4
ZnTe	2.39	1.6	1.4

Experimental band gaps are taken from Huang *et al*., (1993) and theoretical band gaps are taken from Corso *et al*., (1996).

In Fig. 5.9a, 5.9b, 5.9c, we show the density of states DOS for ZnX. It is further observed that the first structure encountered in the total DOS is the structure situated at about 6.20 eV below the zero of energy for ZnS. It consists predominantly of Zn d states with a few contribution of p states of the chalcogen atoms. From the band structure Fig.5.11a, 5.11b, 5.12c, this structure corresponds to the flat bands clustered at —7.09 eV. The near lack of dispersion among some of these bands gives rise to the very narrow nature of the peaks. The structure hump between - 5.50 eV and the zero of the energy in

these compounds which form the upper VB correspond to the chalcogen p states partially mixed with cations s states. Above the Fermi level, the feature in the DOS originate mainly from the s and d states of Zn partially mixed with little of chalcogen p states as seen from Fig.5.10a.

The lowest energy group at around -11eV has mainly chalcogen s states. The second group between -7.0eV and -6.0eV is composed of Zn-d and chalcogen p states. From the partial DOS, we note a strong hybridization between Zn-d states and chalcogen p states.

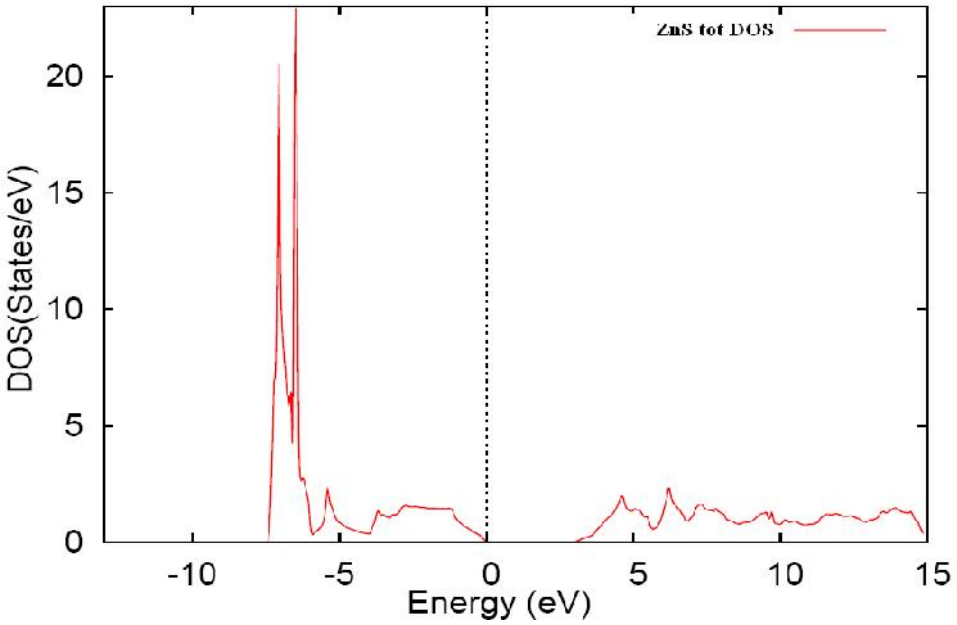

Fig. 5.9a. Total Density of States for ZnS. The vertical dotted line at E = 0 eV indicates the Fermi energy level.

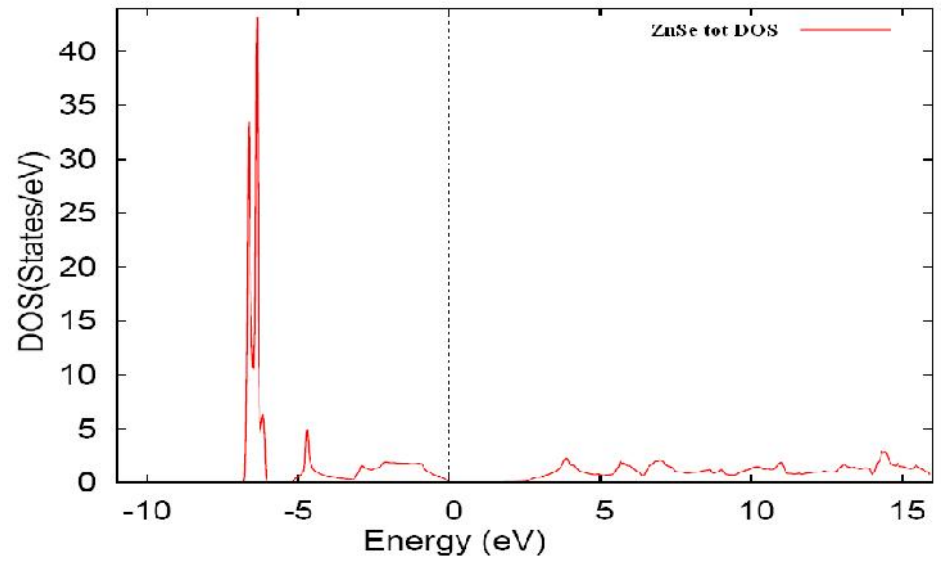

Fig. 5.9b. Total Density of States for ZnSe. The vertical dotted line at E = 0 eV indicates the Fermi energy level.

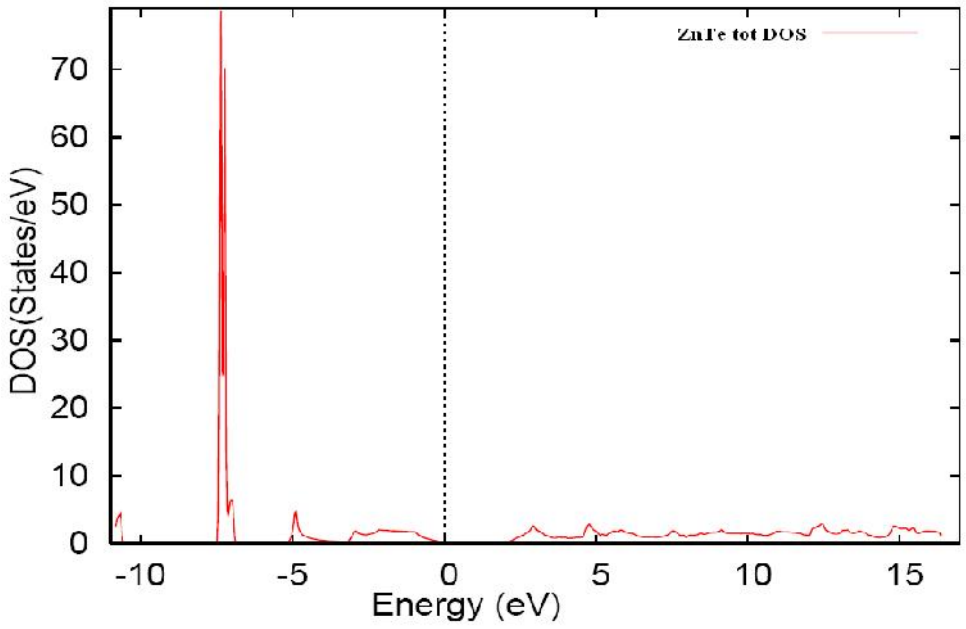

Fig. 5.9c. Total Density of States for ZnTe. The vertical dotted line at E = 0 eV indicates the Fermi energy level.

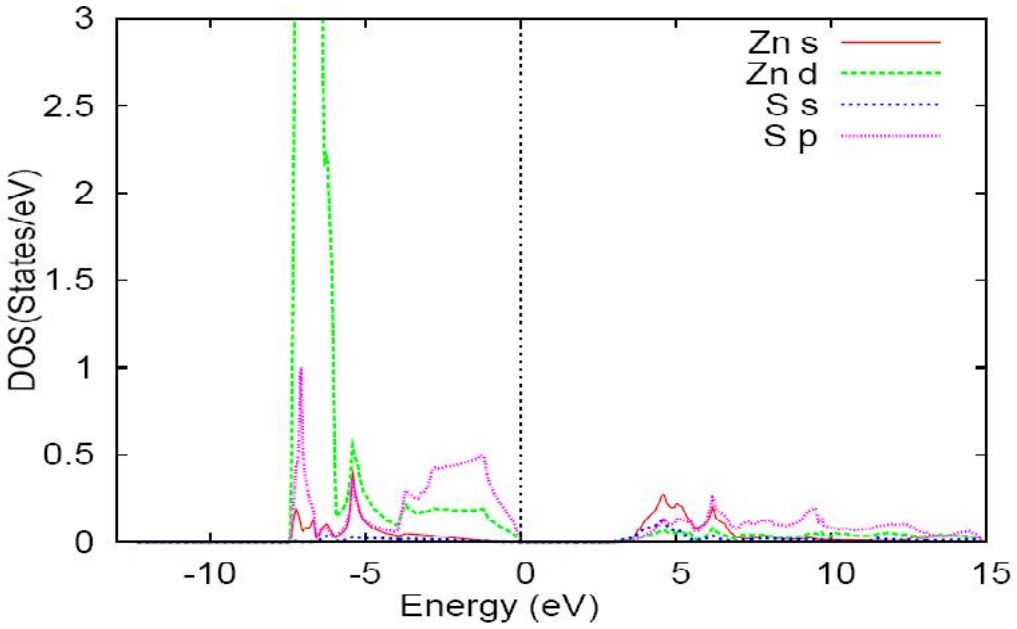

Fig. 5.10a. Partial Density of States for ZnS. The vertical dotted line at E = 0 eV indicates the Fermi energy level.

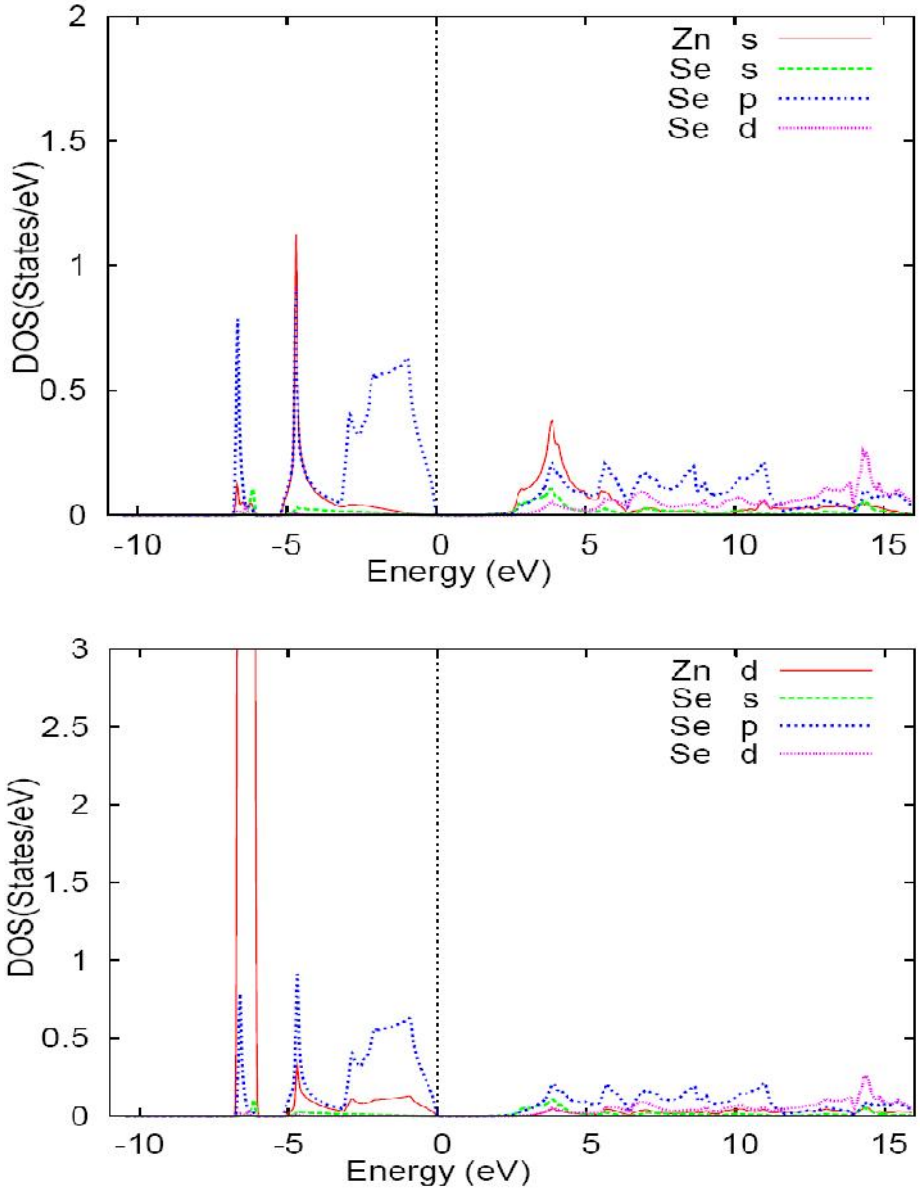

Fig. 5.10b. Partial Density of States for ZnSe. The vertical dotted line at E = 0 eV indicates the Fermi energy level.

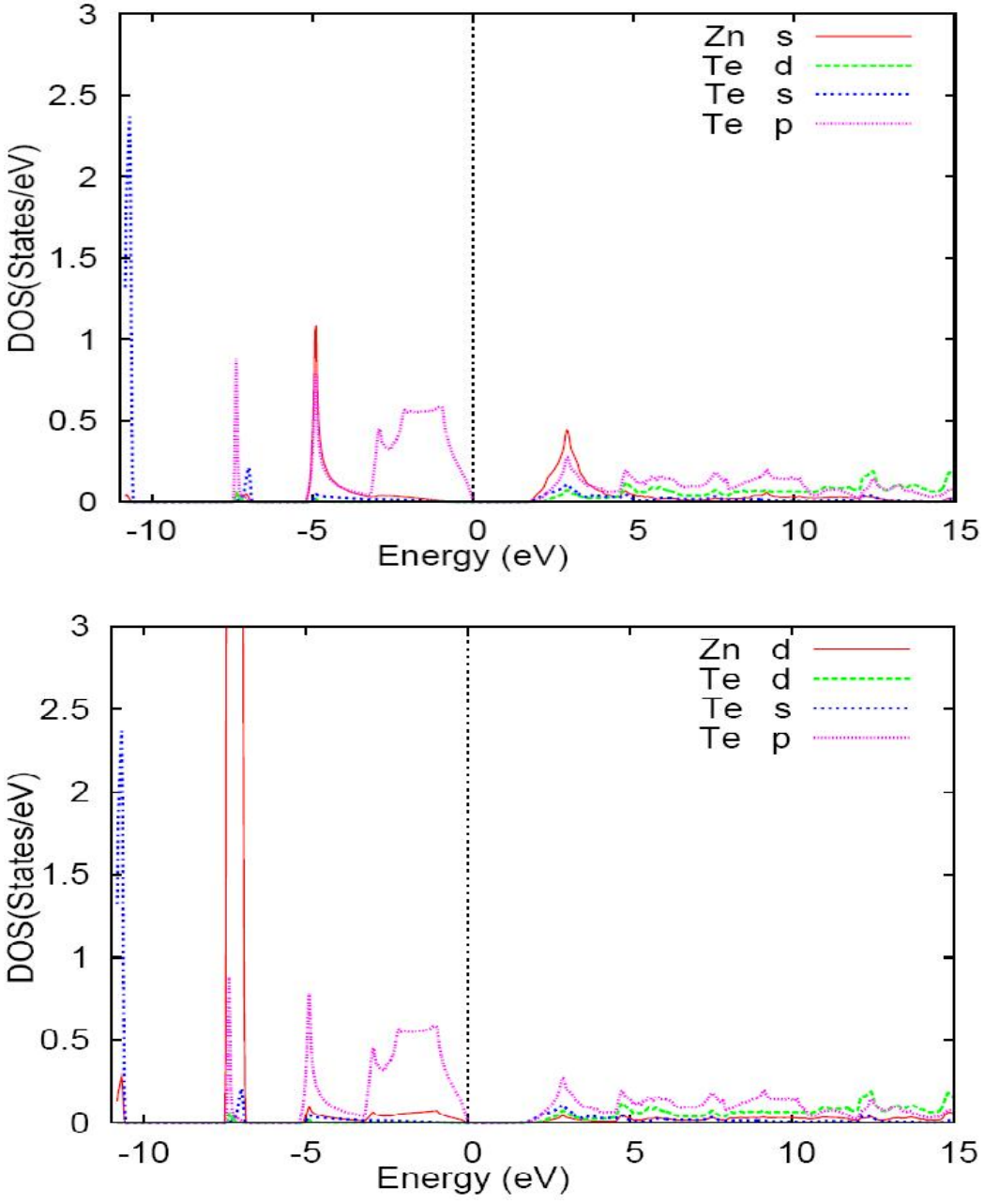

Fig. 5.10c. Partial Density of States for ZnTe. The vertical dotted line at E = 0 eV indicates the Fermi energy level.

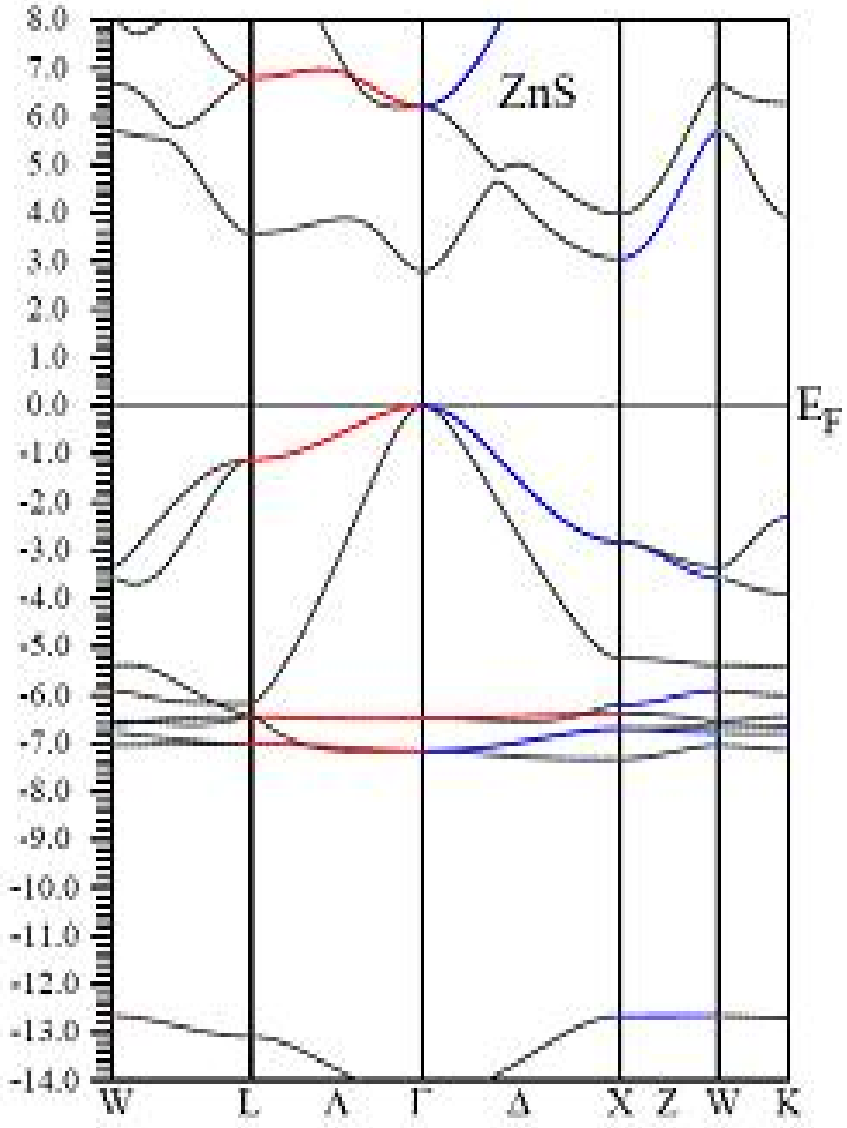

Fig. 5.11a. Energy band structure for ZnS along the high symmetry directions in Brillouin zone. E_F = 0 eV corresponds to the Fermi level.

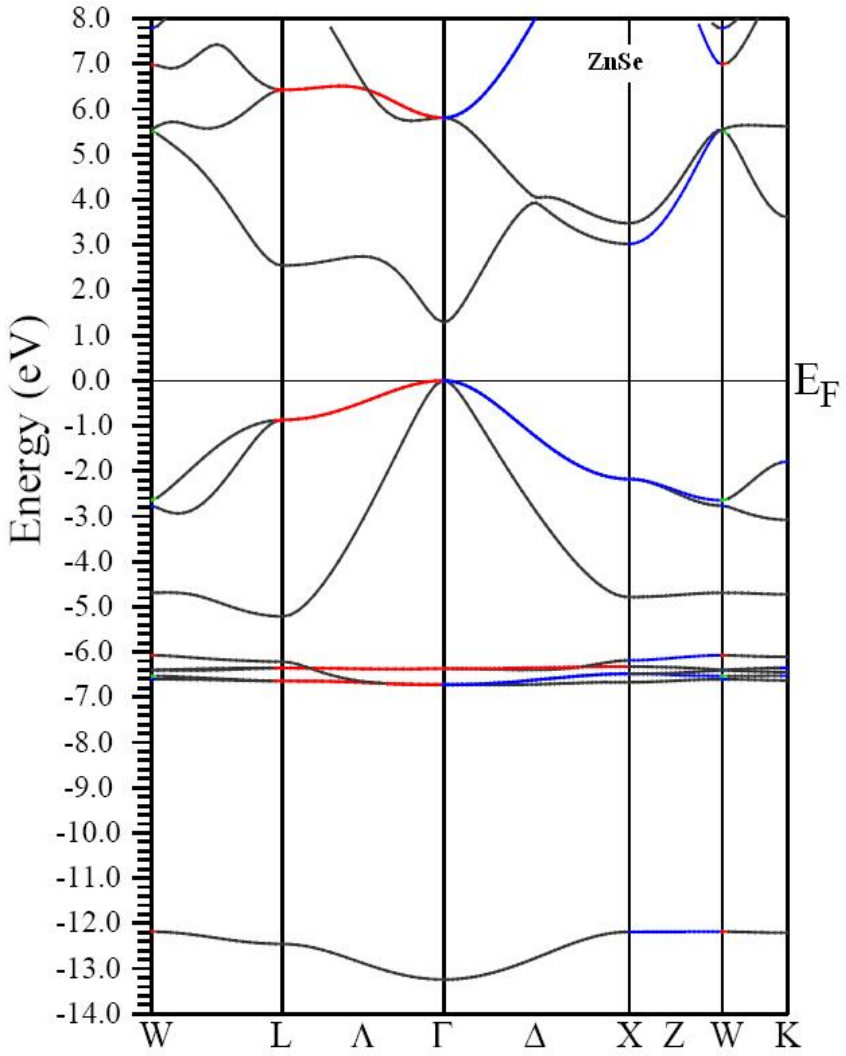

Fig. 5.11b. Energy band structure for ZnSe along the high symmetry directions in Brillouin zone. E_F = 0 eV corresponds to the Fermi level.

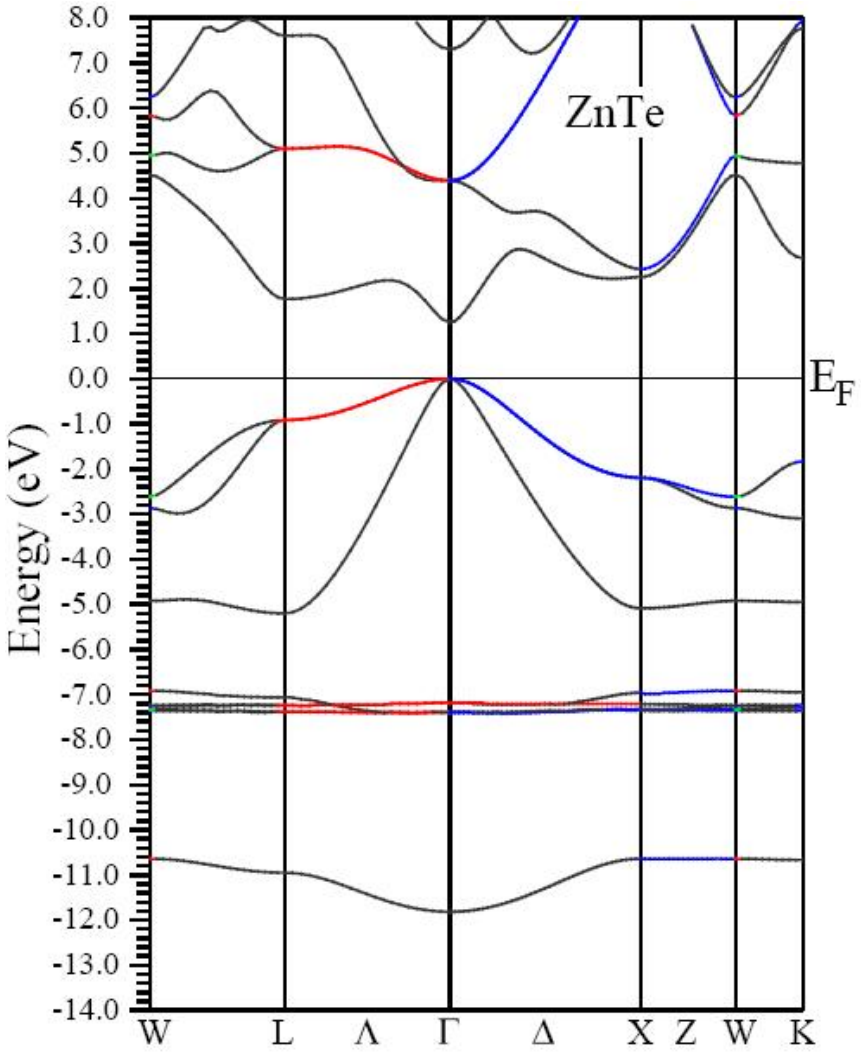

Fig. 5.11c. Energy band structure for ZnTe along the high symmetry directions in Brillouin zone. E_F = 0 eV corresponds to the Fermi level.

5.3.4. Optical properties

In calculations of the optical properties, a dense mesh of uniformly distributed k points is required. The frequency dependent complex dielectric function $\varepsilon(\omega) = \varepsilon_1(\omega) + i\,\varepsilon_2(\omega)$ is known to describe the optical response of the medium at all phonon energies $E = \hbar\,\omega$, using the formalism of Ehrenreich and Cohen (1959). The imaginary part of the $\varepsilon_2(\omega)$ in the long wavelength limit has been obtained directly from the electronic structure calculation, using the joint density of states (JDOS) and the transition moments elements. The knowledge of both the real and imaginary parts of the dielectric function allows the calculation of important optical function such as the refractive index $n(\omega)$.

Fig. 5.12a, 5.12b, 5.12c displays the imaginary (absorptive) part of the dielectric function $\varepsilon_2(\omega)$ for ZnX. Our analysis of the $\varepsilon_2(\omega)$ curves show that the first critical points of the dielectric function occurs at 2.8 eV, 1.3 eV and 1.25eV. These critical points are followed by small structure located at 5 eV in ZnS, 3.7 eV in ZnSe and 2.9 eV in ZnTe related to direct transition (L-L). The main peaks in the spectra are situated at 6.6eV, 5.5 eV and 4.5 eV respectively. The main peaks are followed by pronounced peak situated at 7.9 eV, 7.1 eV and 5.9 eV. These peaks are primarily due to direct transition between valence band and conduction band above the Fermi energy at L-edge. The experimental measurement localized the main peaks at 6.8 eV, 6.2eV, and 5.3 eV for ZnS, ZnSe and ZnTe (Kim et al., 1993; Freeouff, 1973). In comparison with the experimental data, there is slight energy shift in the main peaks. This energy shifts mainly arise from the GGA, which give a smaller band gap in comparison with experiment.

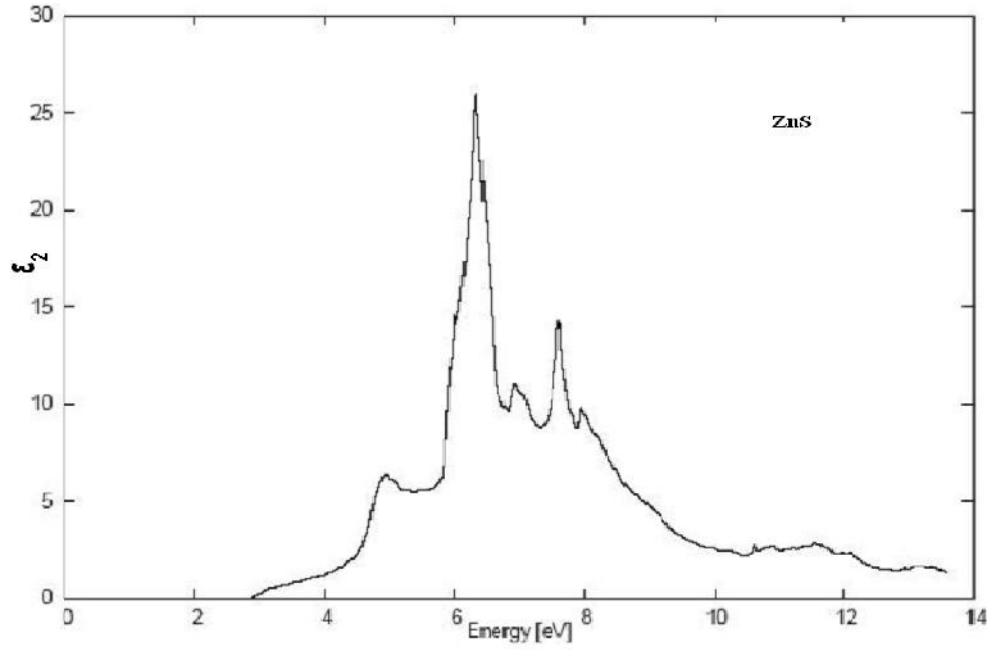

Fig. 5.12a. Imaginary part of dielectric function for ZnS.

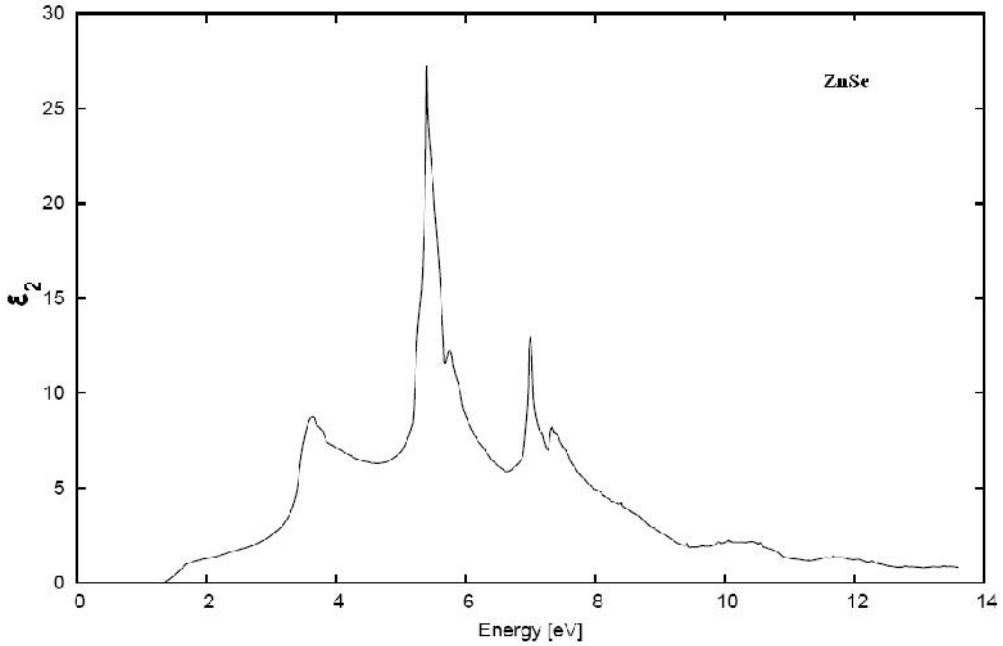

Fig. 5.12b. Imaginary part of dielectric function for ZnSe.

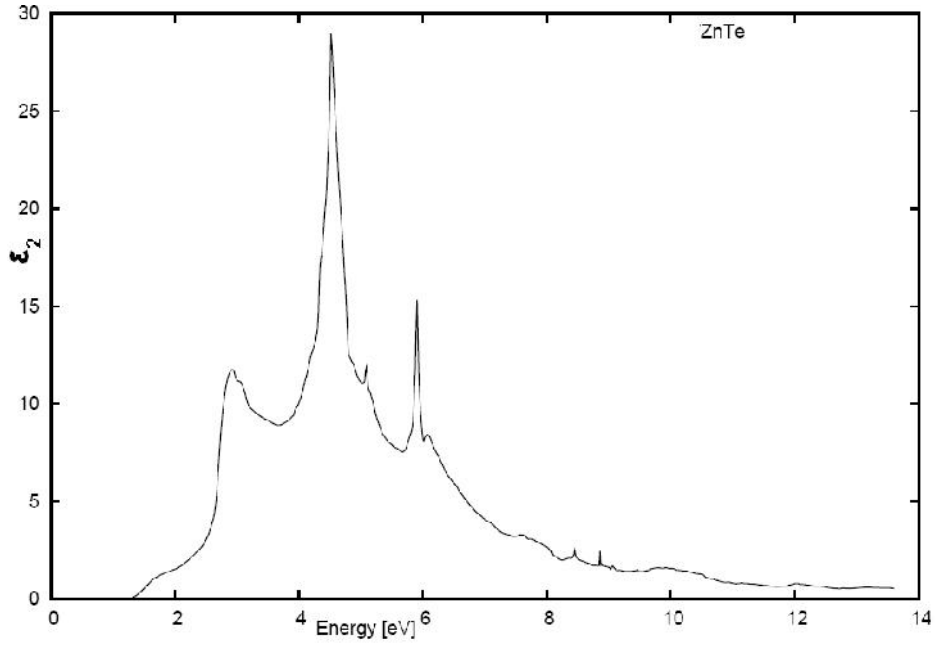

Fig.5.12c. Imaginary part of dielectric function for ZnTe.

5.4 Stibiotantalite ($SbTaO_4$)

A ferroelectric substance exhibits an electric dipole moment even in the absence of external electric field. In these crystals the centre of the positive charge does not coincide with the centre of negative charge. It has wide applications in non-linear optics, ceramics, micro wave and sensor industries. Due to the rapid advances in the field of laser technology, the non-linear optics has been studied rigorously in recent years. Many diverse disciplines such as atomic, molecular, solid state physics, material science, chemical dynamics, surface-interface sciences, biophysics and medicines have tremendous applications due to the inclusion of nonlinear techniques.

5.4.1 Details of calculations

The crystal structure of $SbtaO_4$ in the ferroelectric phase is orthorhombic and belongs to the space group Pbn2_1. There are 6 independent and 24 atoms in a unit cell. The experimentally measured lattice constants are a=4.916Å, b=5.542 Å and c=11.78 Å were used in our calculations. The atomic positions are as follows: Sb (-0.040, 0.0, 0.0), Ta (0.0, 0.375, 0.25), O1 (0.16, 0.33, 0.09), O2 (0.75, 0.12, 0.17), O3 (0.25, 0.12, 0.33) and O4 (0.84, 0.33, 0.41) (Reshak, 2005). Figure 5.13 shows the unit cell of $SbTaO_4$. Kohn-Sham wave functions were expanded in terms of spherical harmonic function inside the non-overlapping muffin-tin spheres surrounding the atomic sites (MT spheres) and in Fourier series in the interstitial region. The *l*-expansions of the wave functions were carried out upto l_{max}=10 inside the muffin-tin spheres of radius R_{mt}. The Fourier expansion for the charge density was upto G_{max}=14. The wave functions in the interstitial region were expanded in the plane waves for the cut-off of K_{max} =7/R_{mt} in order to achieve the energy eigen value convergence. A mesh of 17 X 20 X 42 k points were generated in the irreducible wedge of the brillouin zone for $SbTaO_4$. For the calculations,

the charge convergence criterion is set to be 10^{-5} Ry. With the above k-points, the convergence parameters RK_{max}=7 being the right choice that determines the stability and convergence of the calculations. Under this conditions, the value of the other parameters are chosen as follows: R_{mt} (Sb)= 2.19 a.u., R_{mt} (Ta) = 2.05 a. u., and R_{mt}(O) = 1.82 a.u.

5.4.2 Results and discussions

The total density of states for Stibiatantalite is shown in Fig. 5.15a. From the total density of states, we observe a small energy gap at around 0 eV which is taken as Fermi energy level. The partial densities of states for Sb, Ta and O are shown in Fig. 5.15b, 5.15c and 5.15d respectively.

5.4.3 Band structure

The calculated band structure of $SbTaO_4$ in the orthorhombic phase is shown in Fig. 5.14. The FP-LAPW method yields an indirect band gap of 1.9 eV at Γ-R symmetry point. The band structures near the Fermi level were dominated by the hybridization between 5p bands of Sb, 5d states of Ta and 2p states of O atoms. This conclusion can be drawn from the partial density of states. The peaks above Fermi level had Ta 5d character with a little contribution from Sb 5p-states 2p-states of O atoms. The conduction band arises mainly from d-states of Ta atoms with the minimum energy occurring at Γ point.

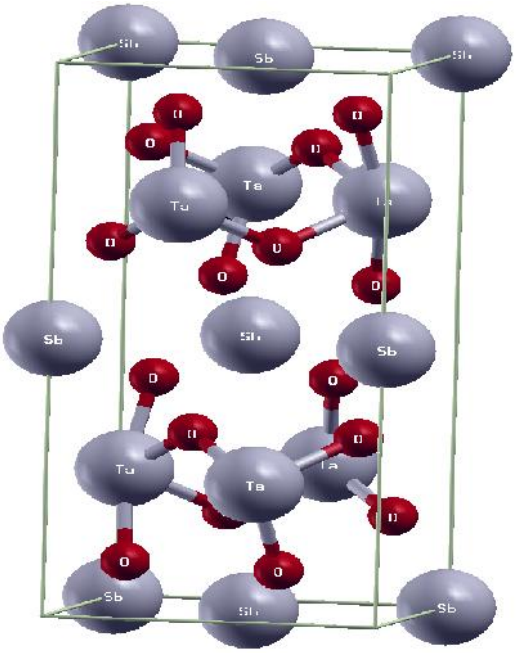

Fig. 5. 13 : Crystal Structure of $SbTaO_4$.

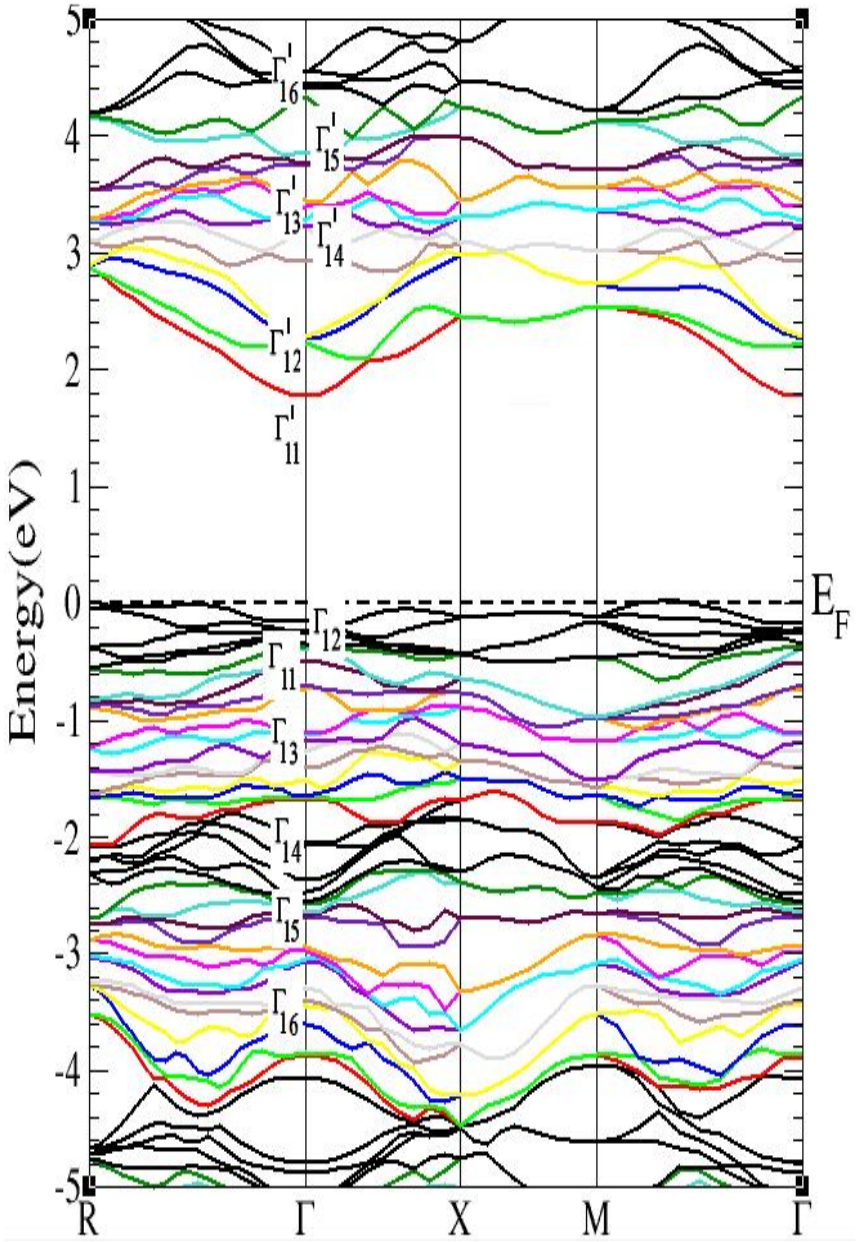

Fig. 5. 14 : Band structure of orthorhombic $SbTaO_4$. E_F = 0 eV corresponds to the Fermi energy level.

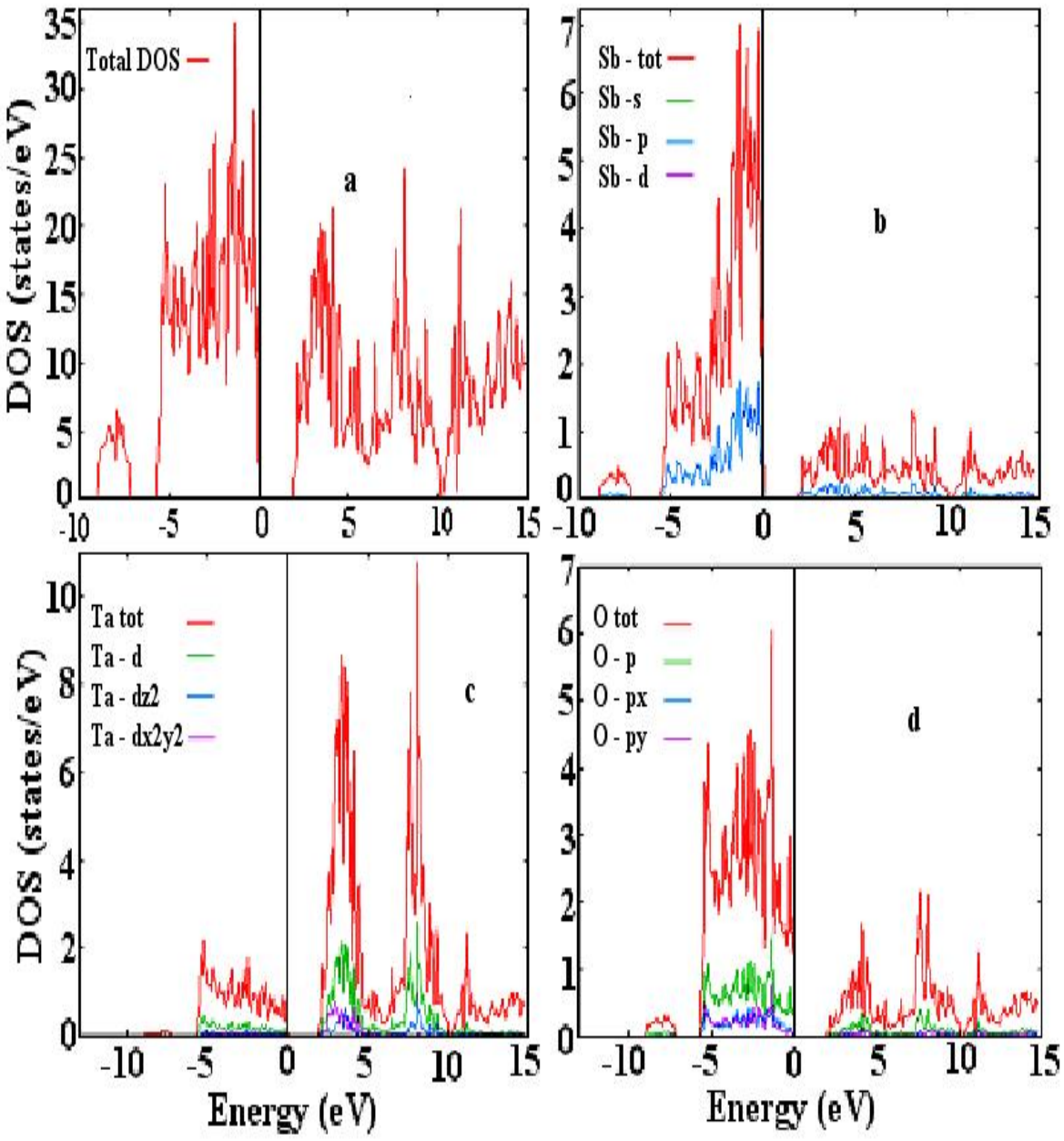

Fig. 5. 15 : Density of states for $SbTaO_4$: (**a**)Total DOS (**b**) Partial DOS of Sb (**c**) Partial DOS of Ta and (**d**) Partial DOS of O.

5.4.4 Optical properties

Our theoretically calculated absorptive part of the dielectric functions for $SbTaO_4$ is shown in the Fig. 5.16. Since the optical spectra are obtained from the interband transitions, the peak structures in Fig. 5.16 can be explained through our band structure Fig. 5.14. As there should be one-to-one correspondence between band structure and optical spectrum, we first look at the imaginary part of the dielectric function $\varepsilon_2(\omega)$. For $SbTaO_4$, the lowest energy peak at 2.5eV in the $\varepsilon_2(\omega)$ arises from the interband transition between the valence band in -0.4eV (Γ_1) and the bottom most conduction band (Γ'_1). The sharp energy peak at 3.5 eV is due to the interband transition from the highest valence band (Γ_1) to the second lowest conduction band (Γ'_{12}). The energy peak at 8.5 eV is due to the interband transition between the valence band in -4.8eV (Γ_{15}) and the conduction band in 4.7eV (Γ'_{16}). The real part or dispersive part of the dielectric function $\varepsilon_1(\omega)$ is shown in Fig. 5.17. The calculated spectra have been obtained by Kramers-Kronig transformation of the imaginary part of the dielectric function $\varepsilon_2(\omega)$. The main feature is a shoulder at lower energies, a rather steep decrease between 2 eV to 4 eV, after which $\varepsilon_1(\omega)$ becomes negative, a minimum at around 5.7 eV and slowly increases at higher energies. With the knowledge of the complex dielectric tensor components all other frequency – dependent optical constants can be obtained.

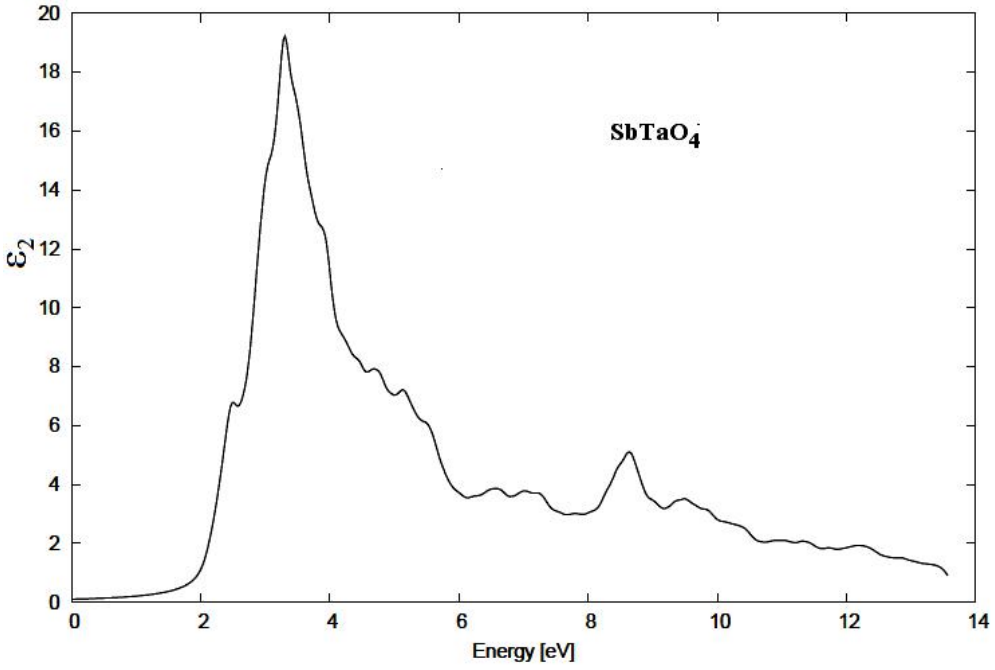

Fig. 5. 16 : Imaginary part of Dielectric function ε_2 for $SbTaO_4$.

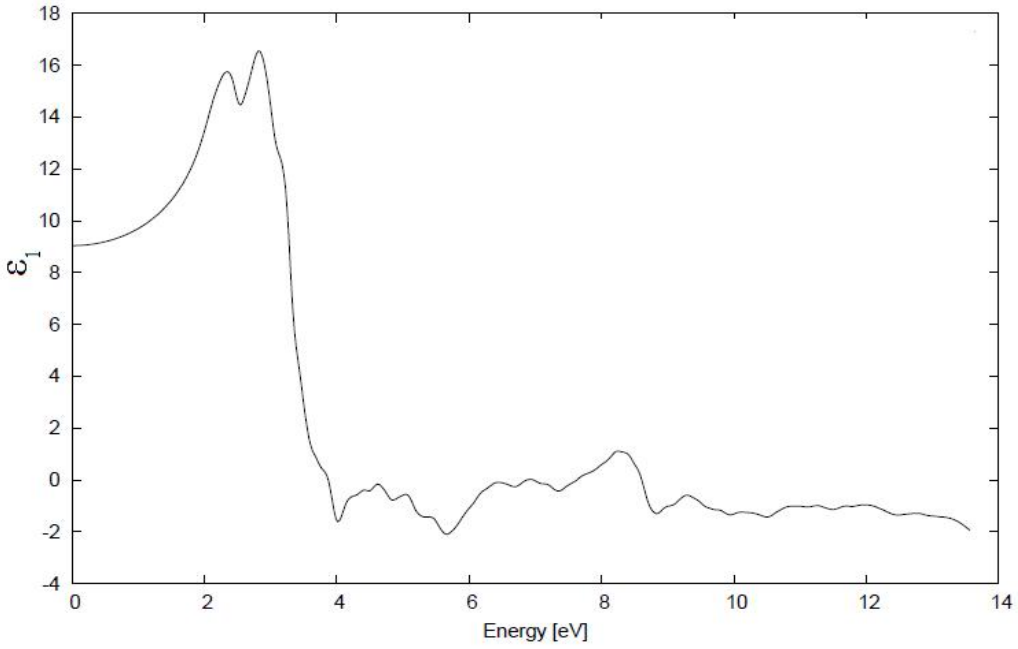

Fig. 5. 17: Real or dispersive part of Dielectric function ε_1 for $SbTaO_4$.

Chapter 6

Conclusions

In this thesis, we have presented the study of optical properties of solids within linear response regime. We have used generalised gradient approximation (GGA) which had been discussed in detail in chapter 2. In Chapter 5, we have presented the calculation of electronic band structures, density of states and optical properties by using FP-LAPW method. We applied it to the case of beryllium chalcogenides (BeS, BeSe and BeTe), lead chalcogenides (PbS, PbSe, and PbTe), zinc chalcogenides (ZnS,ZnSe,and ZnTe) and stibiotantalite ($SbTaO_{4.}$). The band structures are plotted along various symmetry directions in the Brillouin zone. The imaginary part of the dielectric function (ε_2) was also calculated for each system.

The band structures of beryllium chalcogenides (BeS, BeSe and BeTe) show indirect band gaps. Band gaps are 3.1eV, 2.6 eV and 1.9 eV respectively from Γ to X along Δ-direction for BeS, BeSe and BeTe respectively. For BeS, BeSe and BeTe the energy peak at 6.8 eV, 6.2 eV and 5.1 eV in the $\varepsilon_2(\omega)$ arises from the interband transition between the maximum of valence band at Γ - edge and the bottom most conduction band at *W* - edge. In comparison with the experimental data we find that the energy gaps are underestimated which is attributed to our use of GGA. We also identified the microscopic origin of the main features in the optical spectra and found that transitions between highest lying valence band (HVB) at Γ symmetry point and lowest lying conduction band (LCB) at X symmetry point are responsible most of the optical absorption in these systems.

For lead salts, we find direct energy band gaps of 0.40 eV, 0.24 eV, and 0.60 eV for PbS, PbSe, and PbTe respectively at the L symmetry point. Our results were compared with the experimental results and found to agree and also with theoretical results of others using different methods. The main peaks in the spectra are situated at 3.1 eV, 2.6 eV and 2.2 eV respectively for PbS, PbSe and PbTe. The results for band structure and DOS show that the energy gap for lead chalcogenides changes when S is replaced by Se and Te. This trend is attributed to the increase in bandwidth of the conduction band on going from S to Se and Te. For PbS the energy peak at 3.1eV in the $\varepsilon_2(\omega)$ arises from the interband transition between the valence band in -0.9 eV and the bottom most conduction band at W- edge. The sharp energy peak at 2.6 eV for PbSe is due to the interband transition from the highest valence band -0.7 eV to the lowest conduction band at W- edge. The energy peak at 2.2 eV for PbTe is due to the interband transition between the valence band in -0.3 eV and the conduction band in 1.9 eV.

The band structure for zinc chalcogenides also shows direct energy band gap at Γ symmetry point. The experimental band gaps are 3.8 eV, 2.8 eV, and 2.4 eV for ZnS, ZnSe and ZnTe respectively. Our calculated band gaps are 2.8 eV, 1.4 eV, 1.4 eV respectively for ZnS, ZnSe and ZnTe. Our analysis of the $\varepsilon_2(\omega)$ curves show that the first critical points of the dielectric function occurs at 2.8 eV, 1.3 eV and 1.25eV. These critical points are followed by small structure located at 5 eV in ZnS, 3.7 eV in ZnSe and 2.9 eV in ZnTe related to direct transition (L-L). The main peaks in the spectra are situated at 6.6eV, 5.5 eV and 4.5 eV respectively which are followed by pronounced peak situated at 7.9 eV, 7.1 eV and 5.9 eV. These peaks are primarily due to direct transition between valence band and conduction band above the Fermi energy at L-edge.

Our calculation of the electronic structure and DOS of ferroelectric $SbTaO_4$ in the orthorhombic phase using the FP-LAPW method shows that the fundamental gap of $SbTaO_4$ is indirect at Γ-R point with a band gap of 1.9 eV. From the DOS and band structure features, it can be concluded that the system is semiconductor. Further calculations of the x-ray spectra are to be investigated for the improvement of our results.

In the above studied systems, in comparison with the experimental data we find that the energy band gaps are underestimated which is attributed to our use of GGA. For optical calculation, a dense mesh of k points is required for accurate results. In our case, we took only 5000 k points. We are working on higher k points for the improvement of our results. Overall, we can conclude that FP-LAPW method is very appropriate for the calculation of electronic band structure and optical properties of solids.

References

Adachi, S., and Taguchi, T., (1991). Optical properties of ZnSe. *Phys. Rev*., **B43 :** 9569-9577.

Adler, S. L., (1962). Quantum Theory of the Dielectric Constant in Real Solids. *Phys. Rev*., **126** : 413–420.

Agarwal, G.P. and Dutta, N. K., (1993). *Semiconductor Lasers* (Van Nostrand Reinhold, New York, p. 547.

Albrecht, S., Onida, G. and Reining, L. (1997). *Ab initio* calculation of the quasiparticle spectrum and excitonic effects in Li_2O. *Phys. Rev.,* **B55** : 10278–10281.

Albrecht, S., Reining, L., Sole, R. D. and Onida, G., (1998). *Ab Initio* Calculation of Excitonic Effects in the Optical Spectra of Semiconductors. *Phys. Rev. Lett.,* **80** : 4510–4513.

Ali, H.R., (2005). First-principle calculations of the linear and nonlinear optical response for GaX (X=As, Sb, P). *The Eur. Phys. J.,* **B47** : 503-508.

Ambegaokar, V. and Kohn, W., (1960). Electromagnetic Properties of Insulators. *Phys. Rev*., **117** : 423–431.

Andersen, O. K., (1975). Linear methods in band theory. *Phys. Rev.,* **B12** : 3060-3083.

Anna, D., Ravindran, P., Ericsson, P. and Wills, J. M. (1997). Full-potential optical calculations of lead chalcogenides. *Int. Journal of quantum chemistry*., **69** : 349-358.

Arnaud, B. and Alouani, M. (2001). Local-field and excitonic effects in the calculated optical properties of semiconductors from first-principles. *Phys. Rev.,* **B63** : 085208/1-14.

Ashcroft, N. W. and Mermin, N. D. *Solid State Physics*, (Saunders College Publishing, Fort Worth, TX, U.S.A., 1976), p-344.

Benedict, L. X., Shirley, E. L. and Bohn, R. B. (1998). Optical Absorption of Insulators and the Electron-Hole Interaction: An *Ab Initio* Calculation. *Phys. Rev. Lett*. **80** : 4514–4517.

Berghout, A., Zaoui, A., and Hugel, J. (2006). Fundamental state quantities and high-pressure phase transition in beryllium chalcogenides. *J. Phys: Condens. Matt.,* **18** : 10365-10370.

Blaha, P., Schwartz, K., Madsen, G. K. H., Kvasnicka, D. and Luitz, J. (2008). *An Augmented Plane Wave+Local Orbitals Program for Calculating Crystal Properties.*(Revised Edition). Vienna University of Technology: Inst. of Physical and Theoretical Chemistry, Getreidemarkt 9/156, A-1060 2008, Vienna / Austria.

Chatterjee, S. and Pal, U. (1993). *Optical Eng.* **32**: 2923; Chaudhuri, T. K. (1992). *Int. J. Energy Res.* **16** : 481; Mohammad, M.T. (1990). *Sol. Energy Mat*.**20** : 297.

Corso, A.D., Mauri, F. and Rubio, A. (1996). Density-functional theory of the nonlinear optical susceptibility: Application to cubic semiconductors. *Phys. Rev.,* **B53** : 15638–15642.

Dahmani, R., Salamanca-Riba, L., Nguyen, N. V., Chandler-Horowitz, D. and Jonker, B. T. (1994). Determination of the optical constants of ZnSe films by spectroscopic ellipsometry. *J. Appl. Phys.,* **76 :** 514-517.

Ehrenreich, H. and Cohen, M. H. (1959). Self-Consistent Field Approach to the Many-Electron Problem. *Phys. Rev.,* **115** : 786–790.

Fetter, A. L. and Walecka, H. D. (1971), *Quantum Theory of Many-Particle Systems,* (McGraw-Hill).

Fleszar, A. and Hanke W. (2000). Electronic excitations in beryllium chalcogenides from the ab initio GW approach. *Phys. Rev.,* **B62 :** 2466-2474.

Freeouff, J. L. (1973). Far-Ultraviolet Reflectance of II-VI Compounds and Correlation with the Penn—Phillips Gap. *Phys. Rev.,* **B7** : 3810-3830.

Hanke, W. and Sham, L. J. (1975). Local-field and excitonic effects in the optical pectrum of a covalent crystal. *Phys. Rev.,* **B12** : 4501–4511.

Hanke, W. and Sham, L. J., (1979). Many-Particle Effects in the Optical Excitations of a Semiconductor. *Phys. Rev. Lett.,* **43** : 387–390.

Hanke, W. and Sham, L. J., (1980). Many-particle effects in the optical spectrum of a semiconductor. *Phys. Rev.,* **B21** : 4656–4673.

Hashemifar, S. J., Kratzer, P**.,** and Scheffler. M**. (**2005**).** A Density Functional Theory Study**.** *Phys. Rev. Lett.,* **94 :** 096402-096406**.**

Hasse, M. A., Qui, J., Puydt, J. M. D. and Cheng, H. (1991). Blue-green lase diodes. *Appl. Phys. Lett.,* **59** : 1272-1275.

Hassan, F.E.H. and Akbarzadeh, H., (2006). Ground state properties and structural phase transition of beryllium chalcogenides. *Computational Material Science*. **35** : 423-431.

Heciri, D., Beldi, L., Drablia, S., Meradji, H., Derradji, N. E., Belkhir, H. and Bouhafs, B., (2007). First-principles elastic constants and electronic structure of beryllium chalcogenides BeS, BeSe and BeTe. *Computational Material Science*. **38 :** 609-617.

Hedin, L. and Lundquist, B. I., (1971). Explicit local exchange-correlation potentials. *J. Phys. C*: *Solid State Phys.,* **4** : 2064.

Hicks, L.D., Harman,T.C., Sun, X., and Dresselhaus, M.S., (1996). Experimental study of the effect of quantum-well structures on the thermoelectric figure of merit. *Phys. Rev.,* **B53** : R10493- R10496.

Hohenberg, P. and Kohn, W. (1964). Inhomogeneous Electron Gas. *Phys. Rev.,* **136** : B864– B871**.**

Huang, M. Z. and Ching, W. Y., (1993). Calculation of optical excitations in cubic semiconductors I. Electronic structure and linear response. *Phys. Rev.,* **B47** : 9449–9463.

Hybertson, M. S. and Louie, S. G. (1987). *Ab initio* static dielectric matrices from the density-functional approach. Formulation and application to semiconductors and insulators. *Phys. Rev.,* **B35** : 5585–5601.

Jones, R. O. and Gunnarsson, O.**,** (1989). The density functional formalism, its applications and prospects. *Rev. Mod. Phys.,* **61** : 689–746.

Justo, Y., Moreels, I., Lambert, K., and Hens, Z., (2010). Langmuir–Blodgett monolayers of colloidal lead chalcogenide quantum dots: morphology and photoluminescence Nanotechnology. **21**: 295606.

Kalpana, G., Pari, G., Mookerjee, A. and Bhattacharyya, A. K. (1998). *Ab initio* Electronic Band Structure Calculations for Beryllium Chalcogenides. *Intl. J. Mod. Phys.,* **B12** : 1975-1984.

Kell, R.C. (1963). Modern applications of ferroelectricity, *Br. J. Appl. Phys.,* **14** : 249-255.

Kim, C. C. and Sivananthan, S. (1996). Optical properties of ZnSe and its modeling. *Phys. Rev.,* **B 53** : 1475-1484.

Kim, Y.D., Cooper, S.L. and Klein, M.V. (1993). Optical characterization of pure ZnSe films grown on GaAs. *Appl. Phys. Lett.,* **62** : 2387-2389.

Kim, Y. D., Choi, S. G., Klein, M. V., Yoo, S. D., Aspnes, D. E., Xin, S. H. and Furdyna, J. K. (1997). Spectroscopic ellipsometric characterization of undoped ZnTe films grown on GaAs. *Appl. Phys. Lett.,* **70** : 610-612.

Kinto, M., Yagi, Tanigashira, K., Yamada, T., Uchiki, H. and Iida, S. (1992). Photoluminescence studies of p- and n-type ZnS layers grown by vapor phase epitaxy. *J.Cryst. Growth.,* **117** : 348-357.

Kohn, W. and Sham, L. J. (1965). Self-Consistent Equations Including Exchange and Correlation Effects. *Phys. Rev.,* **A140** : 1133–1138.

Kohn, W. (1999). Electronic structure of matter wave-functions and density functional. *Rev. Mod. Phys.,* **71** : 1253-1266.

Levine, Z. H. and Allen, D. C. (1989). Linear optical response in silicon and germanium I including self-energy effects. *Phys. Rev. Lett.,* **63** : 1719–1722.

Levine, Z. H. and Allen, D. C. (1991). Quasiparticle calculation of the dielectric response of silicon and germanium. *Phys. Rev.,* **B43** : 4187–4207.

Lindhard, J. Dan, K. Vidensk and Selsk. Mat.-Fys. Medd. (1954). Random phase approximation. *Mat.-fys. Meddr.,* **28** : 2537-2542.

Luo, H., Ghandehari, K., Greene, R. G., and Ruoff, A. L. (1995) . Phase transformation of BeSe and BeTe to the NiAs structure at high pressure. *Phys. Rev.,* **B 52** : 7058-7064.

Murnaghan, F. D. (1944). *Proc. Natl. Acad. Sci.,* USA 30, p. 244.

Nair, P. K., Fernandez, A. and Nair, M. T. S. (1989). *Proc. SPIE Int. Soc. Opt. Eng*. 1149 : 88.

Nair, P. K., Ocampo, M., Fernandez, A. and Nair, M. T. S. (1990). Solar control characteristics of chemically deposited lead sulfide coatings. *Sol. Energy Mat.,* **20** : 235-243.

Nozieres, P. and Pines, D. (1958a). Electron Interaction in Solids. General Formulation**.** *Phys. Rev.,* **109** : 741–761.

Nozieres, P. and Pines, D. (1958b). Electron Interaction in Solids. Collective Approach to the Dielectric Constant**.** *Phys. Rev.,* **109** : 762–777.

Nozieres, P. and Pines, D. (1958c). Electron Interaction in Solids. The Nature of the Elementary Excitations**.** *Phys. Rev.,* **109** : 1062–1074**.**

Perdew, J. P., Burke, K. and Enzerhof, M. (1996). Generalized Gradient Approximation Made Simple. *Phys. Rev. Lett.,* **77** : 3865-3868.

Rashkeev, S.N., Lambrecht, W.R.L. (2001). Second-harmonic generation of I-III-VI_2 chalcopyrite semiconductors: Effects of chemical substitutions. *Phys. Rev.,* **B63** : 165212-165224.

Reshak, A. H. (2005). First-principle calculations of the linear and nonlinear optical response for GaX (X = As, Sb, P). *The European Physical Journal B.,* **47** : 503-508 .

Rohlfing, M. and Louie, S. G. (1998). Electron-Hole Excitations in Semiconductors and Insulators. *Phys. Rev. Lett.,* **81** : 2312–2315.

Rohlfing, M. and Louie, S. G. (1999). Optical Excitations in Conjugated Polymers. *Phys. Rev. Lett.,* **82** : 1959–1962.

Ronnow, D., Cardona, M. and Lastras-Martınez, L. F. (1999). Piezo-optical coefficients of ZnSe and ZnTe above the fundamental gap. *Phys. Rev.,* **B59 :** 5581-5590.

Samara, G. A. (1983). Temperature and pressure dependences of the dielectric constants of semiconductors. *Phys. Rev.,* **B27** : 3494-3505.

Sarkar, R.L. and Chatterjee, S. (1977). Electronic energy bands of BeS, BeSe and BeTe. *J. Phys. C: Solid State Phys.,* **10 :** 57-61.

Sham, L. J., Rice and T. M. (1966). Many-Particle Derivation of the Effective-Mass Equation for the Wannier Exciton . *Phys. Rev.,* **144** : 708–714.

Singh, D. J. (1994). *Plane waves, pseudopotential and the LAPW method*. Kluwer Academic Publisher, London.

Slater, J. C. (1937). Wave Functions in a Periodic Potential**.** *Phys. Rev.,* **51** : 846–851.

Sole, R. D. and Fiorino, E. (1984). Macroscopic dielectric tensor at crystal surfaces. *Phys. Rev.,* **B29** : 4631–4645.

Strehlow, W.H., and Cook, E.L. (1973). Compilation of energy band gaps in elemental and binary compound semiconductors and insulators. *J. Phys. Chem. Ref. Data.,* **2** : 163-200.

Strinati, G. (1982). Dynamical Shift and Broadening of Core Excitons in Semiconductors. *Phys. Rev. Lett.,* **49** : 1519–1522.

Strinati, G. (1984). Effects of dynamical screening on resonances at inner-shell thresholds in semiconductors . *Phys. Rev.,* **B29** : 5718–5726.

Stukel, D. J. (1970). Energy-Band Structure of BeS, BeSe, and BeTe. *Phys. Rev.,* **B2** : 1852-1858 .

Suzuki, N. and Adachi, S. (1994). Optical Properties of PbTe, *Jpn. J. Appl. Phys.,* **33,** 193-198.

Suzuki, N., and Sawai, K., and Adachi, S. (1995). Optical Properties of PbSe. *J. Appl. Phys.,* **77** : 1249-1255.

Tagantsev, A. K., Sherman,V.O., Astafier, K.F., Venkatesh, J. and Setter, N. (2003). Ferroelectric materials for Microwave Tunable Applications, *Journal of Electroceramics.,* **11** : 5-66.

Tamargo, M.C., Brasil, M. J. S. P., Nahory, R. E., Martin, R. J., Weaver, A. L. and

Gilchrist, H. L. (1991). MBE growth of the (Zn,Cd)(Se,Te) system for wide-bandgap heterostructure lasers. *Semicond. Sci. Technol.,* **6** : A8-A13.

Van der Horst, J. W., Bobbert, P. A., Michels, M. A. J., Brocks, G. and Kelly, P. J. (1999). *Ab Initio* Calculation of the Electronic and Optical Excitations in Polythiophene: Effects of Intra- and Interchain Screening. *Phys. Rev. Lett.,* **83** : 4413–4416.

Verie, C., Gil, B., Aulombard, R.L. (Eds). (1995). *Semiconductors Heteroepiyaxy, World Scientific*. Singapore, p. 73

Ves, S., Schwarz, U., Christensen, N.E., Syassen, K. and Cardona, M. (1990). Cubic ZnS under pressure: Optical-absorption edge, phase transition and calculated equation of state. *Phys. Rev.,* **B42** : 9113-9118.

Waag, A., Fischer, F., Lugauer, H.J., Litz, T., Laubender, J., Lunz, U., Zehnder, U., Ossau, W., Gerhard, T., Keim, M., and Cardona, M. (1996). Molecular-beam epitaxy of beryllium-chalcogenide-based thin films and quantum-well structures. *J. Appl. Phys.,* **80** : 792-806.

Wagner, H.P., Kuhnelt, M., Langbein, W. and Hvam, J. M. (1998). Dispersion of the second-order nonlinear susceptibility in ZnTe, ZnSe, and ZnS. *Phys. Rev.,* **B58** : 10494- 10501.

Walter, J.P., Cohen, M.L., Petroff, Y. and Balkanski, M. (1970). Calculated and Measured Reflectivity of ZnTe and ZnSe. *Phys. Rev.,* **B** : 12661-12667.

Wiser, N. (1963). Dielectric Constant with Local Field Effects Included. *Phys. Rev.,* **129** : 62-69.

Wooten, F. (1972). *Optical Properties of Solids,* (Academic Press, New York and London).

Yim, W. M., Dismukes, J. P., Stofko, E. J. and Poff, R. J. (1972). Synthesis and some properties of BeTe, BeSe and BeS. *J. Phys. Chem. Solids.,* **33 :** 501- 505.

Zachariasen, W. (1926). Simple oxides. *Physik chem.,* **119** : 201-213.

Appendix I

A. l Fourier Series Conventions of Lattice Periodic Functions

A. 1.1 Local Functions

Consider a function *f*(r) which has the lattice periodicity of the crystal, such as the electron density or the crystal potential

$$f(r+R)=f(r) \tag{A.1}$$

where *R* denotes any direct lattice vector. Then, the function *f* may be expanded in the Fourier series

$$f(r)=\frac{1}{\Omega}\sum_{G} f_G e^{iGr} \tag{A.2}$$

with the Fourier coefficients given by

$$f_G(R)=\int_{\Omega} d^3r\, f(r)e^{-iGr} \tag{A.3}$$

The summation runs over the reciprocal lattice vectors *G*, and the integration is over the crystal volume Ω. If the function *f,* however, does not have the periodicity of the lattice, such as an external perturbation, we have to include a sum over the a vector *q* from the first Brillouin zone, and write the Fourier expansion of *f* in the way

$$f(r)=\frac{1}{\Omega}\sum_{q}^{BZ}\sum_{G} f_G(q)e^{i(q+G)r} \tag{A.4}$$

$$f_G(q)=\int_{\Omega} d^3r\, f(r)e^{-i(q+G)r} \tag{A.5}$$

A. 1.2 Nonlocal Functions

Response functions for crystalline systems are in general non-local functions of *r* and *r′* that are invariant, if both space variables are translated by a direct lattice vector *R*, thus

$$f(r+R,r'+R)=f(r,r') \tag{A.6}$$

We use the following convention for the Fourier expansions of functions $f(r, r')$ with the property (A.6)

$$f(r,r')=\frac{1}{\Omega}\sum_{q}^{BZ}\sum_{G}(q)e^{i(q+G)r}f_{GG'}(q)e^{-i(q+G')r'} \tag{A.7}$$

$$f_{GG'}(q)=\int_{\Omega}d^3r\int_{\Omega}d^3r'e^{-i(q+G)r}f(r,r')e^{-i(q+G')r'} \tag{A.8}$$

The quantity $f_{GG'}(q)$ for a given q from the first Brillouin zone can be interpreted as a matrix where the matrix indices are reciprocal lattice vectors G and G'.

A.2 Crystal Lattice Integrals and Summations

In this section, some useful integrals over the crystal volume or unit cell, and some relations involving summations over lattice vectors will be given.

$$\int_{\Omega}d^3re^{iqr}=\Omega\delta_{q,0} \tag{A.9}$$

$$\int_{\Omega_0}d^3re^{iGr}=\Omega_0\delta_{G,0} \tag{A.10}$$

Here, Ω and Ω_0 respectively, denote the crystal and the unit cell volume, and q and G are vectors from the first Brillouin zone, and reciprocal lattice vectors, respectively. The summation over direct lattice vectors R of the plane wave e^{iqR} is given by

$$\sum_{R}e^{iqR}=\frac{\Omega}{\Omega_0}\sum_{G}\delta_{q,G} \tag{A.11}$$

where the factor Ω/Ω_0 is just the number of unit cells in the crystal. Note that the summation

over G is only non-zero if q is equal to zero, provided that q is from the first Brillouin zone.

Appendix II

B.1 k.p Perturbation Theory

In the position representation, the one-electron wavefunction $\langle r|n,k\rangle = \psi_{n,k}(r)$ is the solution of the Schrödinger equation

$$\left[\frac{p^2}{2m}+V(r)\right]\psi_{n,k}(r)=\varepsilon_{n,k}\psi_{n,k}(r) \tag{B.1}$$

Since the crystal potential V (r) has the periodicity of the lattice, using Bloch's theorem we can write

$$\psi_{n,k}(r) = e^{ik.r}u_{n,k}(r) \tag{B.2}$$

$$H_k = \frac{(p+k)^2}{2m} + V(r) \tag{B.3}$$

The periodic part of the wavefunction $u_{n,k}(r)$ obeys

$$H_k u_{n,k}(r) = \varepsilon_{n,k} u_{n,k}(r) \tag{B.4}$$

where

$$H_k = \frac{(p+k)^2}{2m} + V(r) \tag{B.5}$$

We want to obtain an expression for $u_{n,k+q}(r)$ and $\varepsilon_{n,k+q}$ valid for small q in terms of the values for q=0 by perturbation theory. The equation for $u_{n,k+q}(r)$ is $H_{k+q}u_{n,k+q}(r) = \varepsilon_{n,k+q}u_{n,k+q}(r)$ (B.6)

with $H_{k+q} = H_k + \frac{\hbar p.q}{m} + \frac{\hbar^2 k.q}{m} + \frac{\hbar^2 q}{2m}$ (B.7)

where the last three terms can be treated as a perturbation.

We will introduce the notation

$$(r\,|\,n,k) = u_{n,k}(r) \tag{B.8}$$

$$\left(n',k'|\hat{O}|n,k\right)=\frac{1}{\Omega}\int_{\Omega}dr\,u^{*}_{n',k'}(r)\hat{O}u_{n,k}(r) \tag{B.9}$$

for any operator $\hat{O}$ with the integral running over the unit cell of volume Ω. According to this notation, the wavefunction to first order in q for a non-degenerate state is

$$|n,k+q)=|n,k)+\sum_{n'\neq n}|n',k)\frac{(n',k|H_{k+q}-H_{k}|n,k)}{\varepsilon_{n,k}-\varepsilon_{n',k}} \tag{B.10}$$

Only one term from the perturbation Hamiltonian gives a contribution different from zero to the first order correction of the wavefunction

$$|n,k+q)=|n,k)+\sum_{n'\neq n}|n',k)\frac{(n',k|\frac{\hbar}{m}p.q|n,k)}{\varepsilon_{n,k}-\varepsilon_{n',k}} \tag{B.11}$$

To linear order in q the expression for the energy is

$$\varepsilon_{n,k+q}=\varepsilon_{n,k+q}+\left(n,k\left|\frac{\hbar p.q}{m}+\frac{\hbar^{2}k.q}{m}\right|n,k\right) \tag{B.12}$$

Since the states are normalized this expression can be written as

$$\varepsilon_{n,k+q}=\varepsilon_{n,k}+\frac{\hbar}{m}\left[\left(n,k|p|n,k\right)+\hbar k\right]q \tag{B.13}$$

The momentum matrix element can be expressed as

$$p_{l,n,k}\equiv\left\langle l,k|p|n,k\right\rangle=\delta_{l,n}\,\hbar k+\left(l,k|p|n,k\right) \tag{B.14}$$

In terms of this definition, the wavefunctions and energies to first order in q are given by

$$|n,k+q)=|n,k)+\frac{\hbar}{m}\sum_{n'\neq n}|n',k)\frac{p_{n',n,k}}{\varepsilon_{n,k}-\varepsilon_{n',k}}q \tag{B.15}$$

B.2 Matrix elements for small q

In this appendix we use the k.p expressions developed in Appendix B.1 to evaluate the matrix elements for $q \to 0$. We first write the matrix elements in terms

of the periodic part of the wavefunction

$$M^{0}_{l,n}(k,q) = \left\langle l,k \left| e^{-iq.r} \right| n,k+q \right\rangle = \left(l,k \left| n,k+q \right. \right) \tag{B.16}$$

Using the expression of the wavefunction for small q of Eq.(B.15), the matrix element at lowest order is

$$M^{0}_{l,n}(k,q \to 0) = \delta_{l,n} + (1-\delta_{l,n}) \frac{\hbar}{m} \frac{p_{l,n,k}}{\varepsilon_{n,k} - \varepsilon_{l,k}} q \tag{B.17}$$

List of Research Publications

I. Journal Papers

1. Study of electronic and optical properties of lead chalcogenides (PbX) by using FP-LAPW method, **Lalmuanpuia** and R. K. Thapa. Journal of Mat. Sc.Engineer (accepted).
2. DOS and Band structures calculations of Transition metals (W and Nb) using FP-LAPW method, R.K.Thapa, M. P. Ghimire, Rosangliana, Sandeep and **Lalmuanpuia**, Sci. Vis. **10** 88 (2010).
3. A model calculation of Photofield emission by using a simple vector potential, R. K. Thapa, M. P. Ghimire, Rosangliana, Sandeep and **Lalmuanpuia**, Sci. Vis. **10** 31 (2010).
4. Study of DOS and energy band structures in beryllium chalcogenides, R. K. Thapa, Sandeep, M. P. Ghimire and **Lalmuanpuia**, Indian Jour. Phys. **25** (5) : 401- 409 (2011).
5. Study of Co_2MnAl Heusler alloy as half-metallic ferromagnet, R. K. Thapa, Javad Hashemifar, Morteeza Jamal, D. T. Khathing, P. K. Patra, Indrajit Sharma, Rosangliana, **Lalmuanpuia**, M. P. Ghimire, Sandeep and Dibya Prakash Rai., Indian Jour. Phys. **84** (6) 717-721 (2010).
6. Study of photofield emission in tungsten by using free electron model, Rosangliana, M. P. Ghimire, Sandeep, **Lalmuanpuia**, and R. K. Thapa., Indian Jour. Phys. **84** (6) 723-727 (2010).
7. Full-potential optical calculations of beryllium chalcogenides, **Lalmuanpuia** and R. K. Thapa., Bulletin of Material Science. (Communicated)

8. Study of electronic and optical properties of lead telluride (PbTe) by using FP-LAPW method, **Lalmuanpuia**, Rosangliana, and R. K.Thapa Sci. Vis. 10 88 (2010)
9. Study of Co_2MnAl Heusler alloy as half-metallic ferromagnet, R. K. Thapa, Javad Hashemifar, Morteeza Jamal, D. T. Khathing, P. K. Patra, Indrajit Sharma, Rosangliana, **Lalmuanpuia**, M. P. Ghimire, Sandeep and Dibya Prakash Rai., Indian Journal of Physics. (accepted)
10. Study of photofield emission in tungsten by using free electron model, Rosangliana, M. P. Ghimire, Sandeep, **Lalmuanpuia**, and R. K. Thapa., Indian Journal of Physics. (accepted).

II. Conference papers

1. Study of the electronic and optical properties of zinc sulphides, **Lalmuanpuia**, Rosangliana, M. P. Ghimire, Sandeep, B. Zoliana and R. K. Thapa, Symposium on Condensed Matter Physics (CMDAYS-2010), 25^{th} – 27^{th} Aug, 2010, University of Kalyani, Kalyani, West Bengal.
2. Calculation of photofield emission current in tungsten by using transfer Hamiltonian method, Rosangliana, M. P. Ghimire, **Lalmuanpuia**, Sandeep and R. K. Thapa, Symposium on Condensed Matter Physics (CMDAYS-2010), 25^{th} – 27^{th} Aug, 2010, University of Kalyani, Kalyani, West Bengal.
3. Study of optical properties of beryllium chalcogenides, **Lalmuanpuia**, Rosangliana, Sandeep, M. P. Ghimire and R. K. Thapa, Conference on theoretical Condensed Matter Physics-2011, Assam University, 3-5th Feb. 2011.
4. Study of Photofield emission from band states deduced by using Kronig-Penney

potential and a spatially varying photon field, Rosangliana, **Lalmuanpuia**, M.P. Ghimire, Sandeep and R. K. Thapa, Conference on theoretical Condensed Matter Physics-2011, Assam University, 3-5th Feb. 2011.

5. Study of Co_2MnAl Heusler alloy as half-metallic ferromagnet, R. K. Thapa, Javad Hashemifar, Morteeza Jamal, D. T. Khathing, P. K. Patra, Indrajit Sharma, Rosangliana, **Lalmuanpuia**, M. P. Ghimire, Sandeep and Dibya Prakash Rai. Proceedings of the VI National Conference of PANE, Tripura University, 2-4 April, 2009.
6. Electronic and semi-conducting properties of yttrium nitride, M. P. Ghimire, Sandeep, **Lalmuanpuia**, Rosangliana and R. K. Thapa. Proceedings of the VI National Conference of PANE, Tripura University, 2-4 April, 2009.
7. Study of electronic and optical properties of lead telluride (PbTe) by using FP-LAPW, **Lalmuanpuia**, Rosangliana, M. P. Ghimire, Sandeep and R. K. Thapa. Proceedings of the VI National Conference of PANE, Tripura University, 2-4 April, 2009.
8. Electronic and magnetic properties of Gadolinium (Gd), Sandeep, M. P. Ghimire, **Lalmuanpuia**, Rosangliana and R. K. Thapa, VI National Conference of PANE, Tripura University, 2-4 April, 2009.
9. Study of photofield emission in tungsten by using free electron model, Rosangliana, M. P. Ghimire, Sandeep, **Lalmuanpuia**, and R. K. Thapa. Proceedings of the VI National Conference of PANE, Tripura University, 2-4 April, 2009.
10. Study of Co_2MnAl Heusler alloy as half-metallic ferromagnet, R. K. Thapa, Javad Hashemifar, Morteeza Jamal, D. T. Khathing, P. K. Patra, Indrajit Sharma,

Rosangliana, **Lalmuanpuia**, M. P. Ghimire, Sandeep and Dibya Prakash Rai. Proceedings of the IV National Conference of PANE, Tripura University, 2-4th April, 2009.

11. Electronic and semi-conducting properties of yttrium nitride, M. P. Ghimire, Sandeep, **Lalmuanpuia**, Rosangliana and R. K. Thapa. Proceedings of the IV National Conference of PANE, Tripura University, 2-4th April, 2009.

Indian J. Phys. **84** (6), 717-721 (2010)

Study of Co_2MnAl Heusler alloy as half metallic ferromagnet

Dibya Prakash Rai[1], Javad Hashemifar[2], Morteeza Jamal[2], Lalmuanpuia[1], M P Ghimire[1], Sandeep[1], D T Khathing[3], P K Patra[4], B Indrajit Sharma[5], Rosangliana[6] and R K Thapa[1*]

[1]Department of Physics, Mizoram University, Tanhril, Aizawl-796 009, India
[2]Department of Physics, Isfahan University of Technology, Isfahan 84156 Iran
[3]Department of Physics, Jharkhand University, Ranchi-835 205, Jharkhand, India
[4]Science Centre, North-Eastern Hill University, Shillong-793 022, India
[5]Department of Physics, Assam University, Silchar-788 011, Assam, India
[6]Department of Physics, Govt. Zirtiri Residential Science College, Aizawl-796 001 Mizoram, India

E-mail : rktt@sancharnet.in

Abstract : We present the study of half metallacity of Co_2MnAl as half-Heusler alloy in $L2_1$ structure which consists of four inter-penetrating fcc sub-lattices. Density functional theory based electronic structure calculations will be performed by using the full-potential linear augmented plane wave (FP-LAPW). We will use the general gradient approximation method (GGA) and local density approximation method called LDA+U. Density of states and band structure results will be presented in this paper.

Keywords: Half metal, Heusler alloy, Density functional theory, GGA, LDA+U.

PACS Nos.: 71.15.-m, 71.15.Ap, 71.15.Dx, 71.15.Mb, 71.15.Ne, 71.15. Rf, 71.20.Be, 71.20.lp

1. Introduction

Half-metallic ferromagnets (HMF) were predicted to exhibit 100% spin polarization at the Fermi energy (E_F), and have been now intensively investigated in the field of spintronics. Several kinds of Co_2-based full Heusler alloys in $L2_1$ and $B2$ phase structures, have been reported from the theoretical investigations to be HMF or exhibit high spin polarization. In the applicable viewpoints, it is required that the ferromagnetic materials used as an electrode of magnetic tunnel junctions (MTJ) for tunneling magnetoresistance (TMR) have high

*Corresponding Author

Curie temperature T_C as well as the high spin polarization. Co_2-based Heusler alloys have high T_C and are more favorable, display large TMR ratios even at room temperature.

We present a preliminary study of the half metallacity of Co_2MnAl half-Heusler alloy. For this purpose, density of states (DOS), energy bands for spin up and spin down cases, will be studied along with the calculations of magnetic moments. The theoretical value of lattice constant is determined by using the volume optimization method. Density functional theory based electronic structure calculations will be performed by using the full-potential linear augmented plane wave (FP-LAPW). We will use the general gradient approximation method (GGA) and local density approximation method called LDA+U, where the total Coulomb and orbital potentials will be taken into consideration.

2. Crystal structure and calculation details

Co_2MnAl is a type of Heusler compound which crystallizes in the cubic $L2_1$ structure (space group $Fm\bar{3}m^2$). In general Co (red) and Mn (green) atoms are transition metals and Al (blue) is a main group element. The Co atoms are placed on 8c (1/4, 1/4,1/4) and Mn and Al atoms on 4*a* (0,0,0) and 4*b* (1/2, 1/2, ½) Wycloff positions, respectively. The crystal structure of Co_2MnAl Heusler compounds is illustrated in Figure 1.

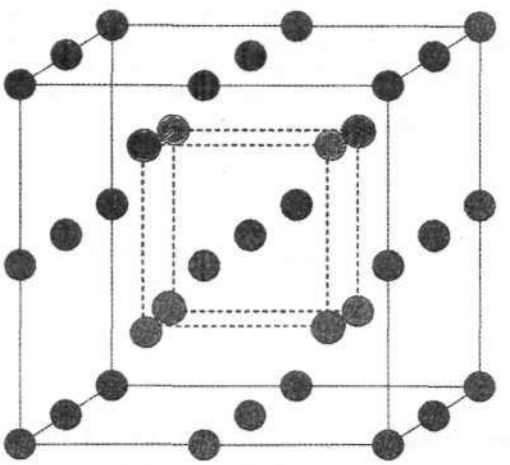

Figure 1. Structure of the Co_2MnAl Heusler compounds.

We have used the experimental [1] lattice constant a_o = 5.749 Å for the initial calculations for which the optimized value of wave vector k = 3000 was used. The optimum value of k was calculated by plotting the converged values of energies against k. The theoretical value of lattice constant a_o = 5.7261 Å was found out from volume optimization. With this value of lattice constant, WIEN2k code [2] was used to calculate DOS, energy bands, magnetic moments *etc* in this Heusler intermetallic system. The energy threshold between the core and the valence states was set to 108.80 eV. Various sets of muffin-tin radii were taken to ensure almost nearly touching sphere. $R_{MT}.K_{max}$ = 7 was used for the number of plane waves, and the expansion wave functions was set up

as l = 14 inside the muffin tins. The self-consistent calculations employed a grid of 104 k points in the irreducible Brillouine zone. LDA+U method [2] was used in which the J = 0, and hence U_{eff} = U = 6.8 eV. The convergence criterion for self-consistence calculations was set up to charge convergence equal to 10^{-5}.

3. Results and discussions

In the half-metallic ferromagnetic compound discussed here, that is Co_2MnAl, we have found that the energy gap stays in the minority spin channel (spin down), whereas E_F cuts through bands in the majority spin channel, that is spin up case (Figure 2). This means that majority-spin states have metallic character while the minority-spin band contains an energy gap at the Fermi level (E_F) which is a semiconducting behaviour. For the majority spin channel, the position of E_F is in the region of the d derived bands. These states are shifted to lower energies with respect to the corresponding minority spin states by the exchange splitting. Thus we find that for spin up case, Co_2MnAl behaves like a metal with DOS concentrated at E_F whereas for spin down case, energy gap exists around E_F. The origin of such gaps has been attributed to be arisen from the hybridization of Co and Mn *d* orbitals. The overall gap is determined by the Co-Co interaction while the effective gap in Mn partial density of states (Figure 3), is much larger as a result of Co-Co-Mn hybridization. This also indicates that the contribution of Mn-atom is more effective than Co or Co_2MnAl atom as a whole to create the band gap in spin down. Further there is not much difference between the behaviour in atomic DOS for Co (Figure 4) and total DOS for Co_2MnAl (Figure 2). The reason for this may be that only the Co-Co interaction contributes to the DOS at the E_F. Similar reports have been also given by Telling *et al.* [3].

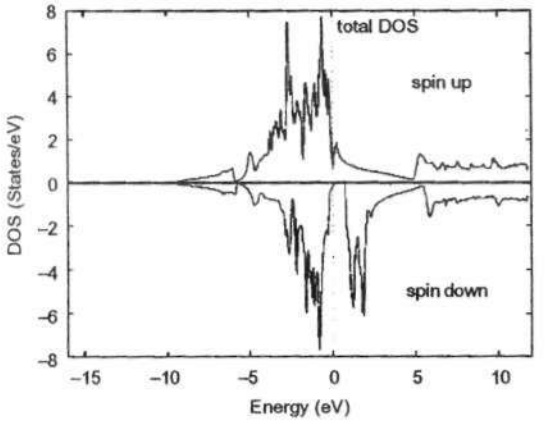

Figure 2. Total DOS for spin up and down case in Co_2MnAl.

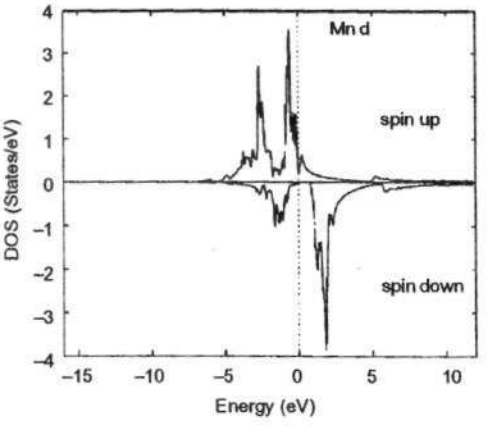

Figure 3. Plot of *d*-states DOS for spin up and spin down cases in Mn.

We have also plotted the energy bands for Co_2MnAl for both the spin up and spin down cases. The value of Fermi level calculated is E_F = 8.501224 eV. It is found that for the spin up the Co_2MnAl alloy behaves simply like a metal in which the majority

bands (spin up) crosses or touch the Fermi-level (E_F) in rather all the directions of the high symmetry (Figure 5). On the other hand, the minority bands (spin down) exhibit a clear band gap (Figure 5), the width of which is given by the energies of the highest occupied band at Γ and the lowest unoccupied band at the X. The value of the energy

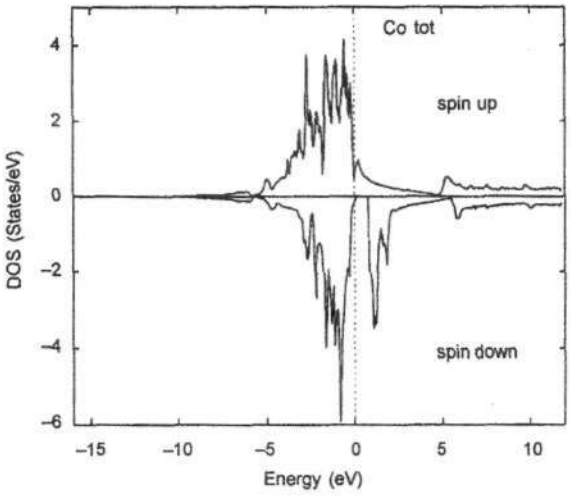

Figure 4. Plot of total DOS for spin up and spin down cases in Co-atom.

gap between Γ and X along Δ - direction is ~ 0.7 eV. This is an indirect band gap. Similar results had been reported by Kandpal *et al.* [4]. The Δ - direction plays an important role in understanding the half-metallic ferromagnets which has been pointed out by others [5-6].

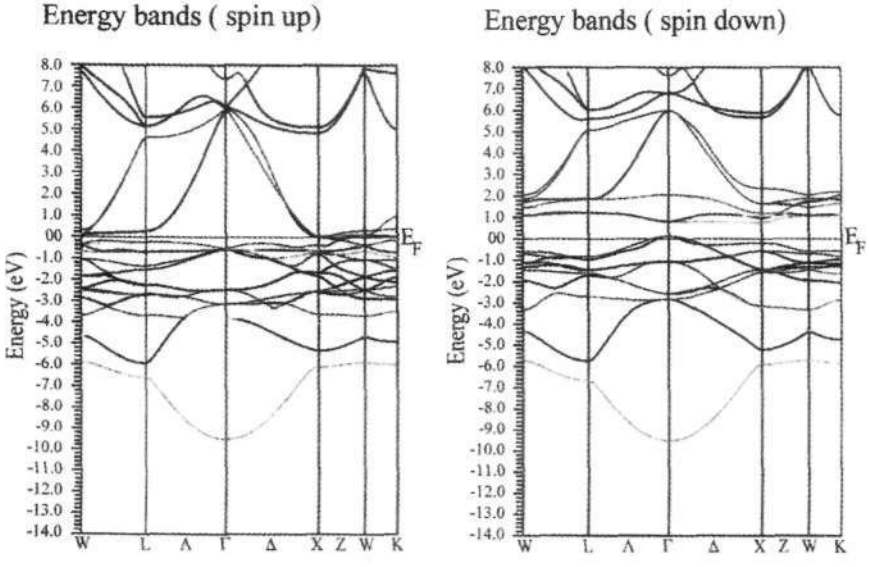

Figure 5. Energy bands plot for spin up and spin down cases in Co_2MnAl.

4. Conclusions

In conclusion, it can be said that due to existence of gap in DOS for the minority spins, Co_2MnAl is a potential half-metallic ferromagnet. This is also evident from the energy band results as discussed. The calculated magnetic moment for Co_2MnAl is equal to 4.02986 μ_B in the unit cell, which is same as experimental value ~ 4.28 μ_B [4].

Acknowledgment

RKT is grateful to DAE(BRNS), Government of India, Mumbai, for the sanction of a research grant. (No. 2008/37/39/BRNS/2482, Dt. 27/01/09). RKT also thanks Prof. Hadi Akbarzadeh for hospitality at ICTP Centre, Physics Department, Isfahan University of Technology, Isfahan, Iran, during his visit in January 2009.

References

[1] J M D Coey and M Venkatesan *J. Appl. Phys.* **91** 8345 (2002)

[2] Peter Blaha, Karlheinz Schwartz, George K H Madsen, Dieter Kvasnicka and Joacim Luitz *An Augmented Plane Wave+Local Orbitals Program for Calculating Crystal Properties*, revised ed. WIEN2k_08.3 (Release 18/9/08)

[3] N D Telling, P S Keatly, G van der Laan, R J Hicken, E Arenholz, Y Sakurba, M Oogane, Y Ando, K Takanashi, A Sakuma and T Miyazaki *Phys. Rev.* **B78** 184438 (2008)

[4] Hem Chandra Kandpal *PhD Thesis* (Gutenberg-University of Johannes, Mainz, Germany) (2007)

[5] S Ogut and K M Rabe *Phys. Rev.* **B51** 51 (1995)

[6] I Galanakis, P H Dederichs and N Papanikolaou *Phys. Rev.* **66** 174429 (2002)